GRID SENSITIVITY SIMULATION OF LOW SALINITY AND POLYMER FLOODING

A Master`s thesis in Reservoir physics

By Vidar Nordaker

Centre for Integrated Petroleum Research (CIPR)

Department of Physics and Technology

University of Bergen

June 2015

Acknowledgement

I would like to thank Professor Arne Skauge for his patience and guidance throughout this year, he has been very helpful and encouraging with a positive attitude. The same gratitude goes to Øystein Pettersen who has given a great amount of help and advice regarding the STARS simulator, and reservoir modeling in general. This thesis could not have been completed without their help.

I would also like to thank my fellow students and friends Morten Meldahl, Hanne Sæle, Ingvild Drønen and Marwan Al-Sawafi for the countless discussions we have had this past year. They have provided a healthy work environment as well as a fun and unforgetable study throughout these years.

My sincere gratitude goes also to my family and friends, who have always supported and believed in me. Special thanks to Mikaela Ödahl who has shown a tremendous amount of support throughout this year, and whose presence has been important to me.

Vidar Nordaker

Bergen, June 2015

Abstract

Water flooding in a reservoir is a well-established recovery method used to maintain the reservoir pressure and to displace the oil towards the producing well. However, after water flooding there is still a substantial amount of oil left in the reservoir, often as much as 60%, leaving a vast recovery potential. By using Enhanced Oil Recovery methods (EOR) it is possible to produce this residual oil and increase our production significantly.

Usually water flooding is used with normal seawater due to its availability, but since the late 1940`s, scientists have been looking at the chemistry of the injected water. Research (Jerauld et al., 2006) have shown that by reducing the salinity of the injection water could increase the recovery by 5-38 % .

Several mechanisms for low-salinity injection have been proposed, but scientists have not yet reached a consensus regarding the main mechanism(s).

The papers published on low-salinity recovery are mostly based on laboratory displacement experiments, and there are therefore few examples of reservoir modeling of low-salinity water flooding. This thesis is based on a laboratory experiment conducted at the Center for Integrated Petroleum Research (CIPR) at the University of Bergen. This thesis will focus on upscaling of the experiments to field-level in order to see how the low-salinity effects can affect a reservoir production. The reservoir rock has the properties of the Berea sandtone core sample presented in Gro Kallevik`s master`s thesis “Implementations of Methods for Modelig Low Salinity Waterflood and Low Salinity Surfactant flooding”. But other than that there are no specific geologic structures other than a difference in absolute permeability between the regions. The horizontal grid-sensitivity of the system and how it affects fluid flow, dispersion, and production will be emphasized in this study.

Table of content

List of figures

List of Tables

Nomenclature

Variables

c	Curvature of interface between two fluids	[Degree]
CC	Geofac, geometric factor for the well element.	Dimensionless
dp	Differential pressure	[kPa]
D/mD	Darcy/ miliDarcy	$[\mathrm{m}^2]$
DISPI	Total dispersion coefficient in I-direction	$[{}^{\mathrm{m}^2}/_{\mathrm{day}}]$
DISPJ	Total dispersion coefficient in J-direction	$[{}^{\mathrm{m}^2}/_{\mathrm{day}}]$
DISPK	Total dispersion coefficient in K-direction	$[{}^{\mathrm{m}^2}/_{\mathrm{day}}]$
ff	Well fraction	Dimensionless
$\mathrm{f_w}$	Fractional flow of water	Dimensionless
$\mathrm{f_{cwell}}$	Well flow factor	Dimensionless
g	Gravitational constant	$[{}^{\mathrm{m}}/_{\mathrm{s}^2}]$
h	Height	[m]
k	Absolute permeability	$[\mathrm{m}^2]$
kr	Relative permeability	Dimensionless
M	Mobility ratio	Dimensionless
PV	Pore volume	$[\mathrm{m}^3]$
$\mathrm{P_o}$	Oil phase pressure	[Pa]
$\mathrm{P_w}$	Water phase pressure	[Pa]
r	Radii	[m]
$\mathrm{r_e}$	Effective well radius	[m]
$\mathrm{r_w}$	Well radius	[m]
Sw	Water saturation	Dimensionless
$\mathrm{S_{wi}}$	Irreducible water saturation	Dimensionless
$\mathrm{S_o}$	Oil saturation	Dimensionless
$\mathrm{S_{or}}$	Residual oil saturation	Dimensionless
t	Time	[days]
tad1	1^{st} parameter in Langmuir expression	[gmol/m³]

tad2	2nd parameter in Langmuir expression	[gmol/m³]
tad3	3rd parameter in Langmuir expression	Dimensionless
u	Darcy velocity	[m/day]
V_p	Pore volume	$[m^3]$
V_b	Bulk volume	$[m^3]$
V_m	Matrix volume	$[m^3]$

Symbols

θ	Contact angle	[degrees]
ρ	Density	[kg/m³]
λ	Mobility	[mD/cP]
σ	Interfacial tension	[dyne/cm]
σ_{ow}	Interfacial tension between oil&water	[dyne/cm]
μ	Viscosity	[cP]
ϕ	Porosity	Dimensionless
Φ	Flow potential	[Pa]

Abbreviations

AVISC	Component viscosity in simulation runs	[cP]
DTMAX	Maximum timestep	[Days]
EOR	Enhanced oil recovery	-
HS	High-salinity	-
HSLS	Combined highsal and lowsal	-
INJ	Injector	-
IPV	Inaccessible pore volume	Dimensionless
LS	Low-salinity	-
LS&P	Combined Low-salinity and polymer	-
MASSDEN	Mass density of components in simulation runs	[kg/m³]
NaCl	Sodium Chloride (salt)	-

OIP	Oil in place	$[\mathrm{cm}^3, \mathrm{m}^3]$
PROD	Producer	-
RF	Recovery factor	Dimensionless
RRF	Residual resistance factor	Dimensionless
S	Skin factor	Dimensionless
SWCTT	Single Well Chemical Tracer Test	-
WBT	Water Breakthrough	-
WOR	Water-oil ratio	-
$\mathrm{X_D}$	Dimensionless distance, x-direction	Dimensionless
$\mathrm{Y_D}$	Dimensionless distance, y-direction	Dimensionless
1D	One-dimension al	-
3D	Three-dimensional	-

Introduction

Since water injection became popular as a recovery method for oil reservoirs in early 1920`s, it has grown to become the most extensive secondary recovery method in use today. The multi-purpose of both maintaining reservoir pressure as well as displacing the oil combined with the availability of water, either nearby rivers or seawater, makes it a practical and easy method to use. However, due to a low recovery factor of oil in place (OIP), different techniques regarding enhanced oil recovery (EOR) have over the years been invented and researched in order to increase production.

Research on whether the brine composition could affect total recovery started over 60 years ago (Brownell, 1948), but the bulk of research on low salinity waterflooding did not take place until recent decades, with published papers such as (Jadhunandan and Morrow, 1995) and (Tang and Morrow, 1999). There has also been an increasing interest since the millennia-change with a yearly increase of published papers on the subject since 2004 (Morrow and Buckley, 2011). Many of these published papers indicated a significant increase in recovery as a suggested effect of wettability alteration in the rock during lowsal waterfloods.

Today, there is a growing interest for low-salinity waterflooding in the petroleum industry since laboratory experiments have shown potential for increased recovery. Several field-tests have also been carried out, but there is not much research on low-salinity modeling. Also, most of the modeling that has been carried out has been simulation of coreflood experiments, thus leaving few examples of low-salinity simulation in field-scale reservoirs.

This thesis is focused on upscaling from a history match of a coreflood experiment to field-size with emphasis on the grid-sensitivity of both highsal- lowsal- and polymer flooding in a reservoir. Each simulation (with a few exceptions) has been performed with 3 different grid models Some processes have been simplified, in regards to data file components, in order to reduce simulation requirements.

This thesis consists of 10 chapters in total, with appendix and references included after. Chapter 1 and 2 consists of some theoretical background of waterflooding and a literature study with past research performed on low-salinity injection. Chapter 3 is a brief

introduction to the CMG STARS simulator and includes some of the most important parameters relevant to the simulations presented. It also includes some numerical background on how STARS handles simulations. Chapter 4 presents a history match of a coreflood experiment performed at Uni CIPR UiB. It also discussed how the history match was made, and a discussion of the results. Chapter 5 can be considered an introduction to the field-scale simulations with a presentation of most of the general properties of the reservoir, and also presents the production scheme. Chapter 6 presents the results from simulations performed in the homogeneous reservoir, and a sensitivity analysis of viscosity and density values for oil. Chapter 7 consists of results and a discussion of the results from the heterogeneous reservoir together with a fluid-flow test of the reservoir with highsal- and lowsal flooding. Chapter 8 is results from the heterogeneous reservoir with added polymer to increase total displacement efficiency. Chapter 9 & 10 is conclusion and recommended further work.

1 Waterflooding

1.1 Petrophysical properties

1.1.1 **Porosity**

The porosity of a rock is defined as the ratio of the total pore volume divided by the total bulk volume of the rock. This void space within the rock is where petroleum hydrocarbons in a reservoir are located. Porosity can be calculated as

$$\varphi = \frac{V_p}{V_b} \tag{1.1.1}$$

Where

$$V_b = V_m + V_p \tag{1.1.2}$$

Where Vb is bulk volume, Vm is matrix volume, and Vp is pore volume.

Porosity of a rock is dependent on:

- The type, content and hydration of the clay minerals present
- Grain size, sorting, packing and orientation
- Cementing or leaching in the rock
- Weathering of the rock

Porosity can be divided into two main categories; primary, the porosity of the rock upon creation, and secondary, porosity created as a result of chemical leaching of minerals or a fracture system. This secondary porosity can either replace the primary porosity or coexist with it.

1.1.2 Permeability

The *absolute* permeability of a rock is a measure of the flow properties of a fluid through it.

A linear and horizontal flow in 1 dimension can by defined through Darcy`s law:

$$q_x = -\left(\frac{k*A}{\mu}\right) * \left(\frac{dp}{dx}\right) \qquad (1.1.3)$$

Where q_x is the Darcy velocity$^{cm^3}/_s$, k is absolute permeability, A is inlet area of the core sample, μ is fluid viscosity, and $\frac{dp}{dx}$ is pressure drop over the core distance. A negative sign implies that the pressure is decreasing through the core sample (see Figure 1-1). The SI-unit for permeability is m^2, but the more commonly used unit is Darcy/milliDarcy (1Darcy≈$10^{-12}m^2$). Darcy`s law operates under the assumption that the fluid is incompressible and flow is linear and horizontal. It is also assumed that the core is 100% saturated by the flowing fluid.

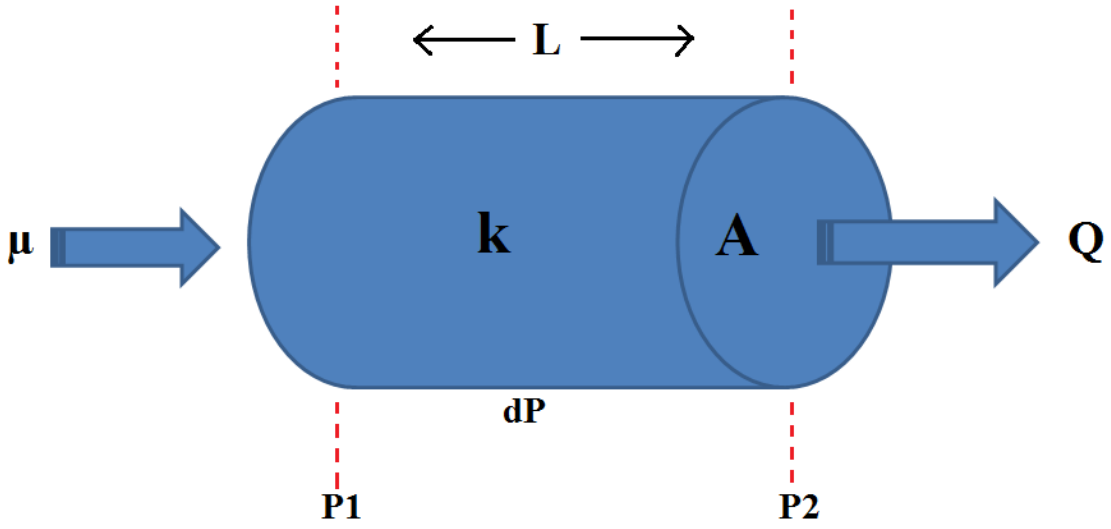

Figure 1-1: *Visualization of Darcy`s law in 1-D, fluid flow through a porous media.*

Since this thesis is mostly focused on field-scale waterflooding, the definition of Darcy`s law as shown in equation (1.1.3) is not sufficient. In order to express it in all 3 dimensions, the flow potential is introduced, and is given as:

$$\Phi = P + \frac{\rho g z}{1.0133 * 10^6} \tag{1.1.4}$$

Darcy's law in 3-D may then be written as

$$\vec{u} = -\frac{k}{\mu}\, grad\, \Phi \tag{1.1.5}$$

Where the permeability *k* is a tensor, meaning it varies for different directions. k will in this thesis be defined in two directions; horizontal permeability, k_h, and vertical permeability, k_v. The ratio $^{k_v}/_{k_h}$ will be 0.1, meaning a 10% vertical permeability throughout the reservoir. Horizontal permeability will be equal in x- and y-direction.

Should there be more than one fluid present and a multiphase flow, each of the fluids will be given an *effective* permeability. This effective permeability is non-dependent on the rock, and instead dependent on saturations of the given fluids, as they are obstructing each other's flow. Therefore, the higher the saturation of a phase at a certain time, the higher the effective permeability for that phase. The effective permeability of different fluids or phases will therefore normally be lower than the absolute permeability. The effective permeability of the normal phases is denoted as $\mathrm{k_w}, \mathrm{k_o}, \mathrm{and}\ \mathrm{k_g}$ for water, oil and gas.

The fraction of effective permeability to the absolute permeability is known as the *relative* permeability, and is given by equation (1.1.4).

$$\mathrm{k_{ro}} = \frac{\mathrm{k_o}}{\mathrm{k}},\ \mathrm{k_{rw}} = \frac{\mathrm{k_w}}{\mathrm{k}},\ \mathrm{k_{rg}} = \frac{\mathrm{k_g}}{\mathrm{k}} \tag{1.1.6a,b,c}$$

Since relative permeability is the ratio of effective and absolute permeability it is dependent on the rock properties, the fluid saturations and distributions, and the wettability. The effect of wettability on petro physical properties will be discussed further in chapter 1.2.

1.1.3 Saturation

A saturation of a fluid is how much of the pore volume the different phases occupy, and is given by:

$$V_p = V_o + V_w + V_g \tag{1.1.7}$$

Where

$$S_o = \frac{V_o}{V_p},\ S_w = \frac{V_w}{V_p},\ S_g = \frac{V_g}{V_p} \tag{1.1.8a,b,c}$$

The sum of the different saturations always equates to 1, and is constantly changing during production. Eventually, some of the saturation will become immobile and settle either at the center of a pore or along the pore walls, depending on the rock`s wettability. The immobile saturation after a displacement is called a *residual saturation* and depends on the wettability and the recovery method used for the displacement.

1.1.4 Wettability

Wettability of a porous media is a very important factor in regards to fluid flow and behavior within a rock. It can be defined as "the tendency of one fluid to spread on or adhere to a solid surface in the presence of other immiscible fluids" (Craig, 1971). Generally, most of the offshore geological formations are fully saturated with water during the diagenesis and are therefore initially strongly water-wet. As hydrocarbons enter the reservoir during a primary drainage process it displaces the water, leaving only irreducible and immobile water saturation.

Therefore, most oil reservoir tends to have a water-wet nature, where water lies along the pore walls in a thin film while the non-wetting phase, the oleic components, lies in the center of the pore.

The basic definition could be described in Figure 1-2 using Young`s equation.

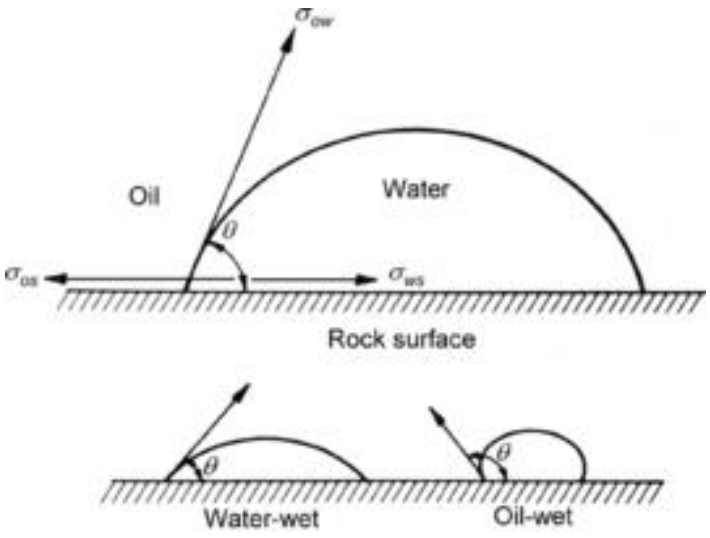

Figure 1-2: *Wettability of oil/water/solid system. Figure taken from Willhite (1986).*

Young`s equation is given by:

$$\sigma_{ow} \cos\theta = \sigma_{so} - \sigma_{ws} \quad (1.1.13)$$

Deriving Young`s equation gives the wettability angle:

$$\cos\theta = \frac{\sigma_{so} - \sigma_{ws}}{\sigma_{ow}} \quad (1.1.14)$$

Where σ_{so} is the interfacial tension between the solid and oil, σ_{ws} is the interfacial tension between water and the solid, and σ_{ow} is the interfacial tension between oil and water. The θ is the contact angle of the drop of water on the solid, and there is a clear correlation between this angle and to which degree it is either water-wet or oil-wet. Table 1 shows a correlation between the contact angle and wettability.

Table 1-1: *Correlation between contact angle and wettability.*

$\Theta \approx 0^{\circ}$	**Strongly water-wet**
$0 < \Theta < 60^{\circ}$	**Weakly water-wet**
$60^{\circ} < \Theta < 120^{\circ}$	**Neutral wet**
$120^{\circ} < \Theta < 150^{\circ}$	**Weakly oil-wet**
$150^{\circ} < \theta$	**Strongly oil-wet**

As seen in Table 1-1, a lower contact angle for water on a surface gives a more water-wet rock.

1.2 Influence of wettability on petrophysical properties

As mentioned earlier, the wettability of a porous media is important in regards to the fluid-flow properties in the rock. The wettability have been proven to influence the relative permeability, waterflood behavior and the residual fluid saturations (Anderson, 1987a). It is therefore essential to mention the different aspects of this influence.

1.2.1 Wettability influence on relative permeability

In a reservoir rock the wetting fluid is located in smaller pores and as a thin film near the pore walls in larger pores while the non-wetting fluid will lie in center of these pores. This distribution affects the mobility of these fluids as it is easier to flow in the center of the larger pores than in the smaller ones. The non-wetting fluid will at high wetting-fluid saturations lie as discontinuous bodies in the pores obstructing wetting fluid flow and therefore lower the permeability of the wetting fluid. During a drainage process where the non-wetting fluid saturation increases the relative permeability of the non-wetting fluid will often approach the absolute permeability, showing us that while the non-wetting phase can restrict the wetting phase permeability, a reverse situation does not apply to the same extent (Anderson, 1987c).

Craig (Craig, 1971) presented several rules of thumb that examines the differences in the relative permeability between strongly water-wet and oil-wet cores. These are illustrated in Figure 1-3.

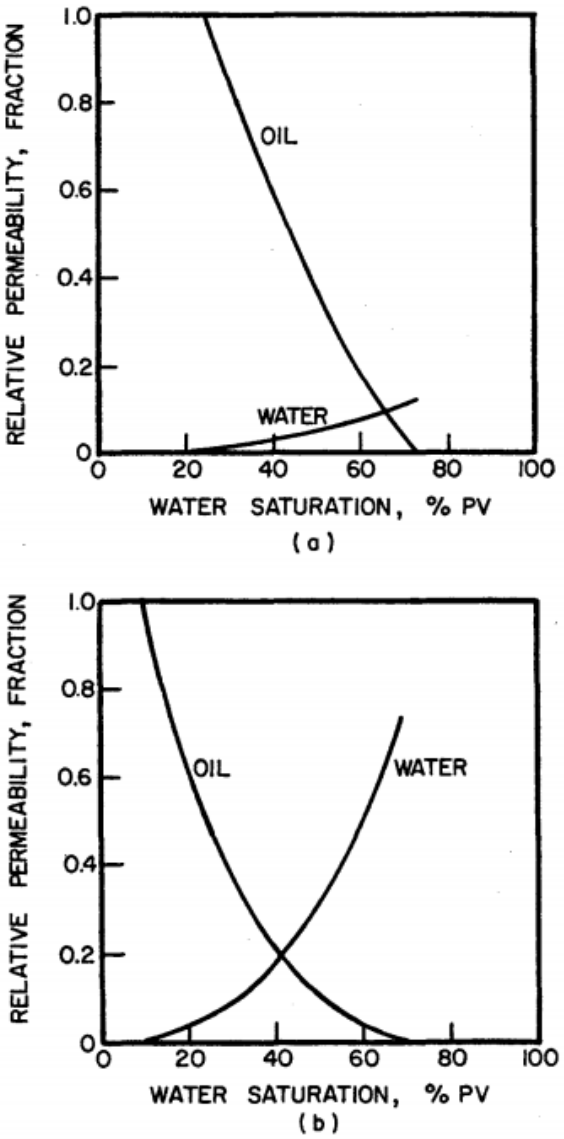

Figure 1-3: *Relative permeability curves in **a)** strongly water-wet cores, and **b)** strongly oil-wet cores. Figures taken from Craig (1971).*

Figure 1-3 shows that in the oil-wet core the water relative permeability at residual oil saturation is much higher compared to the water-wet core. This is caused by residual oil saturation in the water-wet cores is hindering the water flow, while in the oil-wet core the residual oil saturation is located near the pore walls, allowing the water to flow more freely.

The water saturation at which the relative permeability of oil and water are equal is generally beneath 50%PV for the oil-wet, and above 50%PV for the water-wet. Worth mentioning is that the irreducible water saturation is usually less than 15% in an oil-wet system while it is 20-25% in a water-wet system.

1.2.2 Wettability influence on waterflooding

Waterflooding is the most common recovery method in the North Sea where the purpose of injecting water is to maintain reservoir pressure as well as the water displacing the oil. Once water has reached breakthrough in the producing well the oil production will decrease while the water production increases. This waterflood recovery is dependent on fluid relative permeabilities as well as the fluid viscosities. Assuming we neglect capillary effects and a horizontal displacement system, the fractional flow of the water can be expressed as

$$f_w(S_w) = \frac{1}{1+\frac{\mu_w}{\mu_o}*\frac{k_{ro}}{k_{rw}}} = \frac{1}{1+\frac{1}{M}} \quad (1.1.13)$$

Where

$$M = \frac{\lambda_w}{\lambda_o} = \frac{k_{rw}*\mu_o}{k_{ro}*\mu_w} \quad (1.1.14)$$

f_w is the fractional flow of water, S_w is the water saturation, μ_w, μ_o are water and oil viscosities, and k_{rw}, k_{ro} are the relative permeability of water and oil. M is known as the mobility ratio between the oil and water. As discussed in section 1.2.2, the relative permeability is affected by the wettability, and thus the fractional flow of water will also be affected by the wettability by the control of location, flow and spatial distribution of oil and water.

During a waterflood in a water-wet system it is favorable to have a moderate water/oil mobility ratio, as close to 1 as possible. This will give a piston-like uniform displacement through the media, given that we neglect gravitational forces. Injected water will in a water-wet media spontaneously imbibe into the smaller pores and push the oil into the center of the larger pores. This will result in a displacement front, with continuous oil saturation in front of it and discontinuous droplets of residual oil behind it. As long as the oil is connected and continuous, it will be mobile, but once a droplet snaps off through a pore neck it

becomes much harder to mobilize due to the capillary forces. In result, the disconnected residual oil will exist in two basic forms: 1) capillary trapped droplets in the center of the larger pores and 2) larger patches of oil extending over several pores surrounded by water (Anderson, 1987b). A typical production result from a strongly water-wet system is a high percentage of the oil in place (OIP) produced before water breakthrough (WBT) and a rapidly decreasing oil production rate after.

With waterflooding in an oil-wet system we have a reversed locality of the fluids, where the oil is located in the smaller pores and in thin films on rock surfaces while water is located in small drops in the center of the pores. There will initially have a higher OIP but the injected water will now form continuous channels or fingers through the larger pores in the media, displacing the oil. The oil saturation after the displacement front is much higher. As injection continues, water will flow into smaller pores creating additional channels. This will result in earlier breakthrough of water in the producing well and an increasing Water-oil ratio (WOR) over time. Most of the oil will be produced after WBT making the total oil recovery much more dependent on the amount of water injected compared to waterflooding in a water-wet system. This also affects the residual oil saturation and makes it hard to define.

Reservoirs can have wetting states which is neither water-wet nor oil-wet. They can also be mixed-wet, where different parts of the reservoir alternate between being water-wet and oil-wet, or intermediate-wet where the rock has a small attraction to both the oil and water. Such reservoirs would give a higher recovery factor than the oil-wet reservoirs and could result in a sustainable production long after WBT.

2 Literature Study

Oil was primarily produced by pressure depletion of the reservoirs, using the initial reservoir pressure to “push” oil towards the producing well. This pressure rapidly decreased until it no longer could lift oil up to the surface and left most of the oil unproduced. This method is known as the primary recovery method and is very inefficient.

The secondary recovery method is the most outspread method and is injection of water into the reservoir. This technique helps maintaining the reservoir pressure as well as displaces oil and pushes it towards the producing well. But the residual oil saturation after a waterflooding is relatively high, meaning one could produce more of this oil should the capillary number, be more favorable. The capillary number is a result of viscous and capillary forces, and it can be increased by either increasing the viscosity or reducing the capillary forces trapping the oil. This can be done with tertiary recovery methods, and by introducing EOR-techniques.

Among many other techniques, low salinity water injection has shown good potential in lowering the S_{or}. The reduced salinity in the injected water has seemed to induce certain changes in the reservoir and therefore increase the recovery. The specific mechanisms related to this are still uncertain but numerous laboratory-, simulation, and single-well chemical tracer tests done in the field have documented that low-sal injection could improve recovery by 5-38%, or a corresponding reduction in S_{or} of 3-17% (Jerauld et al., 2006). The mechanisms related to increased recovery with low-salinity water injection are presented in chapter 2.2.

2.1 Past Research

In 1967 George G. Bernard performed waterflood experiments on both synthetic and natural water-sensitive cores with varying salinity in the injected brine. His study indicated that when reducing the salinity of the brine from 1 to 0.1 wt% NaCl, the residual oil saturation decreased in the cores. The additional recovery with low-salinity brine injection was accompanied by a high pressure drop over the core. However, when conducting his second experiment with an almost constant pressure drop, no additional oil recovery could be observed (Bernard, 1967).

In 1995, Jahunandan and Morrow performed an experiment with more than 50 slow-rate waterfloods with varying crude oil, brine composition, flooding rate and initial conditions. The low injection rates were utilized to minimize the viscous fingering and end-effect due to capillary pressure. The core wettabilities were measured and were found to be very sensitive to the initial water saturation, aging temperature, and brine composition. The aging time and initial water saturation showed a larger impact on increased recovery than the brine composition, however the general trend gave results indicating an increased recovery when the wettability was changed from water-wet to a more neutral state. The data also showed a maximum in recovery with a wettability close to neutral, but slightly water-wet (Jadhunandan and Morrow, 1995).

Morrow continued the work started by Jadhunandan and published in 1996 a journal with H.O.Yildiz on the effect of brine composition on recovery on Moutray crude oil by waterflooding. Their results confirmed that the most favorable wettability for oil recovery is a weakly water-wet condition and that this can be achieved by altering the injected brine composition (Yildiz and Morrow, 1996).

Tang and morrow performed a waterflood experiment in 1997 further investigating the effect of brine/ oil composition, aging and temperature on recovery by waterflooding, in both displacement and spontaneous imbibition processes. Results showed that an increase in aging time and temperature, and decrease of initial water saturation, increased the waterflood recovery. Also, a decrease in injected brine concentration and connate brine concentration gave a higher waterflood recovery (Tang and Morrow, 1997). Tang and Marrow also observed a change towards more water-wet conditions for both spontaneous

imbibition and waterflooding during the flooding with low-salinity brine. This transition towards a more water-wet system could occur when the temperature was increased or when the samples were aged at high water saturations. These changes were observed for a variety of crude-oil compositions with the addition or removal of light ends, indicating that the crude-oil composition and its interaction with the brine is an issue to take into consideration.

Two year later, in 1999, Tang and Morrow published a paper with a new experiment continuing their work. They investigated the interaction between crude oil and brine, fines migration within cores, and the influence of fines migration had on recovery (Tang and Morrow, 1999). They observed an adsorption of polar components in the crude oil to fines in the core, and that these clays must initially reside within the connate brine. They eliminated other possibilities for this by performing the same experiment on a core sample that was initially saturation with refined mineral oil. This and several other factors led to the hypothesis that "the basic concept of mixed wettability is that adsorption of heavy polar components from crude oils can only occur on rock surface that is not overlain by bulk connate water" (Salathiel, 1973). Assuming that heavy polar components adsorb onto particles at the pore walls giving mixed-wet fines could explain the increase in recovery with low-salinity water injection. This because of the brine chemistry containing the force needed to strip the particles from the pore walls during the course of the waterflooding.

Lager and Webb presented in 2006 their experiment where they performed low-salinity waterfloods on 3" long and 1.5" diameter sandstone cores in order to investigate the specific mechanisms regarding low-salinity injection. The mechanisms they focused on were fines migration, pH variation and Multi-component Ionic Exchange (MIE). Their results questioned the link between fines migration and oil recovery, as though their reached and increased oil recovery in all their waterflood experiments, no fines migration or significant permeability reduction could be observed. They also proved that despite previous research showing evidence for increased oil recovery due to a high pH, this could not be responsible for the increased recovery. This is due to proton buffering from oxides present in the reservoir rocks and the significant amount of CO_2 present in some petroleum reservoirs would most likely make it unsustainable. In order to test the MIE mechanism they replaced the multivalent cations present on the rock surfaces in the cores with sodium. This replacement would

prevent forming of organo-metallic complexes and removing adsorption and cation briding, leaving only van der Waal interactions. This removal led to a higher recovery regardless of salinity and for the first time no improved oil recovery was observed when low salinity water was injected into a clastic reservoir when the mineral structure was preserved. This confirmed MIE as a mechanism of increased oil recovery by low salinity water injection.

Two years later, in 2008, Sorbie et al. followed up on this where they presented a paper demonstrating the importance of MIE and the impact it had on the pore-scale physics. Their model was based on known pore-scale physics and used some ideas from the percolation theory in order to make an estimate of the residual oil. The mathematical model presented in the paper assumed a change in the wetting angle due to injection of low-salinity water. The main assertion in this model was that the $LoSal^{TM}$ (trademarked by BP) effect effectively changes parameters in the Laplace equation for the capillary pressure so that the capillary pressures for high-salinity and low-salinity processes are equal, giving us:

$$\frac{2*\sigma_{ow}^{HS}*\cos\theta_{ow}^{HS}}{R_{HS}} = \frac{2*\sigma_{ow}^{LS}*\cos\theta_{ow}^{LS}}{R_{LS}} \quad (2.1.1)$$

Where $\sigma_{ow}^{HS}\ and\ \sigma_{ow}^{LS}$ are the interfacial tensions between the oil and water for high/low salinity flooding, $\cos\theta_{ow}^{HS}\ \ and\ \ \cos\theta_{ow}^{LS}$ are the contact angles between the oil and water for high/low salinity flooding, and $R_{HS}\ and\ R_{LS}$ are the minimum pore radii for oil to be displaced by water. Rearranging this gives us:

$$R_{LS} = R_{HS} * \left(\frac{\sigma_{ow}^{LS}*\cos\theta_{ow}^{LS}}{\sigma_{ow}^{HS}*\cos\theta_{ow}^{HS}}\right) \quad (2.1.2)$$

Which further implies that either:

$$\left(\frac{\sigma_{ow}^{LS}}{\sigma_{ow}^{HS}} > 1\right) \quad (2.1.3a)$$

Or

$$\left(\frac{\cos\theta_{ow}^{LS}}{\cos\theta_{ow}^{HS}}\right) \quad (2.1.3b)$$

In physical aspects, this means that the effect of low-salinity injection is either due to an increase in the interfacial tension (equation 2.1.3a) or the system becomes more water-wet (equation 2.1.3b). Earlier research (Vijapurapu and Rao, 2004) stated that there is a minimal decrease in interfacial tension when diluting brine, and that in water-wet conditions the contact angle was $\cos\theta_{ow} \approx 1$. Therefore, they concluded that the $LoSal^{TM}$ effect is very unlikely to have an effect in strongly water-wet systems.

However, in mixed-wet systems there could be large pores which are preferentially oil wet and therefore show a larger potential of increased recovery following equation (2.1.3b) in the mathematical model. The low-salinity waterflood method therefore proved to change the water`s contact angle on the rock surface towards a more water-wet condition in mixed-wet systems. This confirmed the MIE theory in which the electrical double layer expands to give less oil-wet conditions. This could also explain why one could observe small or no effect of $LowSal^{TM}$ on strongly water-wet systems.

Rivet, Lake and Pope from University of Texas-Austin conducted in 2010 a waterflooding experiment on a total of 21 Berea Cores with varying ion compositions in the injected brine. They also varied crude oil aging, from 12 hours to 25 days, to induce different wettability settings in the cores. Low-salinity flooding were conducted in both secondary and tertiary mode, with one part of the experiment including parallel waterflooding of five cores, and three other parts including serial waterfloods. The serial waterfloods were conducted in the same core in order to eliminate the possibility that natural variations between the cores would affect the results of high- and low-salinity floodings. They observed an increased recovery in 3 cores which all were measured to be mixed-wet, with an assumption of a wettability change in the cores from mixed-wet to a more water-wet state. No signs of increased recovery were observed in the cores with the lowest clay content, experimental temperature and shortest aging time as these were believed to be more water-wet.

2.2 Suggested Mechanisms

Several hypotheses have been proposed regarding which mechanism(s) is the driving force behind the effect that low-salinity water injection has, but a consensus is yet to be made. Different theories include wettability alteration, fines migration, Multi-component Ionic Exchange, and pH variation. These mechanisms will be discussed further in the following chapters.

2.2.1 Wettability alteration

As discussed in chapter 1.1.6, wettability of a rock has a large impact on how the fluid flow in the rock behaves as it tells us which fluid has an attraction to the pore walls, and to which degree. An alteration of this property will change the flow paths of the fluid and thereafter affect total oil recovery. Several studies have been published (Tang and Morrow, 1997, Agbalaka et al., 2009, Ashraf et al., 2010) suggesting a wettability alteration as the driving mechanism behind the low salinity effect. But the nature of wettability is complex and includes a dependency of the interaction of the chemical composition in both the fluids and the rock. Research done by Buckley, Liu, and Monsterleet (Buckley et al., 1998) presented four different mechanisms of interaction between crude oil/brine/rock that could alter the wettability in a system: Polar interaction, surface precipitation, acid/base interactions and ion bindings/interactions between charged sites and higher valency ions.

Polar interactions are adsorptions of polar compounds in crude oil onto mineral surfaces in the absence of water, and these polar compounds are dissolved in the oil. But should the crude oil prove to be a bad solvent for asphaltenes , the tendency for wetting alteration is enhanced and the compounds will precipitate onto the rock surface. If Ca^{2+} ions are present one can observe a masking of the acid/base in different interactions in the system:

oil-Ca-oil mineral-Ca-mineral oil-Ca-mineral

The two first interactions could limit the wettability alterations while the third could improve it.

Water plays a big part in the oil/solid interaction should it be present. In the presence of water both the solid and oil interfaces become charged and polar functional groups belonging to both the solid and crude oil can behave as acids and bases. In a water-wet or mixed-wet system, water lies as a film near pore walls in a continuous path and the influence of DLVO forces are stabilizing this water film. For oil or solid surfaces the surface charge depends on to which degree the acid/base dissociation react, and in some brine compositions both oil/water and solid/water will have an equal charge thus resulting in an equilibrium case. This equilibrium stabilizes the water film which in turn results in strongly water-wet conditions. Should this equilibrium not be present one could observe a collapse of the water film where crude oil components at the oil/brine interface adsorb onto the solid surface. This collapse in the water film is the first step of wetting alteration. Studies (Basu and Sharma, 1997) showed that the oils ability to rupture the water film is determined by the critical disjoining pressure. If surface forces are repulsive then the capillary pressure would have to exceed the disjoining pressure in order to destabilize the wetting film, but should they be repulsive the solid surface would have an attraction to the drop phase (non-wetting phase) and the water-film will spontaneously rupture.

2.2.2 Fines migration

During their low salinity waterflood experiments in 1999, Tang and Morrow observed a dilution of fines in their samples, but when they fired and acidized the cores in order to stabilize the fines they observed no significant recovery increase due to changes in the brine salinity. Also they did not observe sensitivity for refined oil, meaning no polar components in the oil were present to react with the clay. These results led them to believe that the mobilization of fines within the core is an important part of the low salinity effect.

This mechanism is dependent on the wetting state of the system. It requires a mixed-wet or weakly water-wet system for fines to be mobilized. Adsorption of the polar component in the oleic phase onto the fines cannot occur should the fines be overlain by a water film. Detachment of these mixed-wet fines will expose underlying water-wet rock altering the wettability of the system towards more water-wet, which in turn will lead to an increased oil recovery due to a more favorable mobility ratio (Rivet et al., 2010). Low salinity water

injected will expand the electrical double layer in the aqueous phase and thus releasing even more fines from the solid. The electrical double layer will be further discussed in chapter 2.2.3.

This mechanism was later regarded as *"..quite tentative and was really based on a simple pictorial view of phenomenon, and it was not confirmed in any rigorous manner; it was conjectured as being a plausible mechanism for the low salinity effect"* (Sorbie and Collins, 2010). They sought for more extensive research due to a lack of experimental evidence of fines mechanisms being the reason for increased recovery, and rather preferred the theory of MIE (discussed in next chapter).

2.2.3 Multi-component Ionic Exchange (MIE)

Lager et al. proposed in their revised paper in 2008 that Multi-component Ionic Exchange (MIE) could be the primary mechanism in regards to increased oil recovery with low salinity water injection. Presence of clay (kaolinite) in the rock matrix gives a negative charge to the solid surface and therefore attract positively charged ions like Ca^{2+} andMg^{2+}. This attraction towards the surface will make the overall wettability of the pore more oil-wet by binding acidic compounds in the crude oil to the negatively charged surface in a process known as ionic bridging.

This process occurs when ions in a solvent surround a solid with a charged surface, leading to an electrical double layer with an inner and outer layer of ions where the inner layer consists of adsorbed ions onto the surface, known as the Stern Layer, and the outer layer consists of ions in Brownian motion in the adjacent solvent (Lee et al., 2010). See Figure 2-1 for illustration.

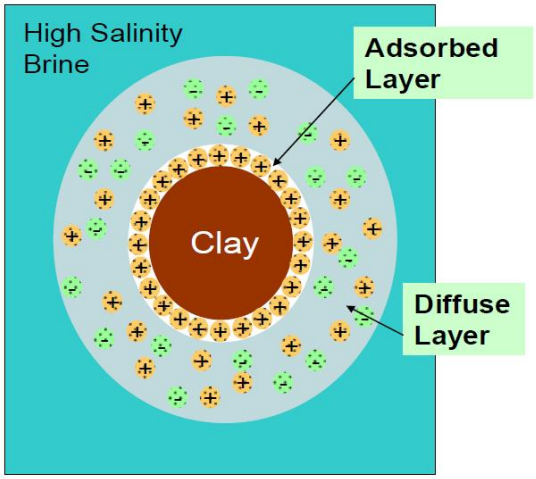

Figure 2-1: *Schematic of the electrical double layer surrounding a negatively charged clay mineral. Figure taken from Lee et al. (2010).*

The thickness of the adsorbed and diffused layer is known as the double layer thickness, or the Debye length, and is dependent upon electrolyte concentration and ion valency. Lower ionic strength and valencies leads to a thicker double layer. During a high salinity water flood, polar components in the crude oil might be retained on the surface, making out the residual oil saturation after a water flood. But when the low salinity brine is introduced to the system, it is possible that divalent cations get exchanged for monovalent cations which will free oil from this surface, leading to an expansion of the electrical double layer due to the ionic strength (salinity) decreasing. An increase of this double layer will alter the wettability towards a more water-wet state. An expansion of this double layer will also result in a higher exchange of Mg^{2+} and Ca^{2+} for low salinity than for high salinity water floods.

Sorbie and Collins (2010) suggested a development of a locally expanding "Self-freshening" zone in which we could observe an even lower salinity than the injected brine which enhances the MIE mechanism. If we inject low salinity water in tertiary flooding after a high salinity brine injection we can observe this zone due to varying adsorption isotherms in the high- and low-salinty floods. The low salinity water will have a higher ion exchange and the HS and LS metal ion fronts will therefore move at different velocities through the core, thus

generating this “fresh” region in which the water film is believed to expand. This zone will to some extent be smeared out, depending on the dispersion.

2.2.4 pH variation

Lager and Webb observed in 2006 an increase in pH in produced brine during their laboratory experiments. This was a result of two concomitant reactions: cation exchange and carbonate dissolution. The carbonate dissolution results in an excess of OH- molecules while the cation exchange is a result of reactions between clay minerals and injected water. The dissolution of carbonates in the rock is slow and widely dependent on the amount of carbonate material present.

$$CaCO_3 \leftrightarrow Ca^{2+} + CO_3^{2-} \quad (2.2.1)$$

$$CO_3^{2-} + H_2O \leftrightarrow HCO_3^- + OH^- \quad (2.2.2)$$

During cation exchange, the mineral surface exchanges previously adsorbed cations to H^+ present in the liquid phase and thus decreasing the H^+ concentration in the liquid which in turn increases the pH. Should the pH increase above 9 the system would resemble an alkaline flooding whereas one would expect a decrease in IFT, wetting alteration, and formation of water drops inside the oil phase(Jensen and Radke, 1988). The decrease in IFT would be a result of creation of surfactants in the alkaline solvent injected. However, the best low salinity coreflood results were obtained from a core from a North Sea reservoir with a very low acidic number in the crude oil. This contradicted earlier experience with alkaline flooding which indicated a higher acidic number for the crude oil to be needed for these reactions to happen (Ehrlich and Wygal, 1977). Also, a presence of CO_2 in most petroleum reservoirs would act as a pH buffer making it very unlikely, if not impossible, for the pH to reach an “alkaline” value of 9-10.

This has led to the conclusion that while laboratory experiments can show an increased pH value during low salinity water flooding and thus pointing towards pH-altering as a key

mechanism, it is very unlikely that such an increase is sustainable in a petroleum reservoir due to the aforementioned CO_2-presence and proton buffering from oxides.

2.3 Field-testing of low-salinity water injection

While experiments with injection of low salinity brine on core samples may show promising results in regards to increased oil recovery it does not necessarily reflect the reality out in the field. Fluid flow can alter as an effect to fluid densities and gravitational forces. Low salinity water injection has therefore been performed in various field tests over the years, with varying results. Webb et al. (2004) performed a Log-Inject-Log test to observe the low salinity mechanics within the near-well region of a reservoir. The test was performed with varying salinities and was designed to ensure to minimize the cross flow and that the results were representative for the total reservoir displacement process. Multiple log passes were done for all the injected brines to ensure a stable saturation value. Their field test showed comparable results with previous laboratory experiments with a 25-50% reduction in residual oil saturation after waterflooding with low salinity brine.

In 2005, a hydraulic unit was converted to inject low salinity brine into an Alaskan reservoir to test how the MIE mechanism would scale up to an interwell distance (Lager et al., 2008). Within a well constrained area, one injector and two producing wells were selected, and a surveillance program was made to capture water samples of the produced water in regular intervals. Response of the low salinity water in the reservoir was confirmed by single well chemical tracer tests. Detailed analysis of the production data and ion analysis of produced water showed a direct field evidence of the effect on low salinity water injection. The results also showed to be consistent with the multi-component ionic exchange theory which was proposed to be the key mechanism in lowsal flooding.

Low salinity water injection was evaluated for increased oil recovery at the Snorre field in the North Sea (Skrettingland et al., 2010). Studies of samples from Statfjord and Lunde formations in the Snorre field had shown rock wettability as neutral to weakly water-wet with the Amott-Harvey index ranging from -0.2 to 0.4, which had shown to be favorable

conditions for the lowsal effect. They performed laboratory core flooding experiments at reservoir conditions and a single well chemical tracer test (SWCTT), in which they could measure the average residual oil saturation within a radius of 10.5 meters. Results from both laboratory measurement and the field test showed a low potential for increased recovery. This was due to the belief that the wetting conditions in the Snorre field were as close to optimal so that seawater brine is sufficient as a recovery method. The tertiary lowsal injection could at best improve recovery marginally.

3 Modeling in STARS

This thesis on reservoir simulation has utilized a simulator developed by the Computer Modeling Group (CMG) known as STARS, Thermal & Advanced Processes Reservoir Simulator. STARS is a thermal, k-value compositional, chemical reaction and geomechanics reservoir simulator in which one can perform advanced modeling of EOR processes with steam, air, solvents and other chemicals. Unlike the widely used reservoir simulator Eclipse100, STARS is a component-based simulator which gives an advantage with simulating chemical composition, temperature changes and dispersion. In STARS you can define your own components and their characteristics and also define how they react with one another. The STARS program also has a good graphical interface in the "Results 3D"-window which is useful when investigating simulations. As of the 2010-version of STARS there is no need for a star-prefix (*) in front of the keywords. Some keywords in the data files presented in the Appendix may include a prefix but this will not make any difference of the simulation outcome.

The following subchapters are focused on how STARS handles some of the processes occurring during waterflooding. These particular processes haven been chosen due to their relevance to this thesis.

3.1 Salt dispersion

Jerauld et al. (2006) states that the bulk of evidence provided by laboratory and field experiments suggests that all connate water is displaced by injecting water with a mixing of the two to some degree. On the other hand, some research has shown evidence that it is not a displacement of connate water, but rather diffusion being the driving force. Thus, the process may not be interpreted as a one-dimensional system with only displacement dispersion, but as a three-dimensional diffusion. Salter and Mohanty (1982) performed tracer floods on a Berea sandstone core in steady-state flow and history matched the results and found that the dispersivity tends to be larger in larger in multiphase flows than in a single-phase flow and thus concluding with that while the water is displaced, a significant amount of salt mixing occurs. They also found that the measured dispersion coefficient

increases almost linearly with velocity, therefore indicating that it is dispersion and not diffusion that governs the flow within a flowing wetting phase.

3.1.1 Dispersion in STARS

Dispersion is by definition a mixing of fluids caused by diffusion, local velocity gradients, heterogeneous streamline lengths, and mechanical mixing (Lake, 1989). The salt in a brine is also dispersed in the continuous water-phase. However, when modelling multiphase flow on a reservoir scale it can sometimes prove useful to alter the specific distinction between the components and the phases. Especially when dealing with surfactants which tend to stabilize smaller dispersion of one phase in another. A surfactant-like component will therefore usually have the same equilibrium properties (such as molecular weight and density) as the true component in which it consists, but the flow-related properties, such as viscosity and resistance factor, will differ substantially.

Dispersion of a component within another, for example salt in the aqueous phase, can in simulations be observed in two ways: numerical dispersion and physical dispersion. The numerical dispersion is a result of calculations performed by the simulator where, in this example, the salt front will “smear out” and develop to a mixing zone with a progressively decreasing salt concentration. Even in uniform reservoirs and simple 1-D core sample simulations, numerical dispersion could affect the simulation results.

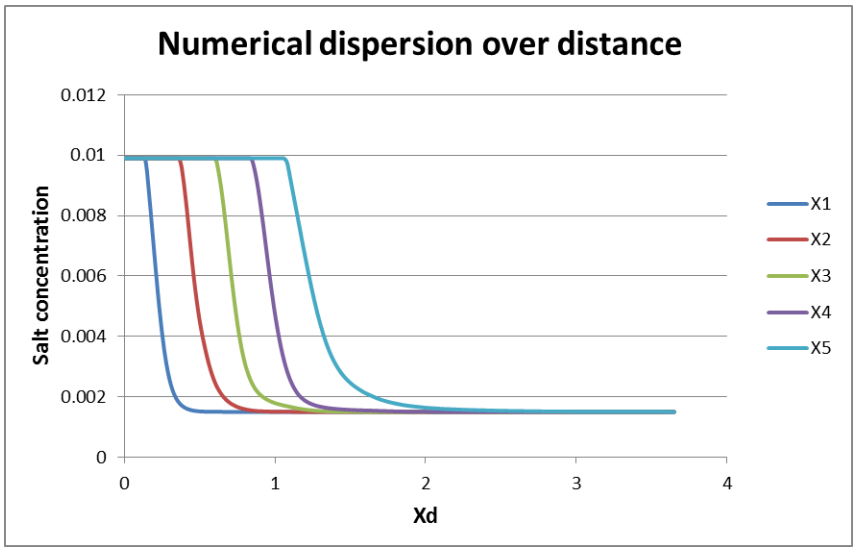

Figure 3-1: *Numerical dispersion of salt in a series of blocks in increasing distance from injector.*

Figure 3-1 shows an example of an expanding mixing zone throughout a core. The graphs X1-X5 represent the salt concentration over dimensionless time in single grid cells placed in an increasing distance from the injector. The further away from the injector, the larger the mixing zone gets as it takes an increasing time for the concentration to reach a minimum level as the salt progresses through cells X1-X5. In other words, the dispersion increases with traveled distance.

Numerical dispersion is greatly dependent on the grid block size and one could minimize the effect by reducing the individual block sizes and increasing the total number of cells, thus making the calculations smaller and reducing the margin of error. A decrease in the block size will therefore result in a decrease of the mixing zone, as illustrated in Figure 3-2.

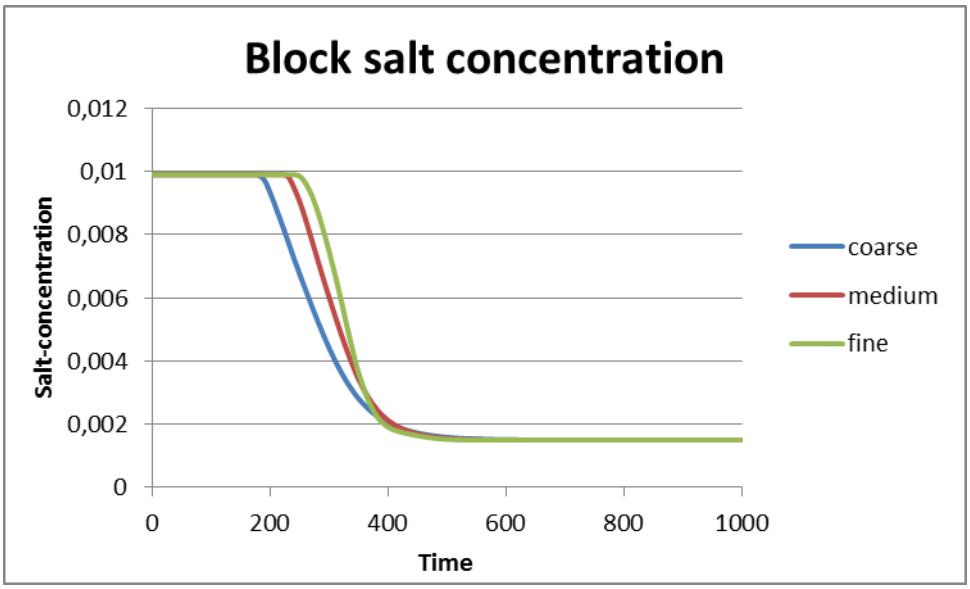

Figure 3-2: *Example of how grid block sizes affects the numerical dispersion of salt in a single grid block over time.*

In Figure 3-2, the grid block sizes have been altered and the total number of grid cells has increased. The graphs are taken from a single grid block located at an equal distance from the injector. One can see that for the finer models the curves have a sharper decrease in salt concentration over time, indicating a smaller mixing zone. A decrease in block size will also delay the progress of the salt as there are more cells to go through, even though they are smaller in size.

STARS have several keywords available to define dispersivity in a system. The keywords *DISPI/*DISPJ/*DISPK allows the user to define the total dispersion coefficients in all 3 dimensions for user-defined components in all 3 phases (gas, oil, liquid). Total dispersion consists of both the effective molecular diffusion and mechanical dispersion. Molecular diffusion is component and phase dependent while the mechanical dispersion is a property of the reservoir rock. In simulation in STARS, the total dispersion input can be viewed as the true physical dispersion coefficient minus the numerical dispersion caused by truncation error, which is a limiting of number digits in equations. Dispersion could be effected by transmissibility multipliers between grid blocks.

3.1.2 Dispersion from lab- to field scale

For one-dimensional flow, as often viewed in core modeling, the longitudinal dispersion coefficient K_l is given by:

$$\frac{K_l}{D_0} = C_1 + C_2 * \left(\frac{|v| * D_p}{D_0}\right)^{\beta} \quad (3.1.1)$$

Where $C_1, C_2,$ and β are properties of the medium, D_p is the particle diameter, and D_0 is the effective binary molecular diffusion. According to (Lake, 1989) it has been experimentally shown that β is usually equal to 1 and with velocities larger than 3 cm/day, which most fluid velocities are on reservoir scale, the latter mixing term in equation (3.3.1) dominates the first term, giving:

$$K_l = \frac{D_0}{\varphi F} + C_2 \left(\frac{|v| D_p}{D_0}\right)^{\beta} * D_0 \cong \alpha_l |v| \quad (3.1.2)$$

Where α_l is longitudinal dispersivity of the medium, a measure of the local heterogeneity scale, classified by (Bear, 1972) as a fundamental property of the medium. The rock property C_1 has been found to be 1/φF, F being the electrical formation resistivity factor. The molecular diffusion will in eq. (3.1.2) be negligible due to the high velocity.

Equation (3.1.2) has shown to be convenient as one now can combine the Peclet number (3.1.3) and dimensionless concentration balance (3.4.4) to become independent of velocity, and thus relate the mixing zone directly to the dispersivity α_l:

Peclet number:

$$N_{Pe} = \frac{uL}{\varphi K_l} \quad (3.1.3)$$

u is fluid velocity, L is length of core sample.

Dimensionless concentration balance:

$$\frac{\delta C}{\delta t_D} + \frac{\delta C}{\delta x_D} - \frac{1}{N_{Pe}} * \frac{\delta^2 C^2}{\delta x_D^2} = 0 \quad (3.1.4)$$

X_D and t_D are the dimensionless values for distance and time, and C is mass concentration.

Giving:

$$N_{Pe} = \frac{L}{\alpha_l} \quad (3.1.5)$$

Where one now can define the inverse Peclet number $\frac{\alpha_l}{L}$ as the dimensionless mixing zone length. If one should assume that a laboratory core should have the same dimensionless mixing zone as in a field, the equality states that:

$$\left(\frac{\alpha_l}{L}\right)_{lab} = \left(\frac{\alpha_l}{L}\right)_{field} \quad (3.1.6)$$

This equation cannot be satisfied if the dispersivity is equal, due to the vast difference in longitudinal length. Therefore, the dispersivity must increase accordingly. (Arya et al., 1988) presented in their paper a collection of measured dispersivity at both laboratory and field scale. They gathered the data in a log-log plot of the measured dispersivity over total length.

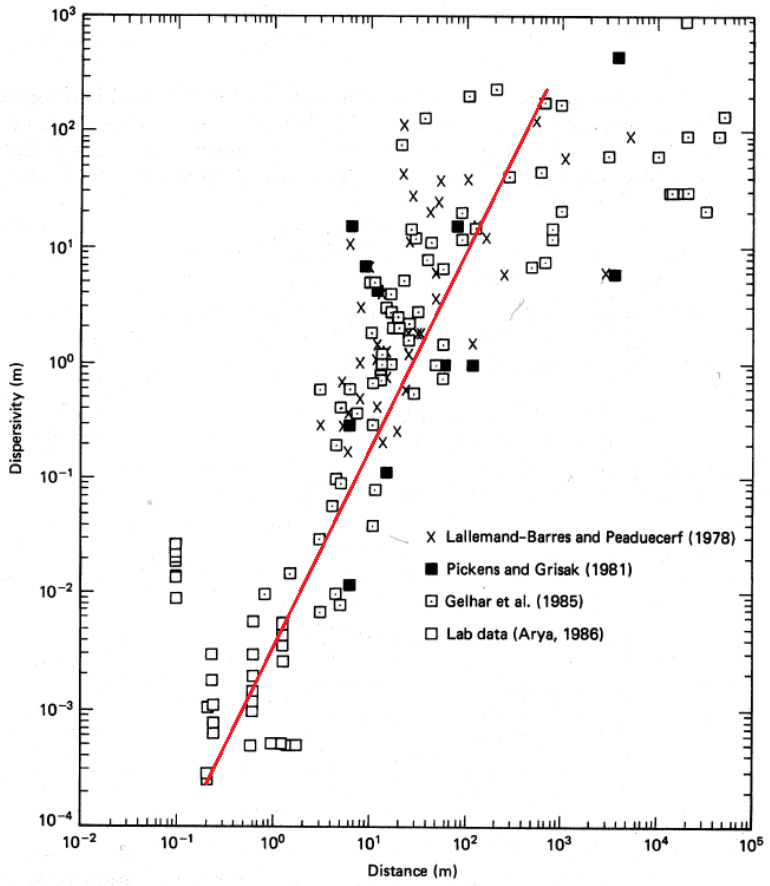

Figure 3-3: *Log-log plot of laboratory and field measurements of dispersivity in porous media. Plot taken from Lake (1989).*

As seen in Figure 3-3, there is a big variation in α_l both at same lengths and formations. Despite this scattering one can clearly see that there is a correlation between the measured dispersivity and the length scale, with an almost linear relationship (red line). This could be explained by stating that the heterogeneity causing the dispersion increases by an increased volume sample.

3.2 Interpolation of relative permeability

Under certain circumstances such as miscible fluids or surfactant concentration changes, will the assumption that rock-fluid properties are only a function of fluid saturations and saturation histories be insufficient. STARS is flexible in regards to a choice in the interpolating parameter, where one can also choose to interpolate as a function of concentration or the capillary number. Should one choose to interpolate using the capillary number, a table including the composition and interfacial tension for the given interpolation component is required, using the *IFTTABLE keyword.

Keyword *INTCOMP indicates which component one chooses to interpolate with, and in which phase it exists. In regards to low-salinity simulation, the interpolation would be based on concentration. Two sets of relative permeability curves will then be given by the *SWT/*SLT keywords, each concerning the high and low salinity concentrations in the brine. This will induce a wettability change as the S_{or} will be lower for the low salinity curve. According to STARS` user`s manual (Ltd., 2012), the relative permeabilities of the water and oleic phase will be interpolated as:

$$kr_w = (wtr) * k_{rw}^{LS} + (1 - wtr) * k_{rw}^{HS} \quad (3.2.1)$$

$$k_{ro} = (oil) * k_{ro}^{LS} + (1 - oil) * k_{ro}^{HS} \quad (3.2.2)$$

Where

$$wtr = ratw^{WCRV} \quad (3.2.3a)$$

$$oil = ratn^{OCRV} \quad (3.2.3b)$$

WCRV and OCRV are additional flexibility parameters should the experimental evidence require it. The *ratw* and *ratn* are the dimensionless interpolation parameters between 0 and 1. They are an indicator on which relative permeability curve is the most dominant at the current timestep, and are given by:

$$ratw = \frac{\log_{10}(N_c) - DTRAPWA}{DTRAPWB - DTRAPWA} \quad (3.2.4a)$$

$$ratn = \frac{\log_{10}(N_c) - DTRAPNA}{DTRAPNB - DTRAPNA} \quad (3.2.4b)$$

N_c is the capillary number, and DTRAPW and DTRAPN are the values for the wetting and non-wetting phase interpolation parameters. The capillary number will be neglected for the simulations in this thesis. At least one of these keywords must be present in order to achieve an interpolation between two sets of relative permeability curves. They could also be equal.

When describing phenomena such as multiple rock types and interpolation of curves based on fluid compositions one may require multiple sets of rock-fluid data. The keyword *RPT allows defining of different rock types in which interpolation may act differently. For each rock type it is possible to define specific interpolation schemes using the keyword for the interpolation set designator, *KRINTRP. An example of this could be as follows:

ROCK TYPE 1: Rock type designator (*RPT)

- Interpolation Definition (*INTCOMP)
- Interpolation Set #1
  - Interpolation Set designator (*KRINTRP)
  - Interpolation parameters (*DTRAPW/*DTRAPN)
  - Relative permeability data (*SWT/*SLT)
- Interpolation Set #2
  - Interpolation Set designator (*KRINTRP)
  - Interpolation parameters (*DTRAPW/*DTRAPN)
  - Relative permeability data (*SWT/*SLT)

ROCK TYPE 2: Rock type designator (*RPT)

- Relative permeability data (*SWT/*SLT)

In this scenario, rock type 1 would interpolate between the two sets while in rock type 2 no interpolation occurs. This allows for a more specific definition of the processes occurring with a core sample or a reservoir. In this thesis, the simulations done in STARS will use the 'NaCl' concentration as the interpolation component.

3.3 Viscosity mixing

In regards to low salinity injection, the water phase viscosity would be dependent on the salt concentration in the water. The default setting for this is a linear relationship between concentration and viscosity. For linear-log mixing, STARS uses the formula

$$\ln \mu = \sum_i^n x_i \ln \mu_i \qquad (3.3.1)$$

in calculation of the phase viscosity. X_i is mole/mass fraction of each component, and $\mu_i$is the pure-component viscosity.

If one should have a reason to believe there is non-linear mixing occurring in the system one needs to specify the components into two groups: those that are key components specified in keyword *VSMIXCOMP, and those that are not. The key components will be known as group S.

Keyword *VSMIXENDP contains the abscissas corresponding to the first and last table entries, and *VSMIXFUNC consists of the 11 table entries that define the nonlinear mixing rule function. These table entries are found by

$$f_a(x_a) = \frac{\ln \mu - M}{\ln \mu_a - M} \qquad (3.3.2)$$

Where

$$M = [\sum_{i \neq S}^n x_i \ln \mu_i]/(1 - x_a) \qquad (3.3.3)$$

"a" is the key component specified by keyword VSMIXCOMP.

3.4 Reservoir pressure

In the “initial conditions” region in the data file the initial reservoir pressure is determined through keyword *REFPRES. One may also include the keyword *VERTICAL *DEPTH_AVE to enable the simulator to calculate a vertical equilibrium using a capillary-gravity method. In the initialization of the reservoir, STARS then builds a table of phase pressure versus depth using the rock-fluid data specified earlier in the data file. This results in an increasing pressure as a function of depth in the reservoir due to overlying rock and fluids.

Pressure in STARS is based on conservation equations, and the grid block size should therefore not affect the overall pressure results. Should a smaller grid block size result in a difference, either in average reservoir pressure or the pressure difference between the wells, the production results would most likely be affected.

The bottom-hole pressure is calculated in a fully coupled manner, meaning that if the well is perforated in more than one layer, all perforations would be accounted for. An average will therefore be calculated.

3.5 Computational concerns

Simulating on a field- or reservoir scale can require a substantial amount of computing memory depending on the size of the reservoir, number of components and grid blocks, grid block sizes, and the timestep sizes. An altering of these will have a large impact on simulation runtime and the data file sizes, which could make storage space an issue. The main-result file (xxx.mrf) makes up for the most of this storage and contains all the information in each individual grid block. One could choose to exclude this file from the output-files, but a viewing of the reservoir in the “Results 3D”-window would then not be possible.

A summary of each simulation timestep (xxx.log) is written for each simulation. This log includes the number of Newton iterations required to solve the non-linear timestep problem and the number of convergence failures (timestep cuts). Depending on the input in the simulator the results can be poor due to various reasons, however there are several

methods for diagnosing a poor numerical performance of a simulation. These methods are discussed in the following chapters.

3.5.1 Timestep size

The keyword *NORM specifies typical changes in the basic variables during a timestep, and these changes are used for an automatic time-step selection. The timestep size is calculated using the following equation:

$$T^{N+1} = T^{N} * \frac{1.75*DNORM(I)}{D(I)^{N}_{MAX}+0.75*DNORM(I)} \quad (3.5.1)$$

Where $D(I)^{N}_{MAX}$ is the maximum change in each variable during the previous timestep.

The timestep size is determined by maximum changes from previous timestep compared to the value assigned in *NORM, the maximum timestep size determined in keyword *DTMAX, or smaller timesteps due to frequent convergence failures which results in timestep-cutting. Each cut reduces the timestep by a factor, ($^{1}/_{2}$ first try, $^{1}/_{3}$ the second try etc.). According to the STARS manual, it is not recommended to reduce *DTMAX as a tool to reduce number of timestep cuts as it merely masks the real cause of a problem instead of fixing it. However, experiences with the convergence problems presented in chapter 8 showed a great improvement of results when reducing maximum timestep size, thus contradicting the advice from the manual.

A certain amount of timestep-cuts can be tolerated, but should cuts occur every 1 to 3 timestep, the cause of the cuts needs to be investigated

3.5.2 Material balance error

The cumulative material balance error is reported for each timestep in the log file and increases smoothly as the run progresses. A final error between 0.1-1% indicates that the convergence is under control. A final material balance error greater than 5% is considered large and should be dealt with. These errors could have several causes:

- Too large convergence tolerances
- Insufficient accuracy of iterative matrix solution
- Erroneous matrix solutions

Convergence tolerances can be handled by the *CONVERGE *TOTRES keyword, in which one check the convergence by comparing scaled equation residuals for each equation with the specified tolerances, both on a grid-average and per-block basis. The tolerance values are found in Table 3-1.

Table 3-1: *Tolerance-values in convergence-checking. Table taken from STARS manual (2012).*

Form	Value used
***TOTRES x**	Specified value
***TOTRES *LOOSER**	1.0e-1
***TOTRES *LOOSE**	1.0e-2
***TOTRES *NORMAL**	1.0e-3
***TOTRES *TIGHT**	1.0e-4
***TOTRES *TIGHTER**	1.0e-5

A reduction in the tolerance value will result in a smaller material balance error at the cost of more iterations, which in turn results in a longer simulation runtime.

3.5.3 Matrix Solver Failure

The matrix solver has several convergence criteria which return with a “failed” flag should they be violated. The matrix solution “fails” when the residual equation does not converge to a value within 10^{-6} (STARS default value). Like the convergence for the material balance, a few failures in the matrix solver is acceptable, but more than one matrix solver failure for every 5-10 Newton iterations is too much. A message will also be written in the log file when more than half of a timestep`s Newton iterations experience a matrix solver failure. They keyword *ITERMAX controls the maximum number of inner iterations allowed to be solved to reach convergence. In general, simulations in reservoirs with somewhat uniform grid and reservoir properties should have little to no matrix failures. But larger and more complex grids need larger *ITERMAX values to avoid matrix solver failures. One may in addition use the *NORTH keyword, to increase the maximum number of orthogonalizations to be performed before the resetting of the iterative solution method.

4 Experimental history matching

In 2011, Gro Kallevik published her master`s thesis "Implementations of Methods for Modeling Low Salinity Waterflood and Low Salinity Surfactant Flooding", where she used the UTCHEM and Eclipse100 simulators to history match waterflood and hybrid EOR experiments done at the Centre for Integrated Petroleum Research by Skauge et al. in 2009. This thesis is based on some of her work on the B7 core with a focus on an upscaling of the core sample to field size. In order to accomplish this, a history matching on the B7 core of the production and pressure curves must first be achieved using the CMG STARS simulator utilized in this thesis. In this history matching of the B7 waterflood experiment, only 3 components were utilized: 'WATER', 'NaCl' and 'DEAD OIL'. Interpolation is based on the concentration of 'NaCl'.

4.1 Core properties

The experiment presented in the paper was performed on cylindrical cores cut from the same block of Berea sandstone. The properties of the B7 core from said experiment are shown in table 4.1:

Table 4-1: *Properties of the B7 core sample presented in "Simulation of Combined Low Salinity Brine and Surfactant Flooding", Skauge et al., 2011.*

Core	Length [cm]	Diameter [cm]	Porosity [%]	PV [mL]	S_{wi}	S_{oi}	$Abs\ K_w$ [mD]	K_o, S_{wi} [mD]
B7	7.95	3.72	25	21.56	0.234	0.766	585.5	700.3

Synthetic sea water, hereafter abbreviated as HS, with a salinity of 36 000 ppm was used as the connate water and the low salinity water, abbreviated as LS, had a concentration of 0.5 wt% NaCl. The oil used was a filtered stock tank crude oil from a North Sea reservoir with a viscosity of 13.8 cP at room temperature (20℃). The B7 core was first flooded with 6.5 pore

volumes of HS water, and thereafter 11 pore volumes of LS water. The following chapters contain a brief description on how the history matching was done.

4.2 Correlation

There is only a certain amount of data one can measure during an experiment. The endpoint relative permeabilities $K_{ro,swi}$ and $K_{rw,sor}$, and the water saturation,S_w, are some of them. $K_{rw,sor}$ and the residual oil saturation S_{or} hold some uncertainties due to capillary end-effects, but this has been disregarded in this thesis. In order to simulate the increased recovery, one must generate relative permeability curves for both the highsal and lowsal water, using the endpoint relative permeabilities as starting points. The LET-correlation (Lomeland et al., 2005)has been utilized for the generation of the relative permeability curves, and are given as:

$$k_{rw=}k_{rw}^{0} * \frac{(S_w^*)^{Lw}}{(S_w^*)^{Lw}+E_w*(1-S_w^*)^{Tw}} \quad (4.2.1)$$

$$k_{ro} = k_{ro}^{0} * \frac{(S_w^*)^{Lo}}{(1-S_w^*)^{Lo}+E_o*(1-S_w^*)^{To}} \quad (4.2.2)$$

Where S_w^* is the normalized water saturation given as

$$S_w^* = \frac{S_w-S_{wi}}{1-S_{wi}-S_{or}} \quad (4.2.3)$$

k_{rw}^{0} and k_{ro}^{0} are endpoint relative permeabilities of oil and water and the parameters L, E and T are empirical values describing the curve. L describes the lower part of the kurve, T the upper part of the curve, and E is the elevation of the slope.

Utilizing the LET-method has its advantages compared to the Corey-correlation (Corey, 1954) in regards to history matching, as it contains more parameters, thus making it easier to adjust the relative permeability curves to match both pressure and production.

4.3 Best match

To achieve a history matching of the B7 core, adjustments had to be made to the relative permeability curves for both highsal and lowsal water. The endpoint relative permeability values were given from the experimental results but the residual oil saturation and the curvature of the relative permeability curves were adjusted. The water relative permeability has largest effect on the differential pressure measured through the core while adjusting the oil relative permeability curve will mostly affect the oil production. The relative permeability curves that produced the best results are shown in Figure 4-1.

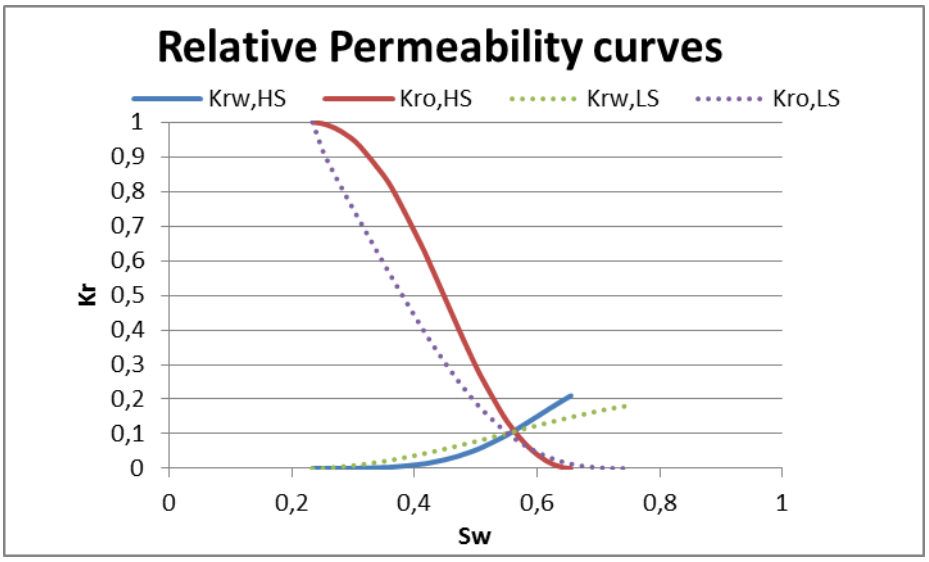

Figure 4-1: *Relative permeability curves which produced the best history match of the B7 core.*

In order to obtain a match, S_{or} was lowered and the shape of the oil curve for HS was adjusted. These changes were made in order to match the sharp curvature of the oil production curve at water breakthrough, which resulted in the S-shaped oil permeability curve. An increase of crossover saturation, the saturation at which the relative permeability curves of oil and water is equal, is by some considered an indication of a wettability change in the system (Craig, 1971), but this is not a certainty.

A history match of a waterflood production experiment does not necessarily have only one "answer", in regards to relative permeability curves. History matching of the B7 core provided a second match with an alternate set of relative permeability curves, shown in

Figure 4-2. However, the relative permeability curve for the LS water shows an unrealistic curvature which would make the interpolation between the curves in this set erroneous.

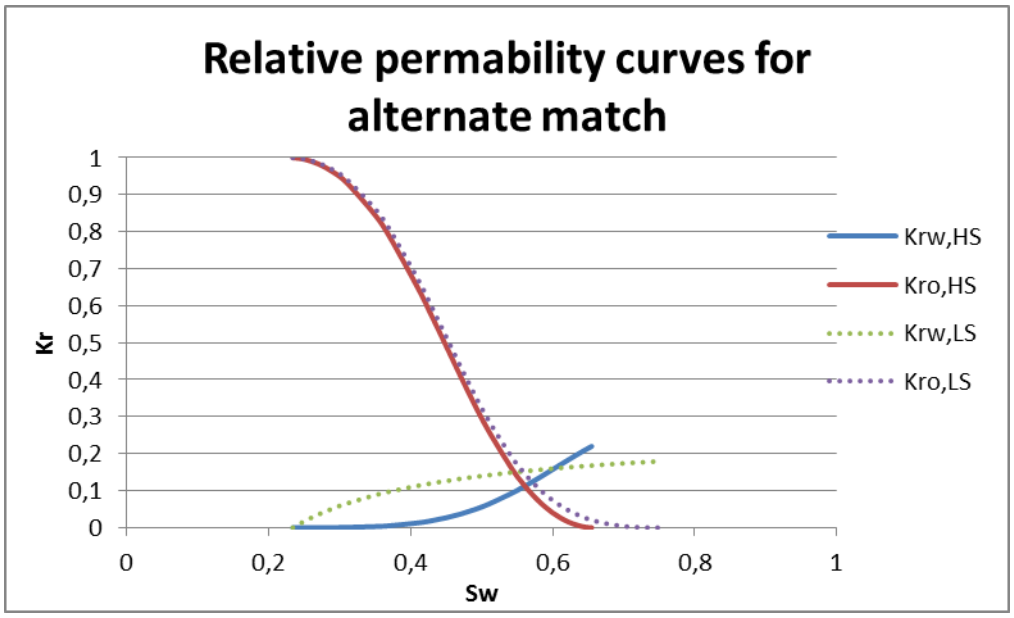

Figure 4-2: *Alternate set of relative permeability curves which also produced a history match for the B7 core.*

The reason why the set in Figure 4-2 produced a match is because of the saturation region of which we experience an interpolation in this experiment. Since it was injected around 6.5 pore volumes of HS water before the LS injection started, the saturation has almost reached S_{or} for HS, and therefore interpolation from the HS to LS curves only occurs in the region above that saturation. Therefore it does not prove to be a problem in this simulation model. However, since this thesis focuses on upscaling to field modeling, utilizing the curves in Figure 4-2 on a field scale, especially if initial water injection was LS water, would produce erroneous results due to the coarse interpolation of the water curves.

History match of the B7 core sample is shown in Figure 4-3.

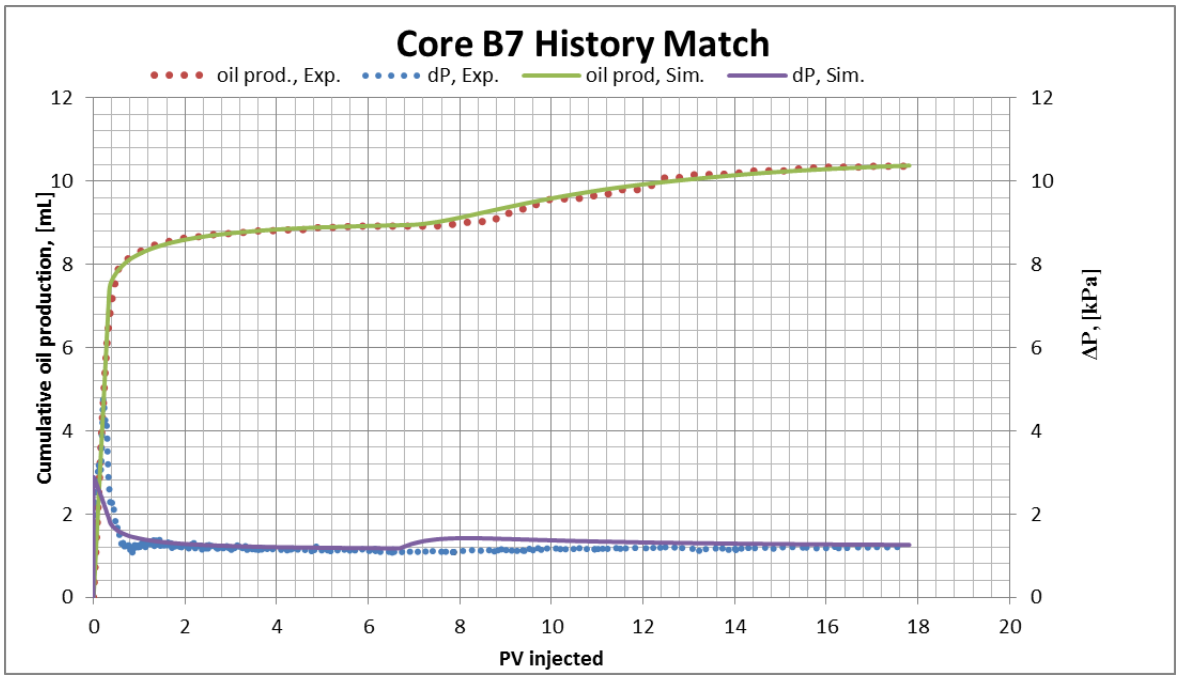

Figure 4-3: *Best-fit history match of the B7 core achieved.*

The production curve shows an accurate match in the initial HS injection part, with both the total production endpoint and the curvature at water breakthrough on-point. The Low salinity injection part shows a slight increase of production ahead of the experimental data but from 12 PV injected they are fairly the same, with a matching endpoint production.

The differential pressure is harder to match, as it is challenging to both match the peak at the initial part of production as well as the plateau level after water breakthrough. A compromise had to be made, as it is hard to adjust the peak value of the differential pressure without affecting curvature of the oil curve. The plateau level after water breakthrough was prioritized and the initial pressure peak is therefore lower. A small bump can be seen at start of the LS injection. This is due to the reduced mobility of the water from HS to LS (See Figure 4-1). One can compensate this by increasing mobility of the oil accordingly and thus maintaining total mobility of the fluids, but this was also restricted by the wish to maintain a match in the oil production curve. Attempts were made to minimize this “pressure bump” and the best match is found in Figure 4-3.

4.4 Results and discussion

Initial waterflooding of the core with ~6.7 PV of high-salinity brine resulted in a recovery of about 54% of OIP. Additional injection of ~11.3 PV of low-salinity brine increased cumulative production with 8.7%, resulting in a total recovery of 62.7%.

Upon simulation of a core waterflooding, water saturation in cells near the injector increases first. The increase is also more rapid, and it takes a larger injection volume for cells further away from the injector to reach an equal saturation. Water saturation in three cells throughout the core is shown in Figure 4-4, and one can see that for both highsal and lowsal injection cell 30, which is closest to injector, increases more rapid. Total number of cells in the core is 120. After lowsal injection initiates there is a small decrease in water saturation which is caused by a small oil bank of liberated oil upon interpolation between relperm curves. At injection end there is a small difference in end water saturation between the cells.

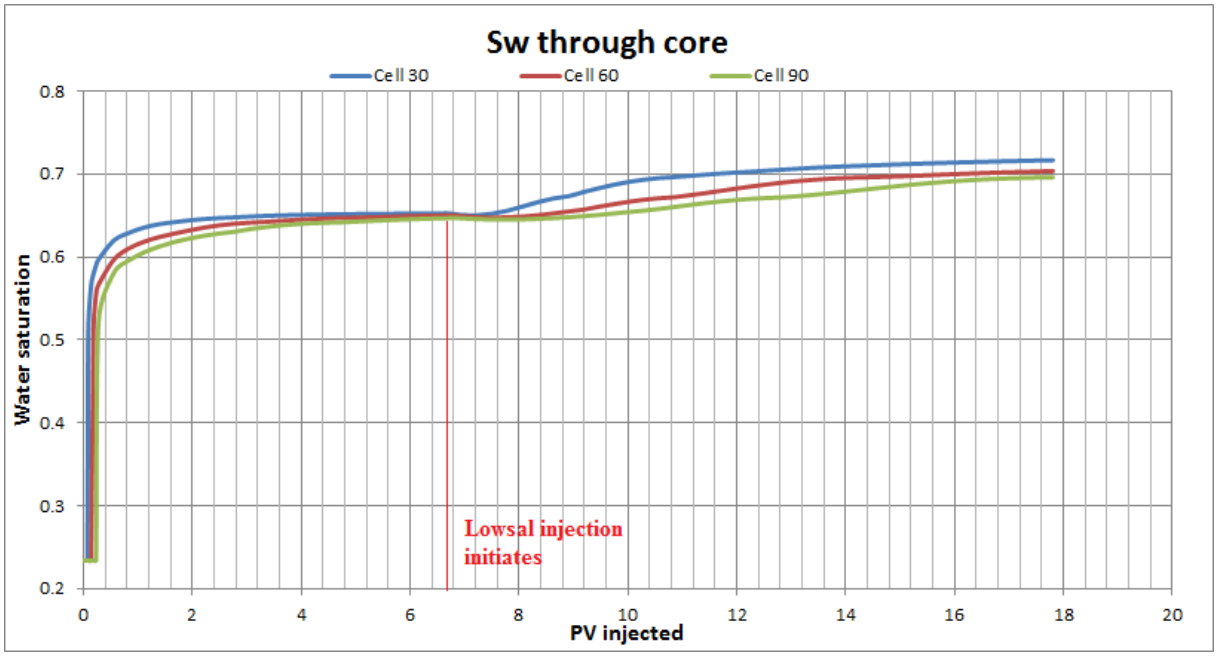

Figure 4-4: *Water saturation in cells throughout B7 core.*

The increased recovery is due to interpolation with NaCl-concentration between the relperm curves shown in Figure 4-1, where the low-salinity curve has a lower S_{or}. Interpolation between highsal and lowsal water is purely dependent on the NaCl-concentration, and so the dispersion of salt is important for the recovery process. Figure 4-5 shows how the salt mixing zone gets larger as it travels through the core, since it requires a larger amount of PV injected for the further cells to reach lowsal concentration.

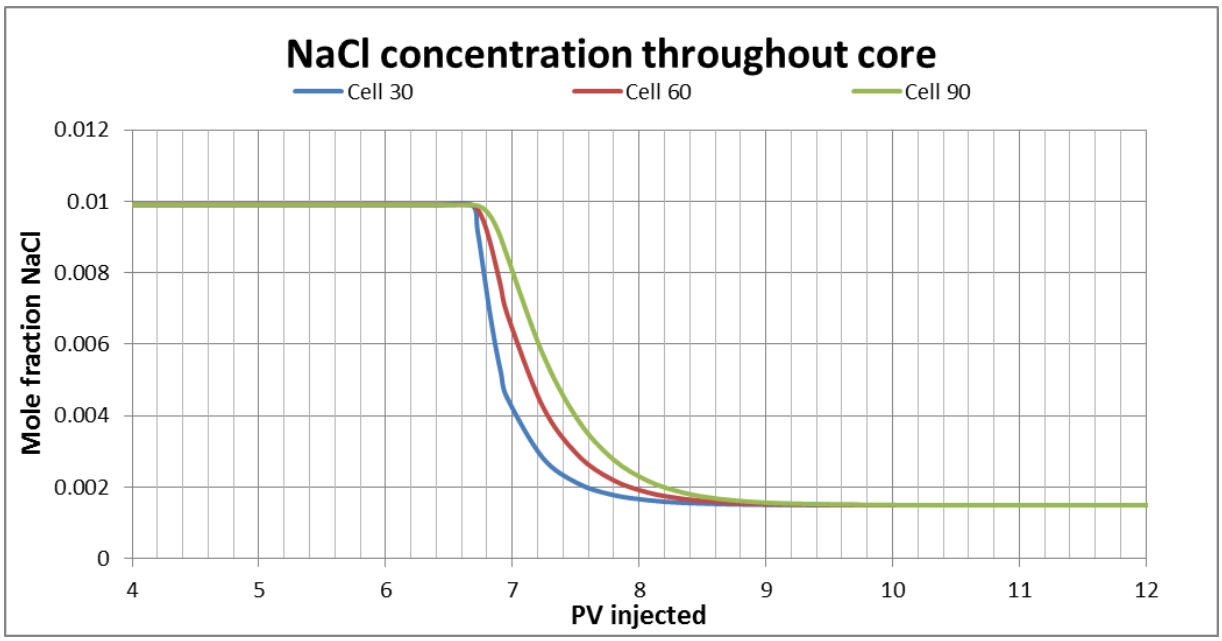

Figure 4-5: *Salt concentration in selected cells through B7 core.*

After lowsal injection starts a decrease in salinity of the produced brine can be observed after only 0.1 PV injected. From Figure 4-5 we see that cell 30 does not reach the lowsal concentration of 0.0015 NaCl until after 1.5 PV lowsal brine injected, indicating a salt mixing zone through the core. Figure 4-6 shows how the NaCl-concentration varies over time after lowsal injection starts at 1440 minutes.

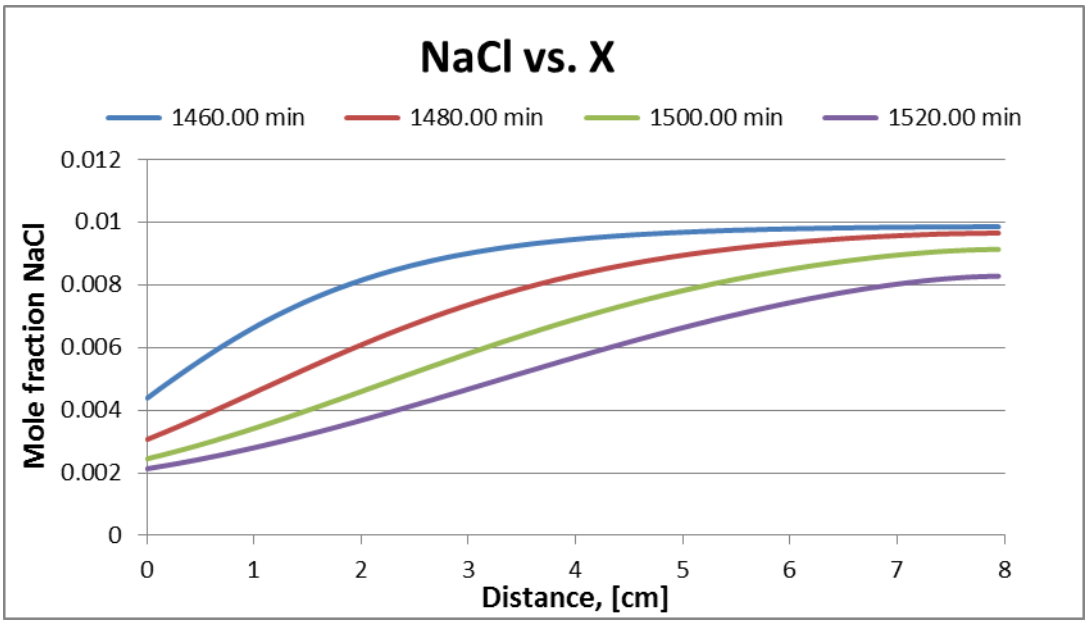

Figure 4-6: *Salt concentration profile as function of distance, for different timesteps.*

Before lowsal injection initiates, the core is filled with highsal water with a saturation close to $S_{w,sor}$. The salt in the lowsal brine mixes with the higher concentration of salt already present in the core, thus creating a mixing zone of salt. This mixing zone stretches through the whole core, as seen in Figure 4-6 where after 1520 minutes all cells have a salt concentration between highsal and lowsal.

A slower decrease in NaCl-concentration leads to a longer interpolation period in which the relative permeabilities of oil and water change accordingly to the relperm curves utilized for the low-salinity brine. Figure 4-7 shows how the relative permeabilities are affected when NaCl enters a grid block. At the exact moment when lowsal brine enters the cell, there is a clear decrease in the water relperm while the oil permeability slightly increases. This behavior is a direct consequence of the interpolation between the relperm curves. It also shows that the water saturation in that cell is close to $S_{w,sor}$. If the water saturation had been lower, say 0.4, one would have observed an inverse reaction in the relperm curves, with an increase in water relperm and decrease in oil relperm. This is due to the specific curvature of the curves utilized.

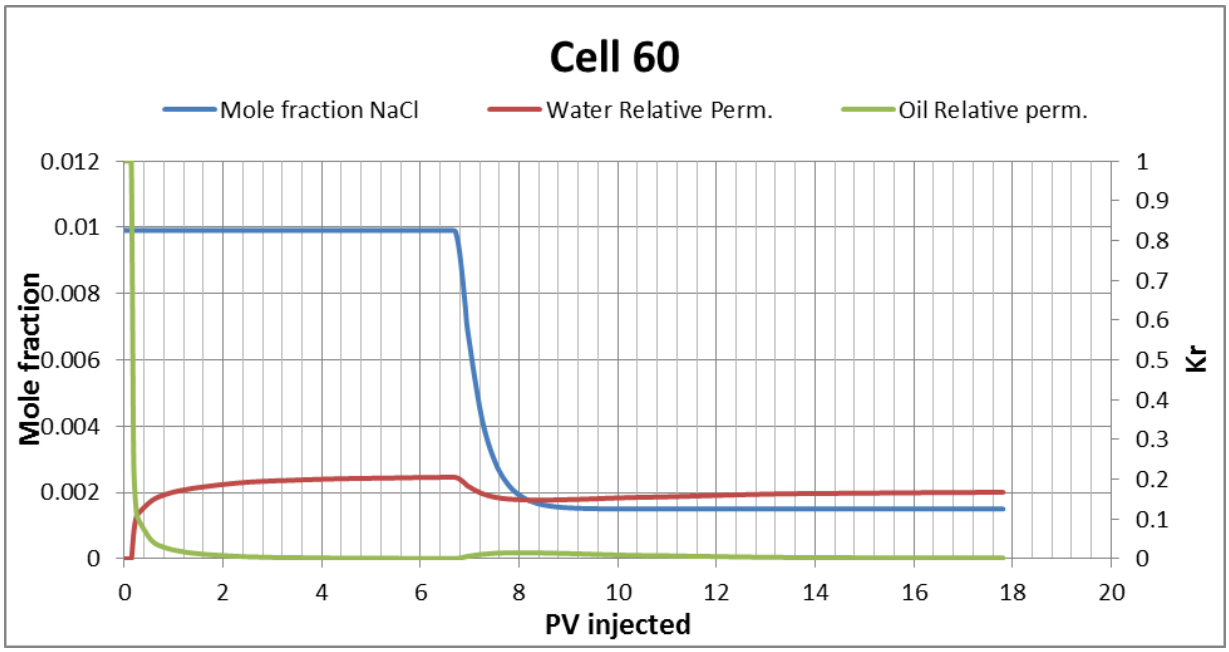

Figure 4-7: *Mole fraction NaCl and relative permeabilities of oil and water in center cell.*

An increase in the oil relative permeability upon a lowering of salinity allows additional oil to flow to be produced. The decrease in water relperm is also the main reason for the increased pressure difference at start of lowsal injection after ~6.7 PV.

5 Reservoir simulation

When upscaling from a core sample scale to reservoir scale there are several things to take into consideration. Firstly, the computational power needed (see chapter 3.4) could become an issue, depending on the number of components and grid blocks. Liu (2001) argues that for compositional modeling one must reduce the number of components included as a prerequisite step in order to achieve an optimal simulation run. Secondly, component properties such as densities and viscosities may play a bigger part in the simulations as the flow is now three-dimensional. Gravitational forces are usually neglected in lab core simulations while cross-flow between layers as a result of density differences are often observed in reservoir simulations. A sensitivity analysis of rock-fluid properties can be found in chapter 6.2. Thirdly, reservoir conditions such as pressure and temperature may alter some of the fluid properties and must therefore be taken into consideration.

The simulation results presented in the following chapters are done in fictive, rectangular reservoirs with and end-to-end displacement of the oil. Although the simulations presented are in field-size, the extents of the simulations are not representable of real-life oil reservoirs in regards to recovery strategies. The simulations are based on highsal/lowsal injection with a focus on how the increased recovery mechanism reacts to the varying grid resolutions, in two different reservoirs; a homogeneous reservoir with no flow obstructions, and a heterogeneous reservoir with two low-permeable regions. A polymer injection will also be carried out in the heterogeneous reservoir, to see how the viscous change will affect the waterflooding. Furthermore, the reservoir processes are simplified with a neglection of the capillary pressure.

5.1 Initial conditions

The two reservoirs are located at 1500m meters below the seafloor with an initial pressure at 400bar and a temperature at 75° C. The temperature in the reservoirs is kept constant to keep the number of variables in the simulations at a minimum. The high temperature negates the viscosity alternation low-salinity water would have compared to laboratory experiments. The water phase viscosity is therefore equal for both highsal and lowsal water. The two reservoirs represent two cases; a homogeneous reservoir with no obstruction of

fluid flow, and a heterogeneous reservoir with two low-permeable regions. The vertical permeability is 200mD, 10% of the horizontal permeability of 2000 mD. This enables for a cross-flow between the layers and allows us to see the gravitational effects on both fluid displacement and salt dispersion. All blocks are filled with an initial water saturation is 0.234, whereas the NaCl-mole fraction is 0.0099. The porosity for all cells is 0.25. Component properties with the corresponding keywords can be found in Table 5-1.

Table 5-1: *Properties of the 3 components included in the simulations presented in this thesis.*

Component	CMM, molecular mass [kg/gmol]	MASSDEN, component densities [kg/m^3]	AVISC, component viscosities [Cp]
Water	0.018	1000	0.5
NaCl	0.058	2165	0.5
Oil	0.4	750	8

As seen in Table 5-1, the oil utilized is a “dead oil” (no gas content) with a high viscosity at 13.8 cP. The viscosities of the water and salt are equal because of the salt being dispersed in the water phase. The viscosity of both water and oil are lower than the ones used in the history match with the B7 core due to a higher temperature, 20℃ -> 75℃. The density difference between water and oil will show an effect in the fluid-flow pattern, where the water will displace the oil both horizontally and vertically.

Since NaCl is dispersed in the water phase, it is common to define *MASSDEN of NaCl to be equal to the water phase value of 1000 $^{kg}/_{m^3}$. However, the density values for highsal- and lowsal brine utilized in Gro Kalleviks master`s thesis (Kallevik, 2010) vary with a different salt concentration. A MASSDEN of 2165 $^{kg}/_{m^3}$ is the chemical density for NaCl in dry powder form, but also happens to fit well with the densities of 1025 $^{kg}/_{m^3}$ for high-salinity brine and

1002 $^{kg}/_{m^3}$ for low-salinity brine. Changing MASSDEN of NaCl to 1000 would not make any significant difference to the presented simulations in this thesis.

All simulations have been run with *ITERMAX and *NORTH values of 300 (See chapter 3.4) to ensure a minimum of matrix solver failures and iterative solution errors. This high value may be considered unnecessary for the coarser models but it was considered preferable to be on the safe side and therefore minimize the risk of errors.

5.2 Grid sizes

The simulations presented in this thesis have all been run with 3 different grid block sizes, while maintaining the total dimensions of the reservoir as 2000m*280m*40m. See Table 5-2 for details.

Table 5-2: *Summary of the grid block dimensions in the simulations.*

	nx	dx [m]	ny	dy [m]	nz	dz [m]	# Grid blocks	Reservoir volume $[m^3]$
Coarse res.	50	40	7	40	20	2	7000	$\mathbf{2.24*10^7}$
Medium res.	100	20	14	20	20	2	28000	$\mathbf{2.24*10^7}$
Fine res.	200	10	28	10	20	2	112000	$\mathbf{2.24*10^7}$

As seen in Table 5-2, the cell count doubles in the horizontal directions for each new grid resolution. The vertical resolution of the grid was decided to remain constant throughout the simulations, due to changes in the vertical resolution proved to alter the flow patterns of the oil and water significantly. This would specifically have an impact on the heterogeneous simulations with low-permeable zones where a finer layering of the reservoir would affect the vertical flow.

5.3 Injection/Production schemes

The injection rate has been chosen to be 10% of reservoir PV each year, with the rate calculated using the following formula:

$$\frac{Total\ reservoir\ volume * Porosity}{10\% * 365 days} = \frac{2.24 * 10^7 m^3 * 0.25}{10 * 365 days} = 1534{,}25\ \frac{m^3}{days} \qquad (5.3.1)$$

The production rate was therefore set to be 1534 $^{m^3}/_{day}$, and the injection rate of water to be a bit less, 1500 $^{m^3}/_{day}$, because of the water being defined as incompressible and the injected water would therefore have a larger volume at reservoir conditions than the oil. Most of the simulations will therefore run over a 10 year period, injecting a total of 1 PV. It is recommended that the producer should be operated under several constraints, with both a maximum oil/liquid rate and a minimum pressure value. The producing well has been set to operate under the conditions of a maximum liquid rate equal to the injection rate, while bottom-hole pressure not going under 100 bar. These rates and conditions have been set to ensure a stable flow in the reservoir and to produce at a high plateau level over time. Both the injecting and producing well are perforated in all 20 reservoir layers.

The wells are located in the center at each end of the reservoir. Table 5-3 shows the XYZ-indices of the perforated sections of the wells in the grid resolution models.

Table 5-3: *XYZ-indices of injecting and producing well.*

	Coarse grid			Medium grid			Fine grid		
	X	**Y**	**Z**	**X**	**Y**	**Z**	**X**	**Y**	**Z**
Injector	1	4	1-20	1	7	1-20	1	14	1-20
Producer	50	4	1-20	100	7	1-20	200	14	1-20

The fact that there is an odd number of rows in Y-direction in the coarse grid (ny=7) and an even number of rows in the medium and fine grid (ny=14 and 28) results in a slightly different well placement, in the sense that the wells are not in the exact center of the

reservoir-ends in the medium and fine grid. This could have a small effect on the flow pattern but is in this thesis considered insignificant due to the wells still being in the approximate centers.

6 Homogeneous reservoir

As mentioned in chapter 5, the homogeneous reservoir has no flow obstructions and the displacement is only affected by the gravitational forces granted by the presence of vertical permeability. To inspect how the grid resolution affects the waterflooding, a series of simulations with two different NaCl-concentrations have been performed for the different grid models.

6.1 High-salinity waterflooding

The first simulation performed was with high salinity water only, abbreviated as HS, over 10 years injecting a total of 1 pore volume. The injected water has an equal salt-concentration as the connate water present in the reservoir, mole fraction of 0.0099 NaCl, and therefore no salt-mixing will occur.

6.1.1 Production results

Earlier simulations (Haajizadeh and Begg, 1993) have presented that for waterflood simulations, a horizontal coarsening of a homogeneous grid had a tendency of resulting in lower recovery factor. The results from the highsal waterflooding confirm this, see Table 6-1.

Table 6-1: *Production results from high salinity waterflooding of homogeneous reservoir.*

Grid resolution	Cumulative production [m^3]	Recovery factor, RF
Coarse	$2.2695*10^6$	0.5291
Medium	$2.2750*10^6$	0.5303
Fine	$2.2780*10^6$	0.5311

The recovery factor, RF, of a production is given by

$$RF = \frac{Oil\ recovered}{OIP(Original\ Oil\ in\ place)} = \frac{Oil\ recovered}{V_b * \varphi * S_{o,i}} \quad (6.1)$$

Where V_b is the bulk volume of reservoir, φ is reservoir porosity and $S_{o,i}$ is initial oil saturation.

Although the differences are small, about 7000 m^3 oil produced between the coarse and fine grid resolution, there is a trend showing an increased recovery with finer grid resolutions. Plotting of the cumulative production shows almost identical graphs with only a minor variation at time around breakthrough. Investigation of this can be done by studying the production rates around WBT, Figure 6-1:

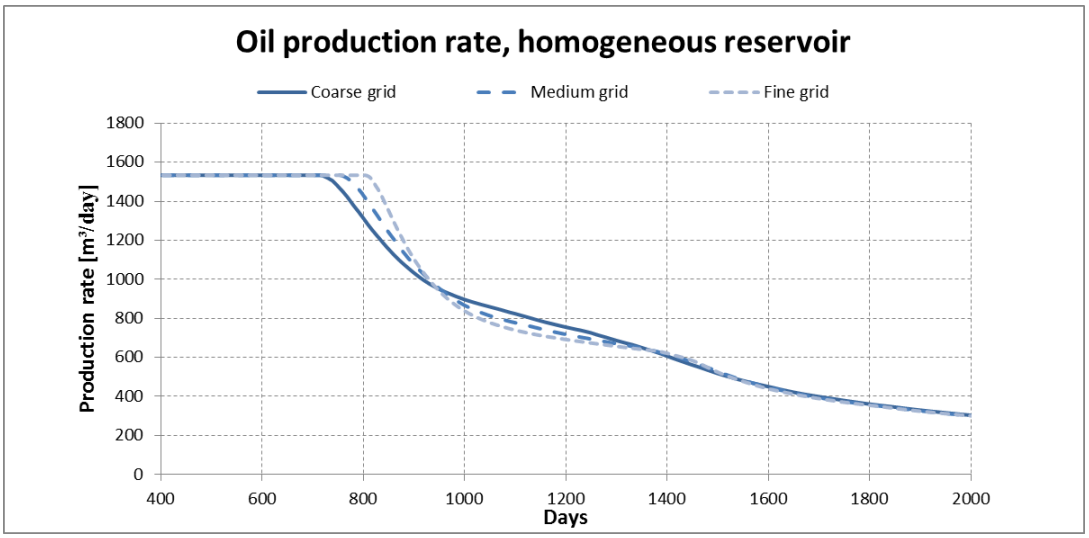

Figure 6-1: *Oil production rates in homogeneous reservoir with highsal waterflooding.*

Looking at Figure 6-1, one can notice that a finer grid resolution will result in a slightly longer production plateau level. In other words, the water breakthrough is delayed due to the increased grid block count even though each individual cell is shorter in the horizontal directions. STARS` saturation calculation is based on a grid block average that follows the relative permeability curves utilized. Water cannot flow into cell (*n*+1) until the water saturation in cell *n* is high enough for the water relative permeability to allow the water to flow freely into the adjacent cell(s). The process of water entering a cell and thus increasing the water relative permeability must for each finer grid in this case be done to twice the number of cells in the horizontal direction, thus resulting in the delayed water breakthrough.

The production graphs in Figure 6-1 shows a noticeable “bump” in oil production after 1000 days, where the decreasing oil production slightly stagnates between 1000-1500 days. This can be investigated further by partitioning the layers in the reservoir into regions and then studying the oil production within each layer. The region partitioning is shown in Table 6-2.

Table 6-2: *Layer partitioning of the reservoir into regions.*

	Layers
Region 1	1-5
Region 2	6-10
Region 3	11-15
Region 4	16-20

These regions will be equal for all three grid resolutions, as they have an equal amount of layers in Z-direction, and will be featured throughout this thesis. Investigating the production within these regions could show a more detailed picture of the flow path of the water and might give an explanation to why the oil production rate differs for the different grid models, and why the stagnation in the production appears. Henceforth, all graphs and tables will specify whether the data is showing total well production or individual region/layer production.

Studying the region production for each grid resolution shows almost identical production curves for regions 1,2, and 4. The production in region 3 however, showed a variation. This can be seen in Figure 6-2.

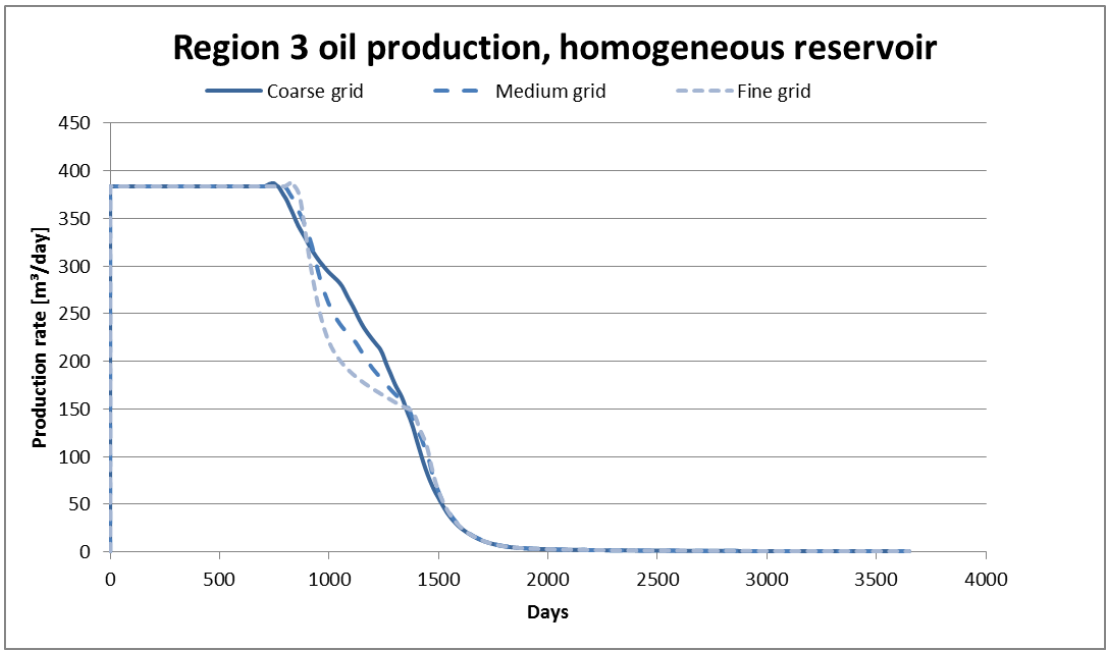

Figure 6-2: *Production rates for the different grid resolutions in region 3, homogeneous reservoir.*

At the end of the plateau level in Figure 6-2 there is a tiny increase in the production due to water breakthrough in region 4, but this is short-lived as the production starts to decrease shortly after. The noticeable difference is the curvature of the different graphs, where a finer grid resolution result in an initially steeper declining rate before stagnating and having an approximately equal production as the coarser version. This difference in production rates could imply an impact of grid resolution on fluid flow patterns.

STARS has a 3D-viewing option which allows the user to inspect the reservoir as a whole for a wide range of properties. Looking at the water saturations as a function of depth at any given timestep is a useful tool to utilize in order to achieve a better understanding of the results. It also allows the user to follow the water-front as it progresses through the reservoir. Figure 6-3a,b,c shows the sectional view of the water saturation at breakthrough time for the coarse grid, the medium grid, and the fine grid, respectively. Note that the color scale ranges from 0 to 1.

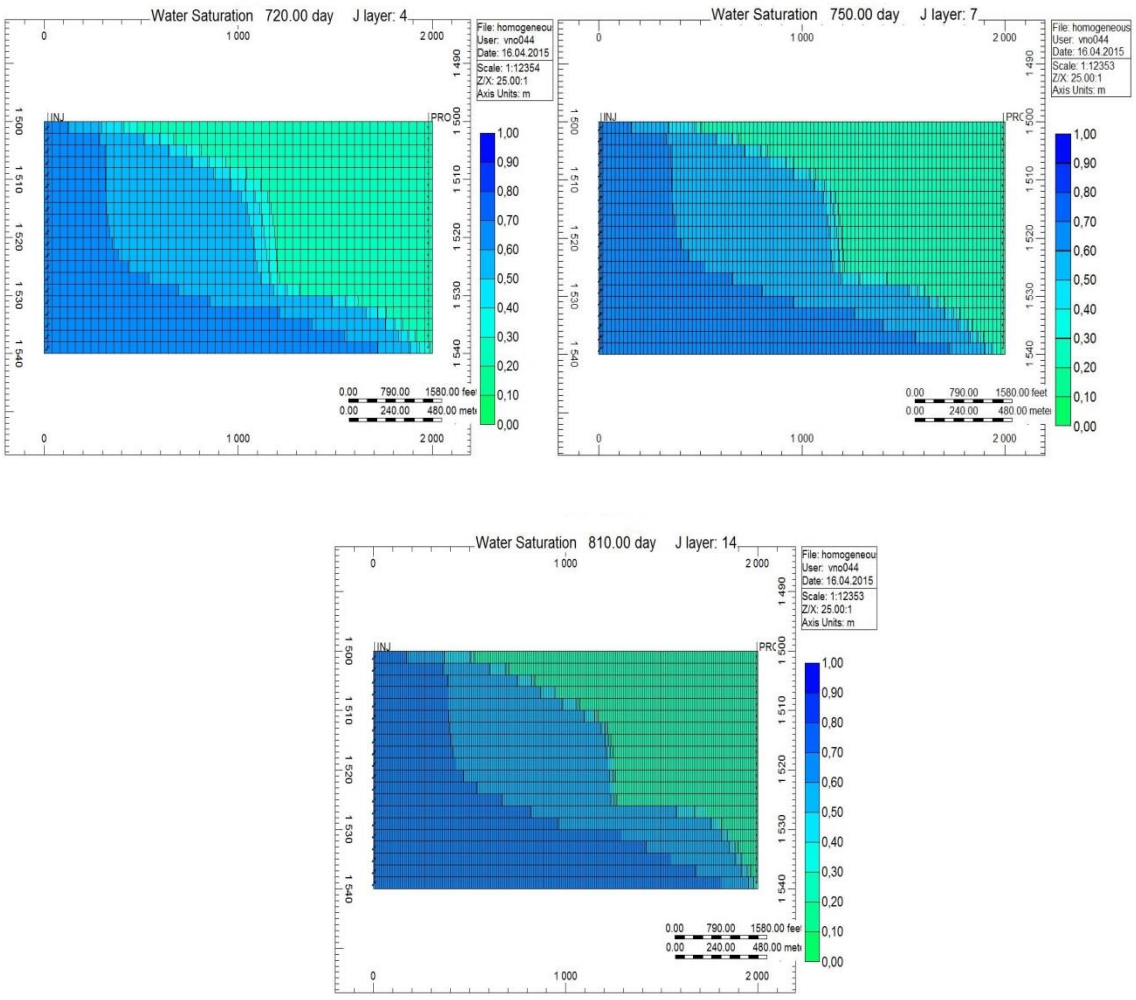

Figure 6-3a,b,c: *Sectional view in XZ-direction of water saturation in coarse, medium and fine grid, respectively, at breakthrough time.*

As discussed in chapter 3.3, numerical dispersion is increasing by the coarsening of grid blocks. The physical dispersion of the water front will behave in the same way, with a steeper front with finer grid resolutions. One can see that for the fine grid the waterfront is sharper in the middle regions, indicating a more piston-like displacement front. However, due to the gravitational forces the denser water will flow towards the bottom of the reservoir thus reaching the producing well in the lower layers first. As the grid resolution increases, this eventually develops into two fronts; a lower and a middle front (see Figure 6-3c). Due to the lower front being higher in the fine grid, stretching over the layers 14-20, this will affect the region production shown in Figure 6-2.

6.1.2 Block saturations

Figure 4-1 shows the relative permeability curves utilized for the highsal water injection, where the endpoint water saturation,$S_{w,sor}$,is 0.655. Inspection of the grid block saturations in the bottom layer, layer 20, showed a reluctance of the water saturation to reach this upper value, even though the injection rate and time is sufficient for the saturation to reach $S_{w,sor}$. Figure 6-4 shows the saturations in every 10^{th} cell in X-direction over time.

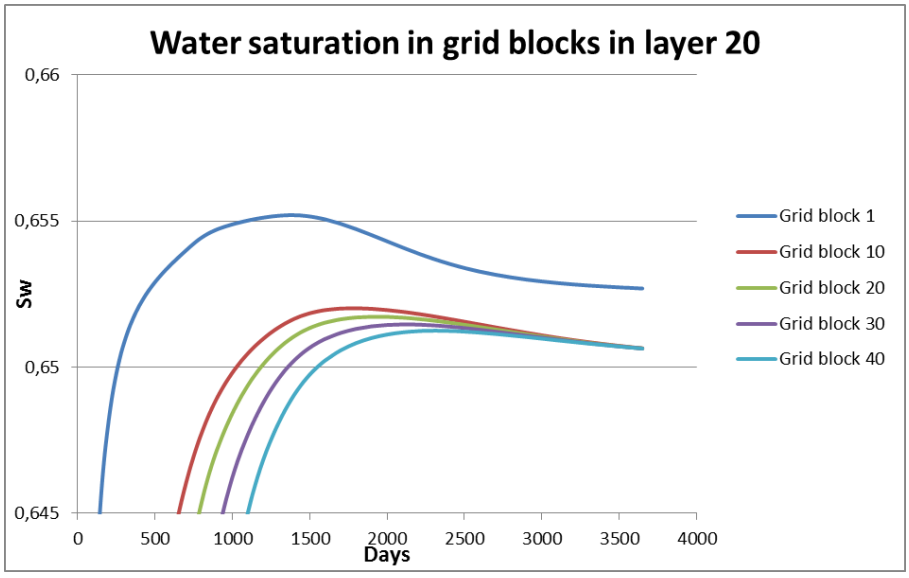

Figure 6-4: *Water saturation in grid blocks in layer 20, coarse grid.*

As seen in Figure 6-4 the saturation in grid block 1, the well perforated grid block, actually surpasses the maximum saturation value in the utilized relperm curve for a short period before decreasing. At increased distance from the injector the cells have lower maximum water saturation, before decreasing and reaching the same saturation value at simulation end. It is possible that since the injected volume only equals to 1 pore volume, more water is needed for the saturation to reach $S_{w,sor}$, however the general trend of a saturation decrease is noteworthy. Given that this simulation has only included injected highsal water and therefore no interpolation of relperm curves or change in NaCl-concentration takes place, makes these results slightly surprising. However, this saturation deviation is relatively small and can therefore be considered to be within the computational error margins, as it will not have any noticeable impact on the final results.

The grid blocks viewed in Figure 6-4 are taken from the coarse grid. The equivalent grid blocks from the medium and fine grids showed an equal saturation trend. It is worth mentioning that the data file used to produce the results in Figure 6-4 included the relative permeability set for the lowsal water, but since the injected water was of a high-NaCl composition no interpolation between the two sets should occur. However, to exclude the risk that the merely presence of the lowsal relperm set in the data file affects the outcome, another simulation was run without the lowsal relperm set. No significant difference was observed.

A saturation profile as a function of distance was made from the bottom layer for all three grid resolutions. The bottom layer was chosen due to no water flowing further down in the reservoir from that layer, and was chosen at a time before water breakthrough for all grid resolutions. Grid blocks from the center row (Y=center) were chosen. The saturation profiles correspond to the saturation fronts seen in Figure 6-3a,b,c, with a smaller physical dispersion for the finer grids, see Figure 6-5.

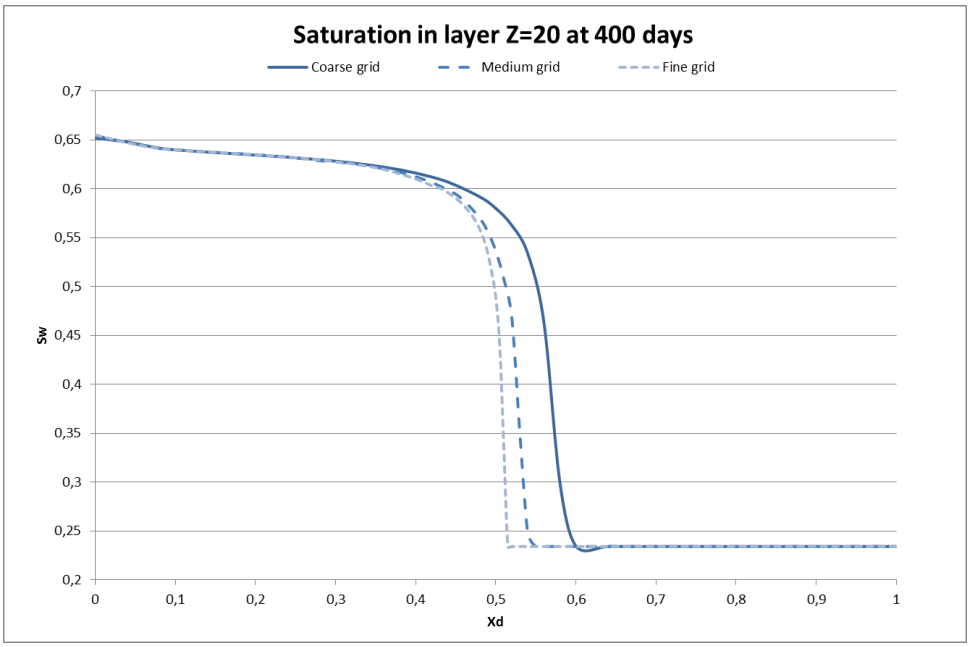

Figure 6-5: *Saturation profile of layer 20 as a function of distance. Y=center.*

One can see that the coarse grid has a more dispersed waterfront, while the finer grids have a steeper saturation profile implying a more stable front. The “tail” saturation, the upper part, is equal for all three resolutions as this is an already flushed area. It appears that even after the water front has passed the saturation gradually increases until it reaches a value close to$S_{w,sor}$.

6.1.3 Pressure

Figure 6-4 shows the pressure difference between the injecting and producing well. The difference is highest right after start of production as the bottom-hole pressure increases for the injector and decreases for the producer. As time goes by, the pressure starts to stabilize within the reservoir and the difference decreases. At time of water breakthrough, around 800 days, the pressure decrease stagnates and eventually settles at a difference of 5000 kPa. A consistent result for the bottom-hole pressure is the slightly higher values for the finer grids. Finer grid resolution equals smaller grid blocks, and therefore smaller grid block calculation averages performed. This would result in a higher grid block pressure in the cells near the injecting well and a lower pressure in cells near producer, resulting in a slightly higher pressure difference with a finer grid resolution.

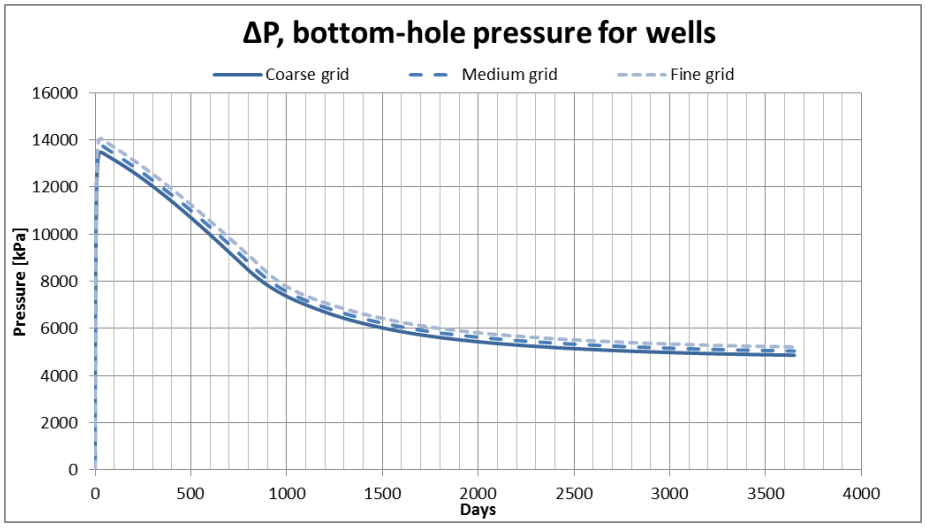

Figure 6-4: *Pressure difference of the wells in the different grid resolutions.*

A variation in the bottom-hole pressure with varying grid block size is not very critical to the simulation as long as it does not surpass the operating constraints. It is more important that the average reservoir pressure remains unchanged. Figure 6-5 shows the average reservoir pressure for the different grid resolutions, and one can see that the reservoir pressure is unaffected by the grid resolution. There is a small deviation around 800-1000 days, however this is considered as an isolated anomaly.

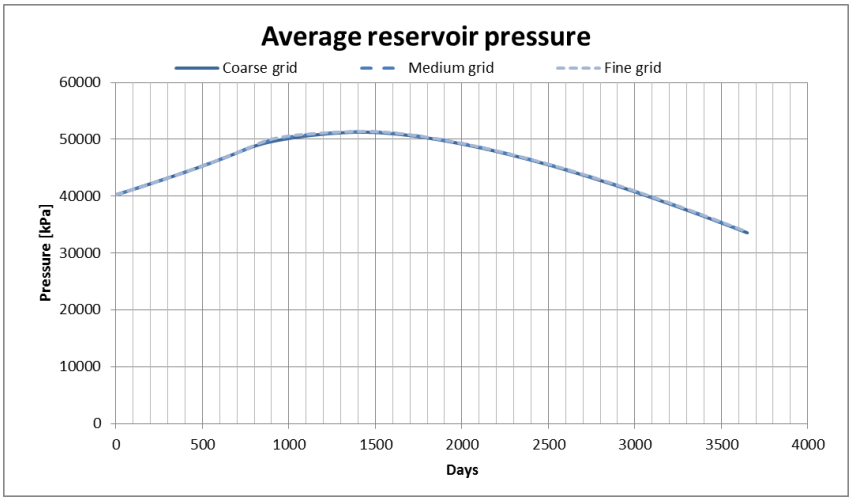

Figure 6-5: *Average reservoir pressure in different grid resolutions.*

The results reported in this subchapter are representable for all other simulations in this thesis, as they all follow the same trend with a slightly increase pressure difference in the bottom-hole pressure and an unaffected average reservoir pressure. Pressure results from the other highsal&lowsal simulations will therefore not be included for the rest of this thesis.

6.2 Sensitivities of fluid properties

In the "Component Properties" section of the data file one assigns the components to be present and injected in the simulation as well as their properties. One must also include a reference temperature and pressure using the TEMR and PRSR keywords corresponding to densities entered in MASSDEN and SOLID_DEN.

When simulating in field-scale there are several other aspects to take in account compared to simulation of core samples. The gravitational forces are usually neglected in core sample simulation while it could have a big impact on fluid-flow and behavior in field scale.

The results in chapter 6.1 use the component properties shown in Table 5-1. It is well known that a displacement process can vary greatly depending on the fluid properties, especially in a 3-dimensional displacement. Should the viscosities or densities differ, one would expect to see a different outcome. Since water is denser it tends to flow towards the bottom, and therefore faster in the lower layers, forming an "S-shape" of the waterfront in XZ-direction, as seen in Figure 6-3a,b,c. After water breakthrough in the lower layers the injected water will flow through the path of least resistance which will lead to increased water cut thereafter. This could lead to a poorer displacement efficiency of the reservoir leaving the upper layers untouched.

This chapter is a sensitivity study where the viscosity and density of the oil and water would be varied and the effect on fluid behavior and production results studied.

6.2.1 Viscosity sensitivity

This subchapter will consist of a sensibility analysis of the effect of oil viscosity on fluid flow and reservoir production. The values in the keyword *AVISC are changed from 8cP to 13.8cP for the high-viscosity run (initial laboratory viscosity value), and to 3cP for the low-viscosity run.

6.2.1.1 High viscosity oil

Increasing the oil viscosity would result in an increased water mobility rate, thus making it harder for the water to displace the oil which would result in a more uneven water front.

Table 6-3: *Cumulative oil production for highsal waterflooding of homogeneous reservoir with high-viscosity oil.*

Grid resolution	Cumulative production [m^3]	Recovery factor, RF
Coarse	$2.0863*10^6$	0.4863
Medium	$2.0872*10^6$	0.4865
Fine	$2.0859*10^6$	0.4862

The differences in the production results between the models are less than 1000 m^3 and could therefore be deemed insignificant as it makes up for less than one tenth of a percent of the total production. Also, the recovery factor only differs with a total of $^3/_{10000}$. A plot of the cumulative production results could not produce any significant conclusion other than that the production is equal. However, the oil production rates gave more intriguing results.

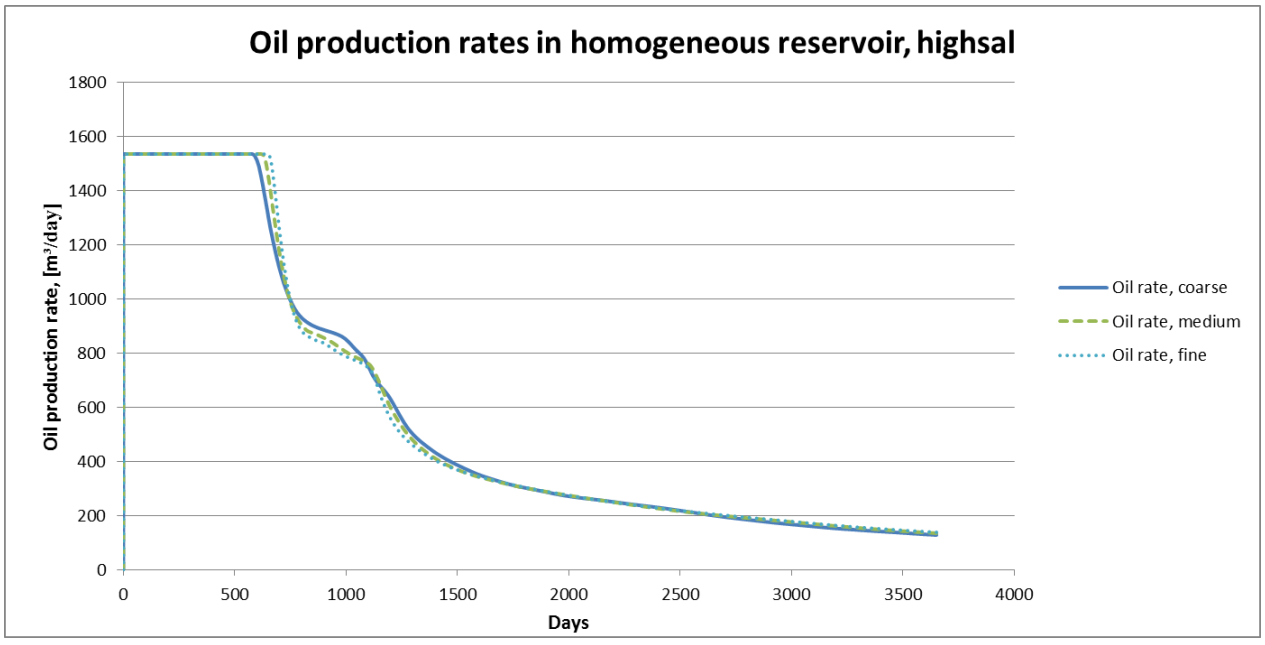

Figure 6-6: *Oil production rates of continuous highsal injection in homogeneous reservoir.*

The shapes of the curves are noticeable as there is a “bump” in the oil production after the water breakthrough, where the production decrease stagnates to some degree before continuing to decrease and reaching the tail production period after around 1500 days. This “stagnation” is highest in the coarse model and lowers with grid resolution. Also, while the water breakthrough for the medium and fine grid is delayed, the curvatures of the graphs are steeper after breakthrough and different in shape until they reach the tail production period after around 1500 days. This could give an indication of the impact the grid resolution has on the fluid flow pattern. Given that the reservoir is homogeneous, no other factors than the gravitational force and the fluids properties should affect the flow paths. To investigate this further, the reservoir is split into 4 regions:

The production in regions 1 and 2 proved to be fairly equal for all three grid resolutions, with only the coarse grid model having a slightly higher production. This was expected due to the water breakthrough occurring in the lower layers first, and therefore the production variations due to gravitational forces and viscous fingering could have an impact on the production in the lower regions.

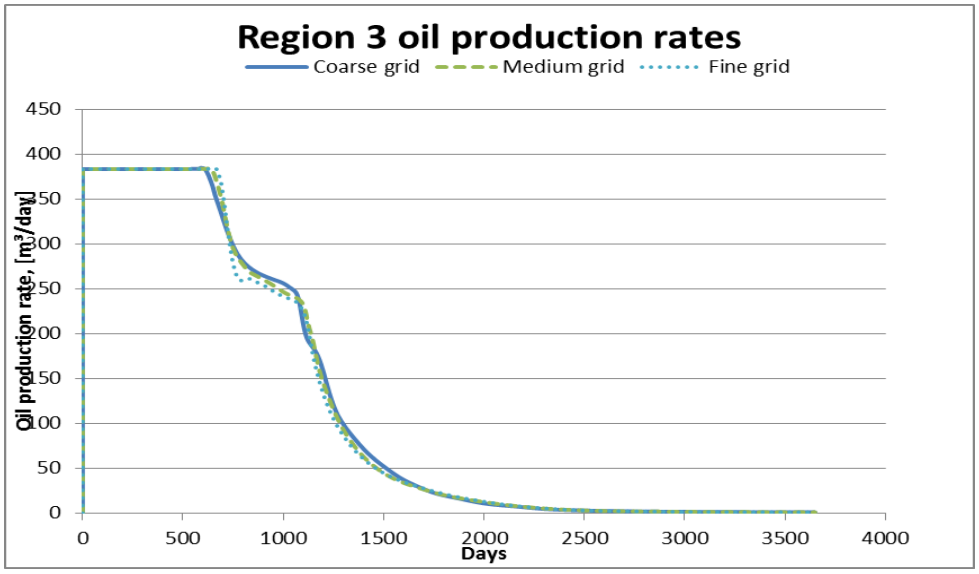

Figure 6-7: *Oil production rates in region 3 in homogeneous reservoir.*

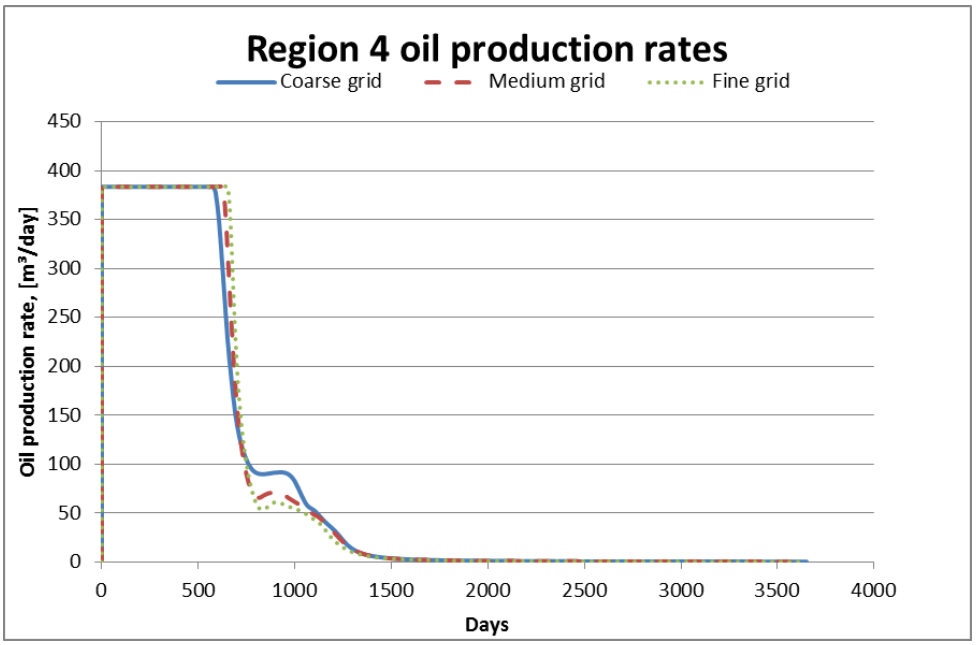

Figure 6-8: *Oil production rates in region 4 in homogeneous reservoir.*

Figure 6-7 and Figure 6-8 show the oil production in region 3 and 4. In region 4 the production rate increases after the initial water breakthrough, indicating some sort of either oil banking or water banking. Should the region already be flooded with highsal water, an injection of low salinity water could lead to a development of an oil bank due to the residual oil saturation lowering when interpolating between the highsal and lowsal water. However, since these results only represent a high salinity injection in a secondary flooding then no such phenomena can occur. This could point towards the phenomena of viscous fingering. Given the large viscosity difference between the two phases (water=0.5 cP, oil 13.8 cP) with a mobility ratio high above 1, the water will displace the oil in an irregular fashion resulting in various flow channels. Looking at the water front in the 3D viewer proves an irregular flow pattern:

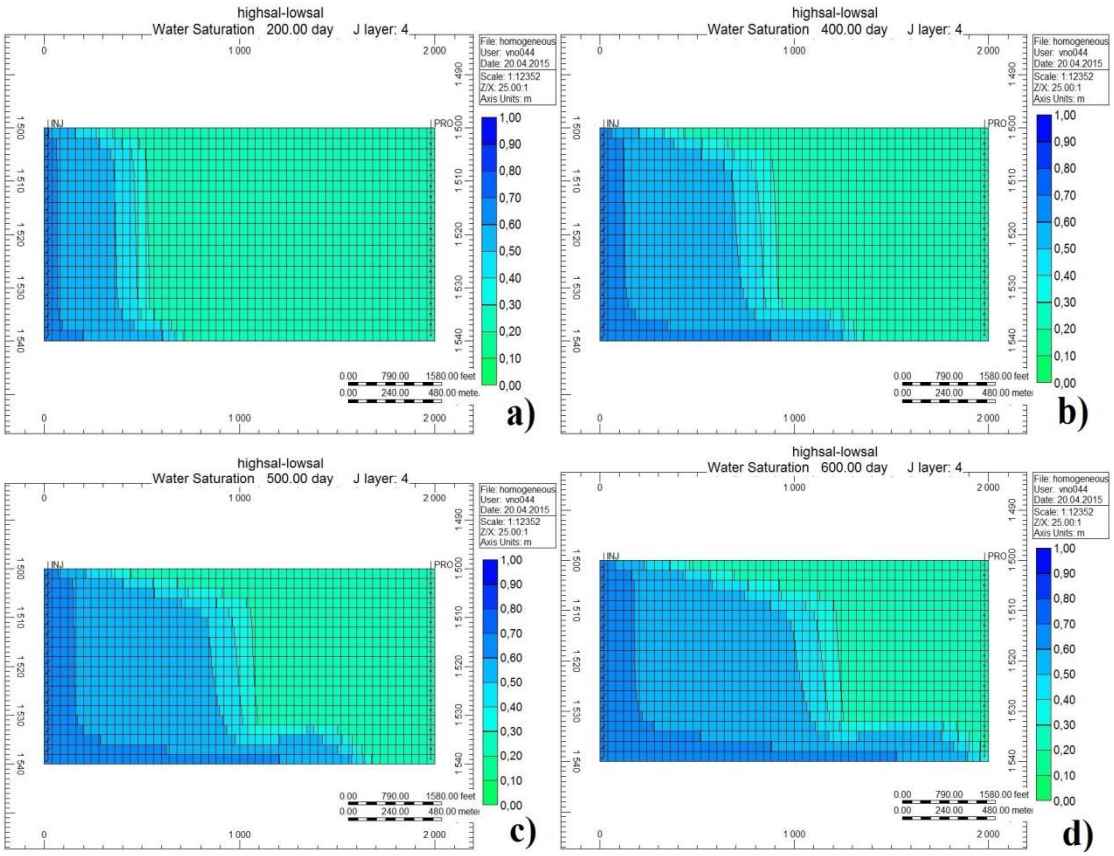

Figure 6-9a,b,c,d: *Sectional view in XZ-direction of water front with high-viscosity oil, coarse grid.*

Figure 6-9a,b,c,d shows the water front after 200,400,500 and 600 days, respectively. One can see from Figure 6-9a) that the water front starts out in a normal manner, but as the front progresses the water flows faster in the lower layers and eventually creates a “bump” of water where it seems to flow vertically upwards in addition to horizontally towards the well. This could occur due to the water being unable to mobilize the more viscous oil, and therefore choosing an alternate route vertically in the system and thus overcoming the gravitational force and the fact that the vertical permeability is 10% of the horizontal. This flow behavior explains the results shown in Figure 6-7 and Figure 6-8 where the decreasing oil production either stagnates or increases again after initial water breakthrough.

As discussed in chapter 6.1.1, a finer grid resolution could lead to a tendency of increased vertical movement of fluids. Comparing the waterfronts with the high-viscosity oil for the different grid resolutions confirms this tendency, see Figure 6-10a,b,c.

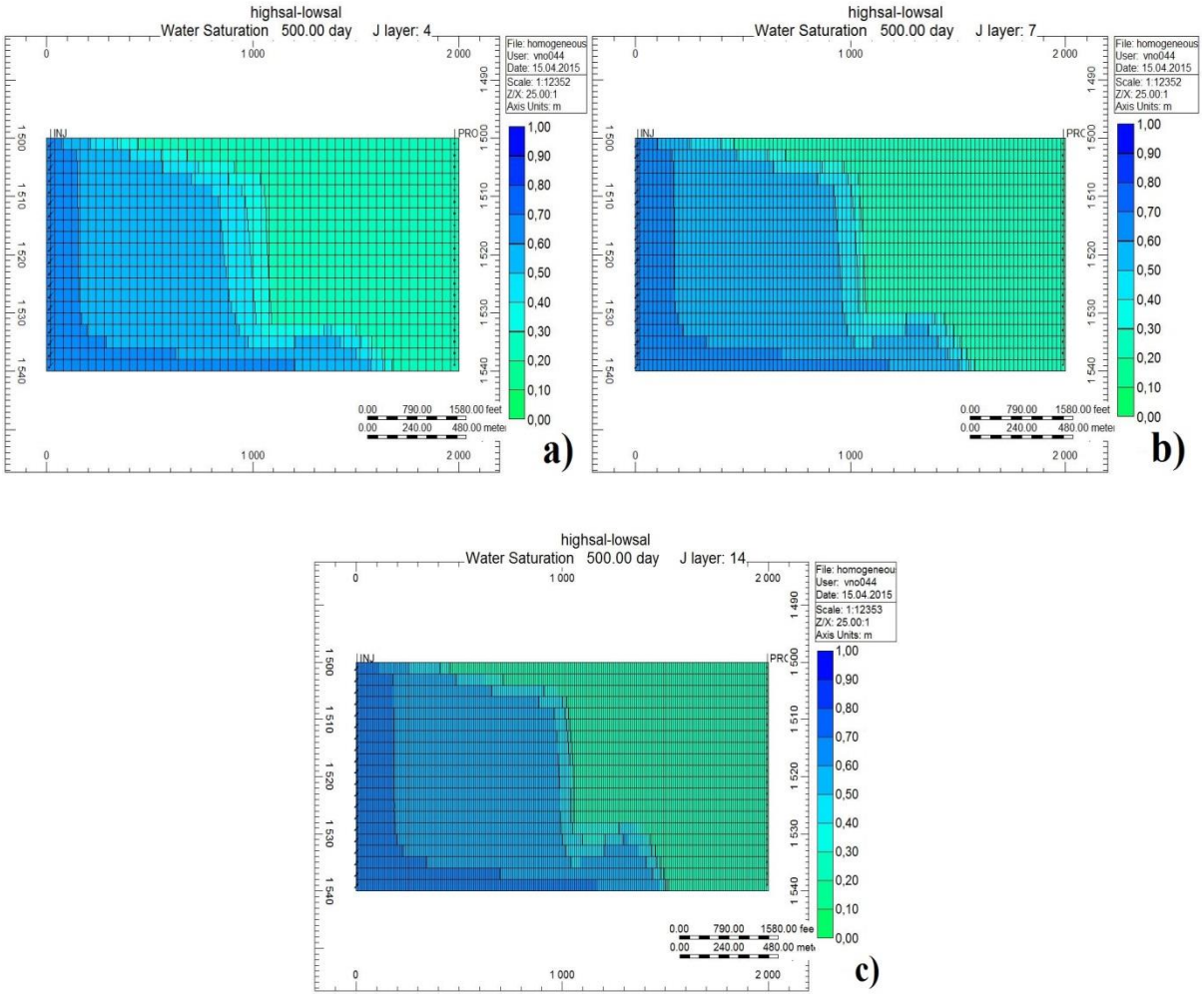

Figure 6-10a,b,c: *Sectional view in XZ-direction of waterfronts with high-viscosity oil with varying grid resolutions at 500 days.*

Figure 6-10a,b,c shows the waterfronts for the coarse, medium and fine grid respectively, after 500 days. As suspected, the water front for the coarse grid is more spread out and the water "bump" is lower in height. The sharpness and height of this bump seems to increase with a finer grid resolution which in turn will have an impact on the production profiles of the different simulations.

The results in Figure 6-10a,b,c are somewhat unexpected due to the water being heavier than oil, and the fact that the vertical permeability is 10% of the horizontal permeability. No capillary forces are included either, which gives no obvious reasons to why the water flows

upwards in the lower water front. The expected water front form would be a “tongueing” of water at the bottom of the reservoir. However it is possible that the water is experiencing challenges displacing the highly viscous oil, hindering the water front velocity to some degree, which in turn leads to an accumulation of water directly behind the water front. This accumulation could therefore flow vertically upwards in addition to the already horizontal flow. To test this hypothesis a single simulation was run in the coarse model with an increased injection rate. The increased injection rate will give a higher water velocity and therefore maybe remove the water “bump”.

The increased injection rate from 1500$^{m^3}/_{day}$ to 2500 $^{m^3}/_{day}$ will in turn result in an earlier breakthrough so a view at the same timestep as in Figure 6-10a) is therefore not preferable because it is after the water breakthrough. However, Figure 6-11 shows the water front at water breakthrough time, and it is clear that while the bump is still present, it is smaller and does not occur until right before breakthrough. The before mentioned hypothesis is therefore considered as a plausible explanation to why the bump occurs.

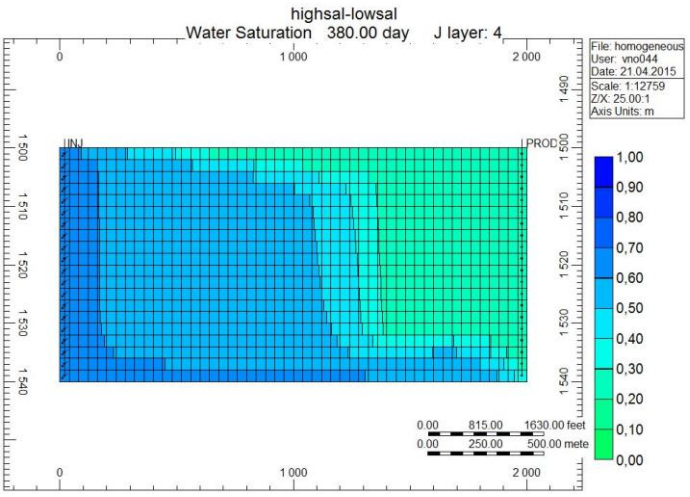

Figure 6-11: *Sectional view in XZ-direction of waterfront of with high-viscosity oil, increased injection rate, at breakthrough time.*

It is worth mentioning that even though the 3D viewer may be a useful tool in interpreting reservoir behavior, it is easy to over-exaggerate the differences between cells. Small differences may appear much larger due to the color scale utilized, e.g. two neighboring cells

with saturations 0.499 and 0.500 may have different colors in the viewer but still have the approximate equal value.

6.2.1.2 Low viscosity oil

For the Low-viscosity test, an oil viscosity of 3cP was used. A lowering of the oil viscosity would imply a lower mobility ratio between the oil and water and therefore a more stable displacement process. However, the production results show the same slight deviation as with the high-viscosity oil. That is, the medium grid resolution gave the highest cumulative production.

Table 6-4: *Production results from simulation with low oil viscosity.*

Grid resolution	Cumulative production $[m^3]$	Recovery factor, RF
Coarse grid	$2.4258*10^6$	0.5608
Medium grid	$2.4086*10^6$	0.5615
Fine grid	$2.4085*10^6$	0.5614

The difference in production between the medium and fine grid resolution is very small, but it contradicts the common agreement of increased production with finer grids nonetheless.

The recovery factor is higher compared to the high-viscous results, with an increase from 0.48 to 0.56. This is due to the stable water front providing a more efficient sweep of the reservoir, resulting in a longer plateau-production level.

The regional production rates are fairly equal for the different grid resolutions, with the largest difference being time of water breakthrough. However, compared to the high-viscous runs, when the lower regions reach water breakthrough, the other regions seem to compensate this with an increased production for a period before decreasing due to water breakthrough. Figure 6-12 shows an example of this in the coarse grid.

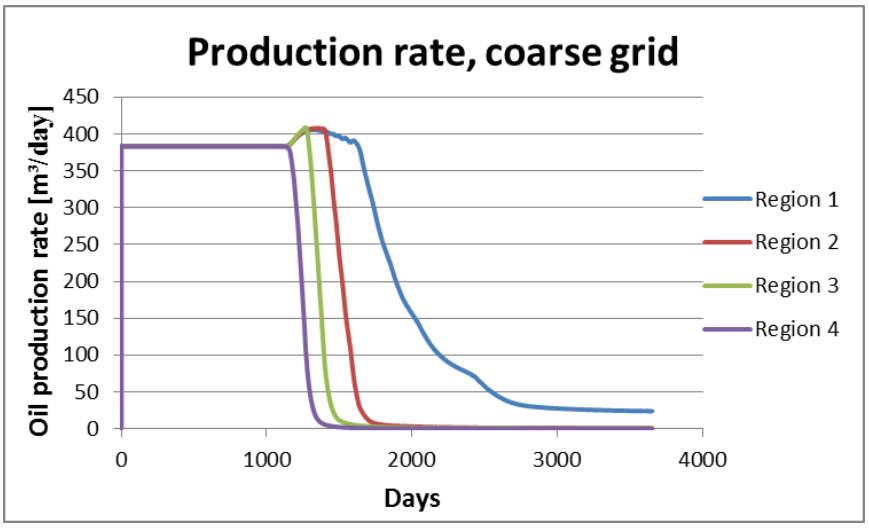

Figure 6-12: *Oil production in coarse grid resolution with low-viscous oil.*

All regions except region 1 have an increase in production before reaching water breakthrough and immediately decreasing towards a zero-value oil production rate. Region 1 maintains a certain level of production due to a poorer displacement in the upper layers, especially layer 1. The density difference makes the water flow downwards in the reservoir and thus resulting in a certain amount of residual oil in layer 1. The regional production for the medium and fine grid is almost identical with only a steeper decline rate after breakthrough.

Figure 6-13 shows the production rates of oil, water and liquid in a randomly chosen layer. At time of water breakthrough, the total liquid production from this layer drops until the water production has reached a certain level and then increases again. Since the producing well is being controlled by the minimum bottom-hole pressure and a total liquid rate, the production well therefore compensates the decrease by increasing the oil production in layers which have not yet reached water breakthrough.

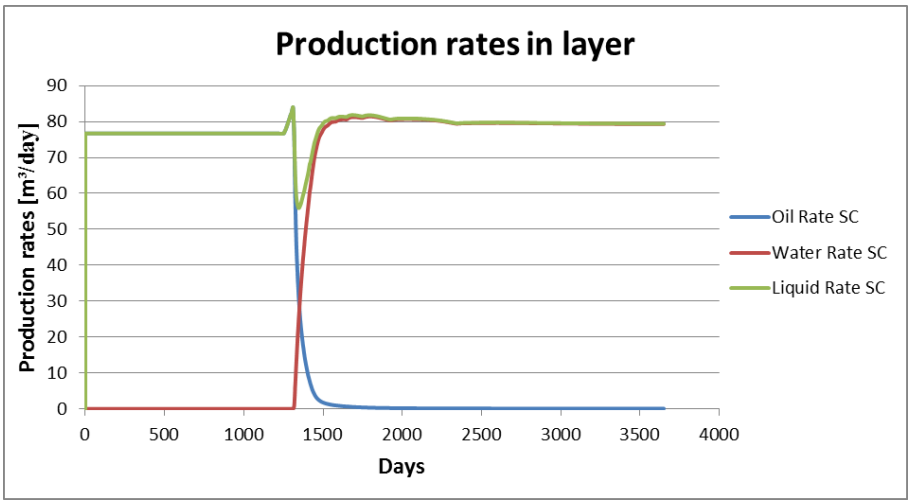

Figure 6-13: *Production rates of oil, water and total liquid in a random layer.*

6.2.1.3 Comparison to initial run

When comparing the results from the viscosity sensitivity to the initial run one can see a clear effect of the oil viscosity, both in the production rate and the cumulative oil produced. The clearly favorable recovery is with the low-viscosity oil, which resulted in a longer plateau level of production and a faster decline after water breakthrough, minimizing the time needed to produce the reservoir. One could achieve a higher recovery in all three cases with an increased production time, but seen from an operational point of view this is not desirable. For Figure 6-14 and Figure 6-15 the data is chosen from the fine grid resolution runs, following the assumption that the finest grid resolution gives the most accurate results.

Table 6-5: *Production results from viscosity sensitivity runs*

	Prod. [m^3]	**RF**
Initial run	$2.2780*10^6$	0.5310
Highvisc. run	$2.0859*10^6$	0.4862
Lowvisc. run	$2.4084*10^6$	0.5614

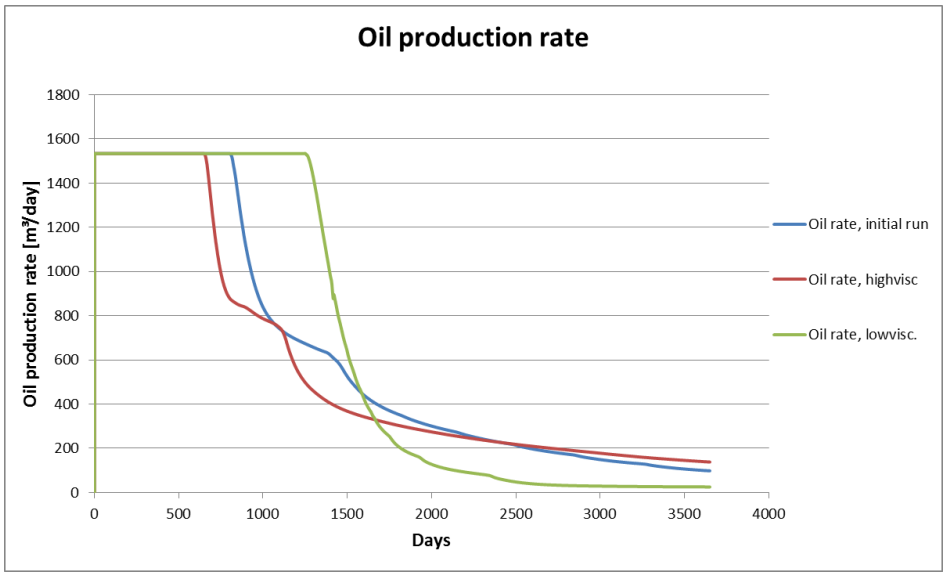

Figure 6-14: *Comparison of oil production rate in the viscosity sensitivity runs.*

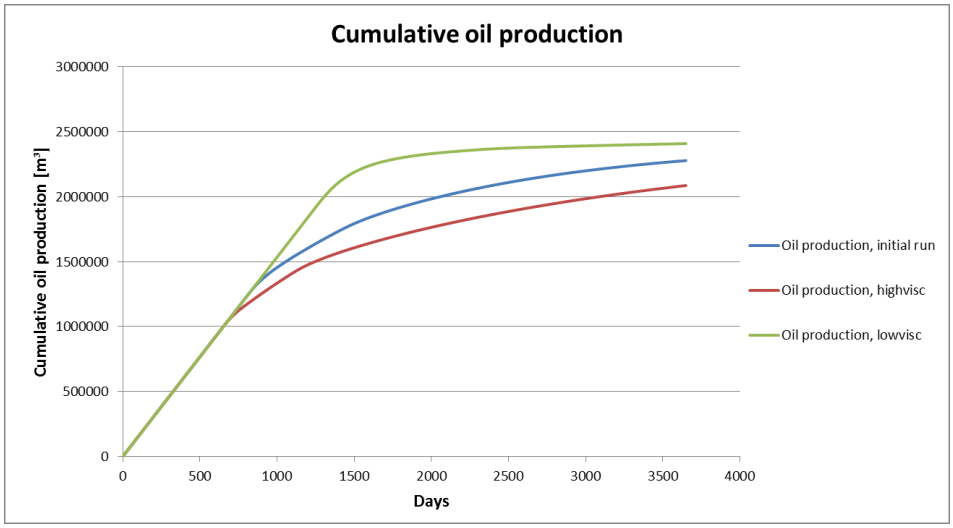

Figure 6-15: *Comparison of the cumulative oil production in the viscosity sensitivity runs.*

6.2.2 Density sensitivity

In this chapter, the density of the oil is varied to see how this affects the flow patterns and the production profiles. The values in keyword *MASSDEN are changed from 750$^{kg}/_{m^3}$ to 650$^{kg}/_{m^3}$ for the low-density runs, and to 850$^{kg}/_{m^3}$ for the high-density runs. The mass densities of the salt and water will remain at the values listed in Table 5-1.

6.2.2.1 High-density oil

A heavier oil will lower the density difference between the water and oil, and therefore lower the water`s tendency to flow towards the bottom of the reservoir. One would therefore expect the lower part of the waterfront not to be as prominent as in the initial run with an overall more stable front. A comparison of the cumulative production in the different grid resolutions showed the same trend as with the initial run, with a slightly increasing production with a finer grid. The oil production rate did not show any specific variation by grid size other than a delay in WBT to some degree. The most significant difference between the grid resolutions observed was the production in region 3, as shown in Figure 6-16.

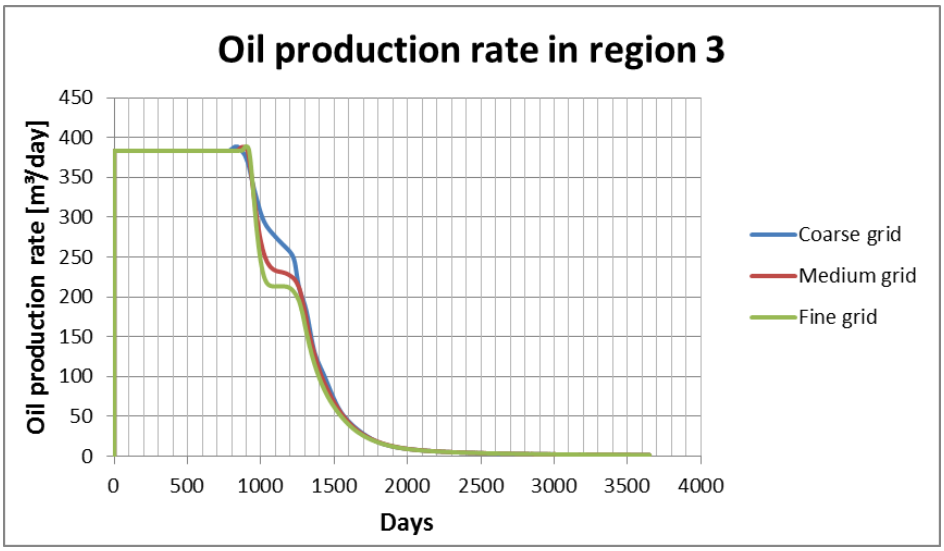

Figure 6-16: *Oil production rate in region 3 for the varying grid resolutions, high density oil.*

Figure 6-16 shows that the finer grids have a larger decline in oil production after initial water breakthrough. It appears that some sort of water banking occurs and that the water bank is higher for the finer grids as the production declines more initially. The production rate is equal for all grid resolutions after around 1300 days, meaning that it is only the initial water breakthrough that differs for the grid resolutions.

When comparing the results from the high-density oil simulations with the initial simulations, the first noticeable difference is the breakthrough time. The high-density oil resulted in, as expected, a later water breakthrough due to the smaller density difference making the gravitational effects on the water work slower. The water fronts are also more stable, meaning a faster production of the reservoir in total. However, in the fine grid simulation run, the same kind of water banking occurs as with the high-viscosity sensitivity run, meaning an accumulation of water behind the water front, stretching the water front upwards, see Figure 6-17.

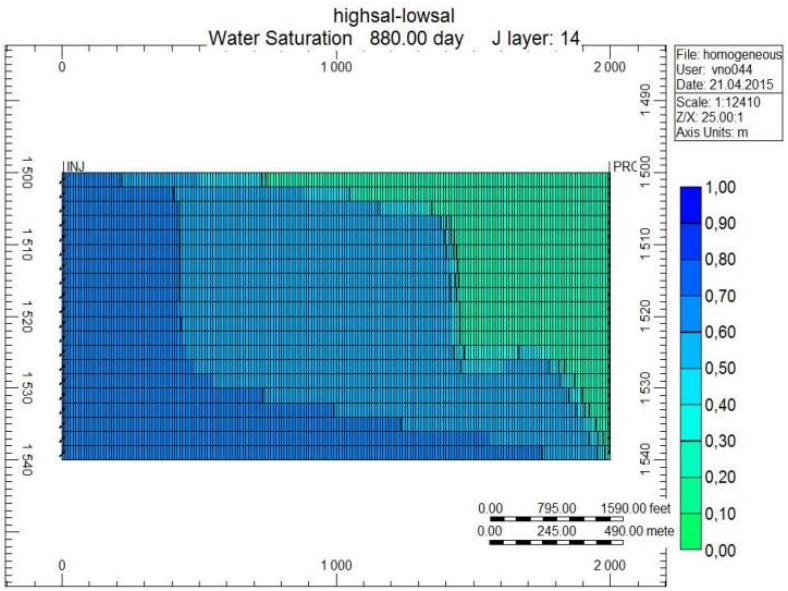

Figure 6-17: *Sectional view in XZ-direction of water front at water breakthrough time in fine grid.*

Figure 6-17 shows the same kind of water banking as seen in the high-viscosity oil simulation. This does not occur in the initial run presented in chapter 6.1, meaning that the

elevated oil density is the main cause of the water banking in this simulation. It is possible that the water bank is a combined effect of the viscosity and density properties of the oil. A viscosity difference of 0.5cP-8cP between the water and oil is still significant even though the initial run resulted in no such water bank, and an increased density from 750-850 $^{kg}/_{m^3}$in the water component might contribute to making the displacement of oil by water harder, and therefore resulting in the accumulation of water behind the water front. Figure 6-11 showed a reduction of this water bank by increasing the injection rate. This could also be relevant for this simulation, but the surprising factor is that it only occurs in the fine grid simulation with the elevated oil density.

6.2.2.2 Low-density oil

Lowering the oil density will increase the density difference between the oil and water, and therefore increasing the water`s ability to flow downwards in the reservoir. This will in turn lead to a higher flux of water flowing in the bottom layers and the water will reach breakthrough earlier. The early breakthrough will lead to a longer tail production which in turn gives a slow production rate with a long tail production. Comparison of the different grid resolutions can be seen in Figure 6-18.

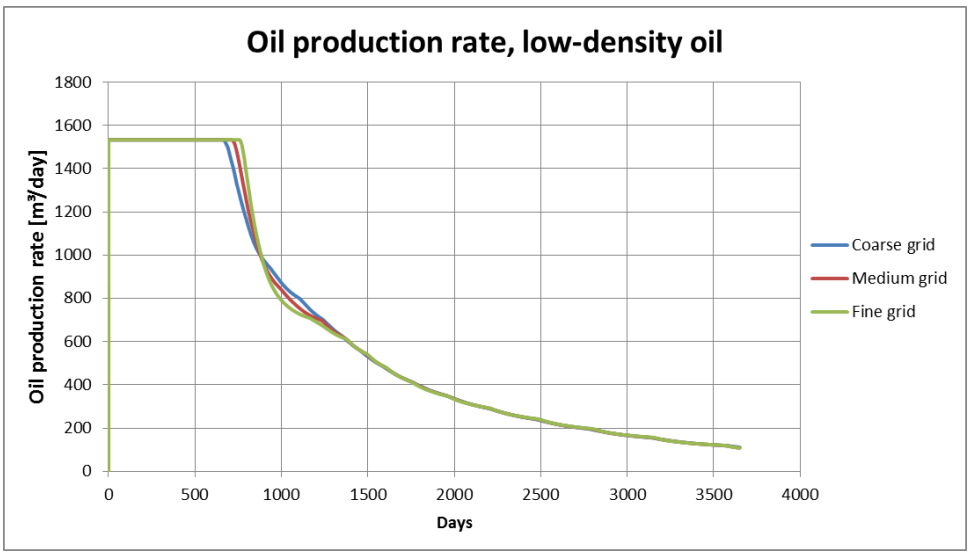

Figure 6-18: *Oil production rates for the different grid resolutions with low-density oil.*

As seen earlier in this thesis, the finer grids result in a later breakthrough and a steeper declining production rate after the initial water breakthrough. As with the high-density oil, the largest variation in regional production between the different grid resolutions occurred in region 3. It showed the same curvatures as Figure 6-18, where the fine grid had a steeper production decline after breakthrough before having equal production rates after 1250 days.

Figure 6-19a,b,c show the waterfront at breakthrough time for the different grid resolutions.

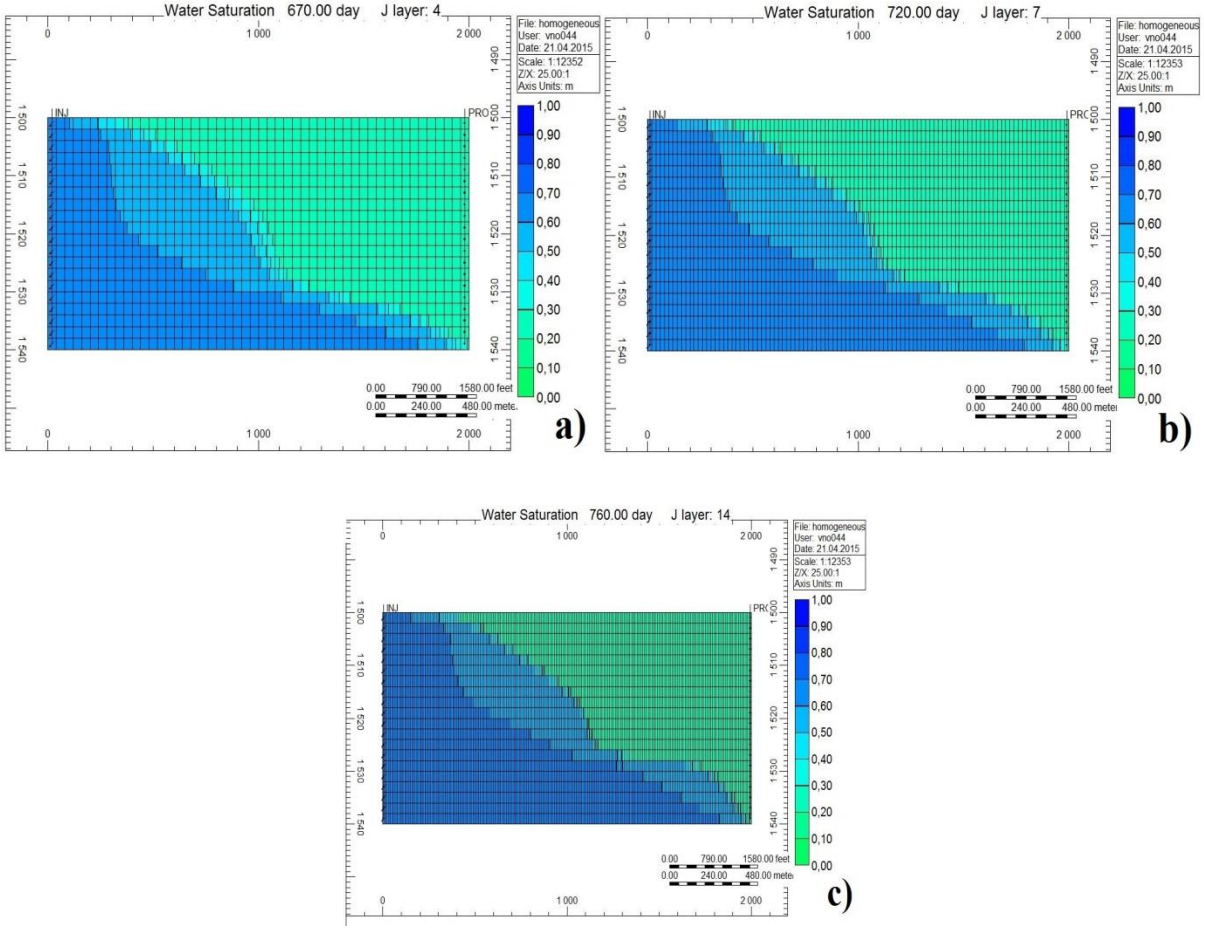

Figure 6-19a,b,c: *Sectional view in XZ-direction of water front at breakthrough time, low-density oil.*

As suspected, the water front in the lower layers is proceeding faster, resulting in an almost diagonal waterfront at time of breakthrough with the finer models having a steeper front. With a displacement like this the water-cut in the lower regions will increase rapidly as much

of the oil will flow upwards due to the density difference. This will result in a longer production in the upper regions, leaving only an oil production from the uppermost layers in the end.

6.2.2.3 Comparison to initial run

When comparing the results from the density sensitivity simulations to the initial run, there were not as large differences in production rates and cumulative production as first expected. Looking at Figure 6-20 shows that it is actually the low-density oil simulation that had the highest cumulative production, in spite of it having the earliest breakthrough and longest tail production.

Table 6-6: *Production results from density sensitivity runs.*

	Prod. [m^3]	**RF**
initial	$2.2780*10^6$	0.5310
highdens	$2.2543*10^6$	0.5255
lowdens	$2.2896*10^6$	0.5337

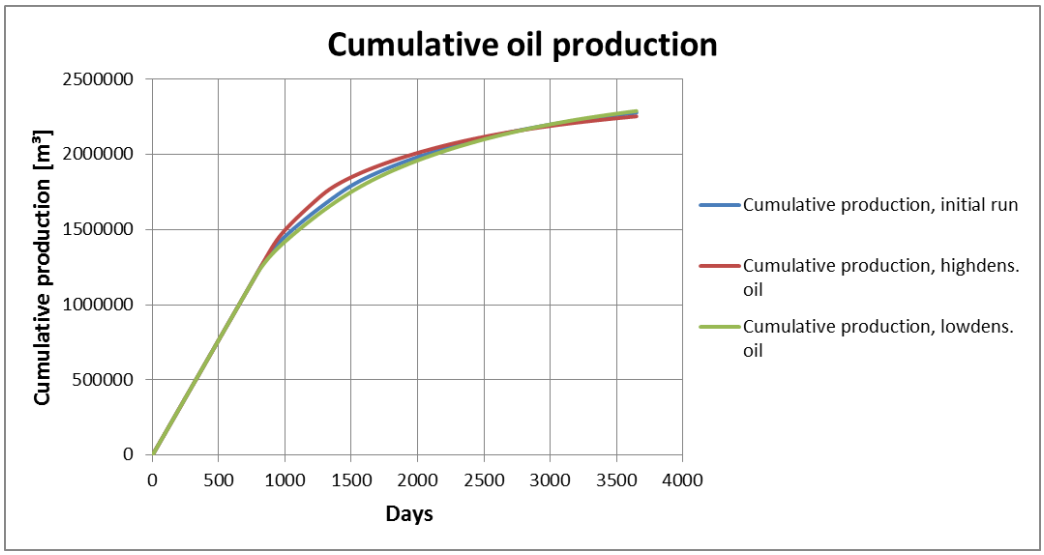

Figure 6-20: *Comparison of cumulative production with varying oil density.*

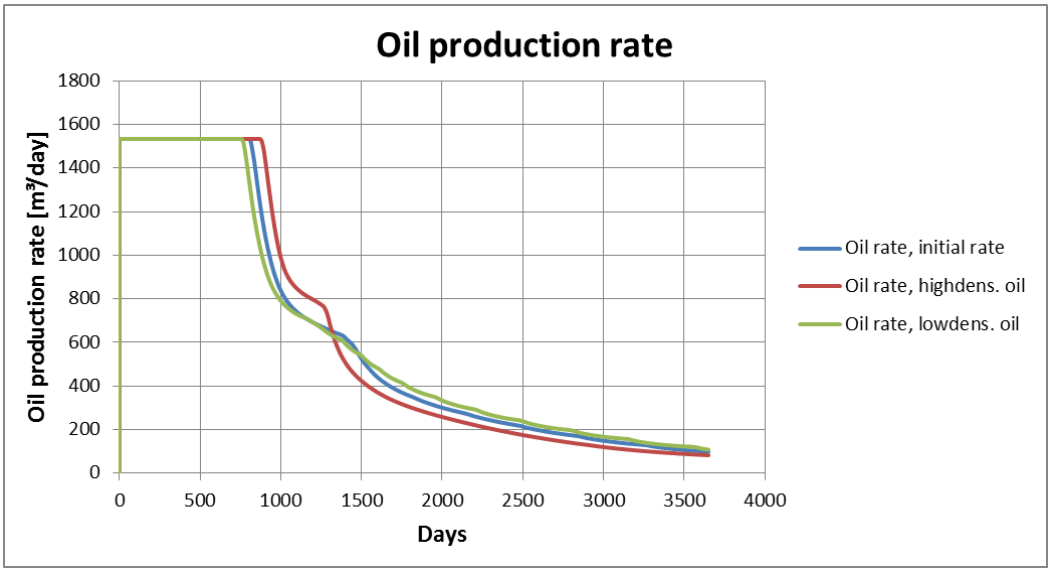

Figure 6-21: *Comparison of production rates with varying oil density.*

The high-density simulation runs showed a delayed water breakthrough time due to a smaller density difference between the oil and water making the water flow slower downwards. The decline slope after breakthrough is fairly similar to the initial and lowdens-runs but the “bump” from 1100-1300 days is shorter and the rate drops faster afterwards, ending with a slightly lower rate at ended simulation.

6.3 Low-salinity waterflooding

Injection of low-salinity brine into a reservoir with connate high-salinity water will lead to a salt mixing process. This chapter will focus on the salt mixing and recovery when utilizing lowsal injection of water. This will be investigated in two cases: Low-salinity injection as a tertiary recovery method, where most of the reservoir has been flooded with highsal (abbreviated as HSLS), and as a secondary injection where the injected water is lowsal only. In the second case an interpolation will occur immediately as the injected lowsal water will mix with the connate highsal water, reducing the water mobility and thereby affecting the flow. The salt dispersion will also be different in the two cases as the water saturation at start of lowsal injection is different and will therefore have an effect on the salt front throughout the reservoir.

The theoretical increase in recovery with a low-salinity injection is deemed to be around 13%, due to the decrease of S_{or} in the relative permeability curves utilized in the simulations. However, larger increases may be observed due to additional injection volume.

Table 6-7: *Residual oil saturations for high-salinity and low-salinity relative permeability curves.*

	$S_{w,sor}$
HS	0.655
LS	0.744

6.3.1 Secondary low salinity brine injection

In the simulations presented in this subchapter low salinity brine is being injected from day 1 over a 10 year period, injecting a total volume equal to 1 pore volume. Injection of lowsal water will lead to a direct interpolation between the connate water and the injected water, and thus affecting the water flow since the relative permeability curves for both oil and

water are different. It is expected to observe a higher recovery compared to the results from the highsal-only injection in chapter 6.1 since the S_{or} in the lowsal curve is lowered. Also, the dispersion of salt is bound to be different from the HSLS simulation as the water saturation will initially be lower in this subchapter.

6.3.1.1 Production results

As with the results from the highsal injection presented in chapter 6.1, the water-cut is delayed with a finer grid resolution and the oil production decreases faster after initial water breakthrough as a result of a more stable water front. The production rates for the grid models can be found in Figure 6-22:

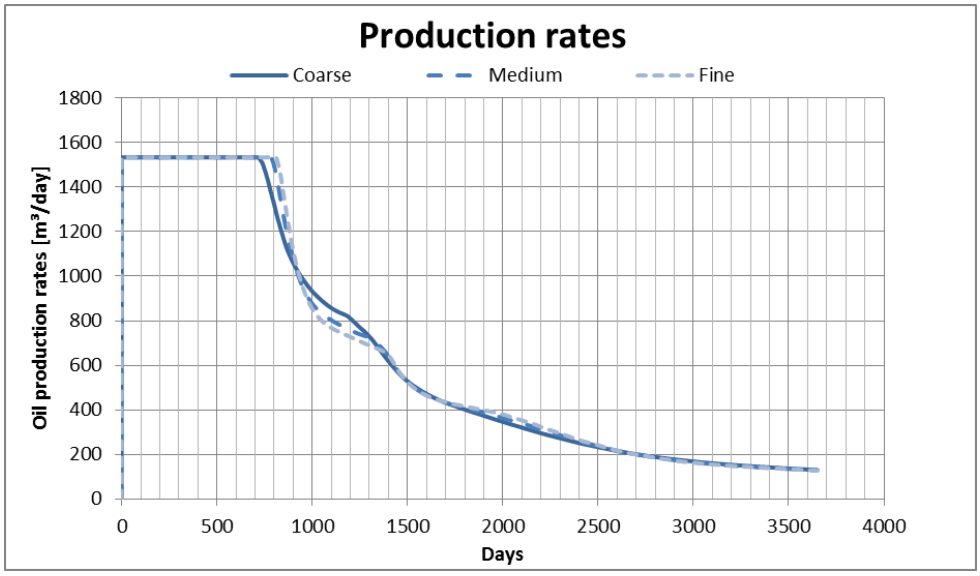

Figure 6-22: *Production rates for secondary lowsal injection for the grid models.*

The production rates for the different grid resolutions are very much alike to the rates presented in chapter 6.1.1 with highsal injection. Both the delay before water breakthrough between grid resolutions and the shape of production curves after water breakthrough are fairly similar. There are some minor variations between them, such as a small deviation between the grid models in Figure 6-22 around 2000 days, but in total they are very similar.

This shows that even though lowsal injection introduces interpolation between relperm-curves, this does not affect the variations between the grid resolutions.

The regional production for secondary lowsal injection in the different grid models is very much alike in region 1 and 4 (as with the highsal injection results), but region 3, and to some extent region 2, differs with grid block size. We know from chapter 6.2.1 that the viscosity difference between the oil and water reacts to the grid resolutions with a different displacement pattern thus affecting the regional production. In the secondary lowsal injection, this difference can also be seen in region 2, as opposed to being exclusive for production rates in region 3. Figure 6-23 and Figure 6-24 show the oil production rate for region 2 and region 3 for the grid models.

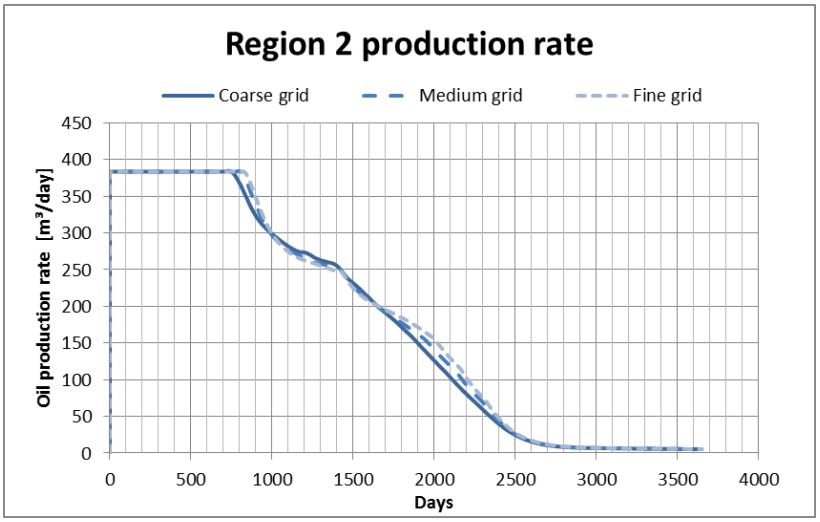

Figure 6-23: *Oil production rates for the different grid resolutions in region 2.*

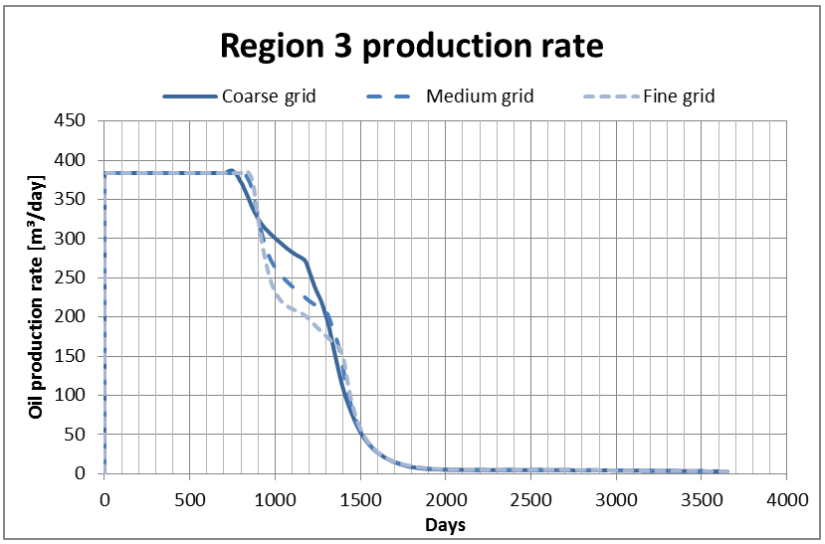

Figure 6-24: *Oil production rates for the different grid resolutions in region 3.*

The production in region 3 shown in Figure 6-24 shows the same variation between the grid models as for the highsal injection shown in Figure 6-2, with a sharper decrease in production for the finer grids after water breakthrough before it evens out and has an equal decline for all grid resolutions. Figure 6-23 shows a slower oil production decrease for the fine model than for the coarser models between 1700-2400 days.

6.3.1.2 Salt dispersion

Due to the salt partly following the water flow pattern we would expect to see a certain amount of gravitational segregation of the salt front, with a faster advance in the lower layers. However, due to diffusion of salt and the connate water being connected in the grid blocks, the salt will to a certain degree advance in front of the water front. This will occur in the upper layers where the water will have a harder time displacing the oil. Since the injected water advances at a faster pace in the lower layers, the displacement of connate water by the injected water will lead to the water front advancing faster than the salt front. Figure 6-25a,b,c shows the NaCl-concentration in the grid models after 500 days.

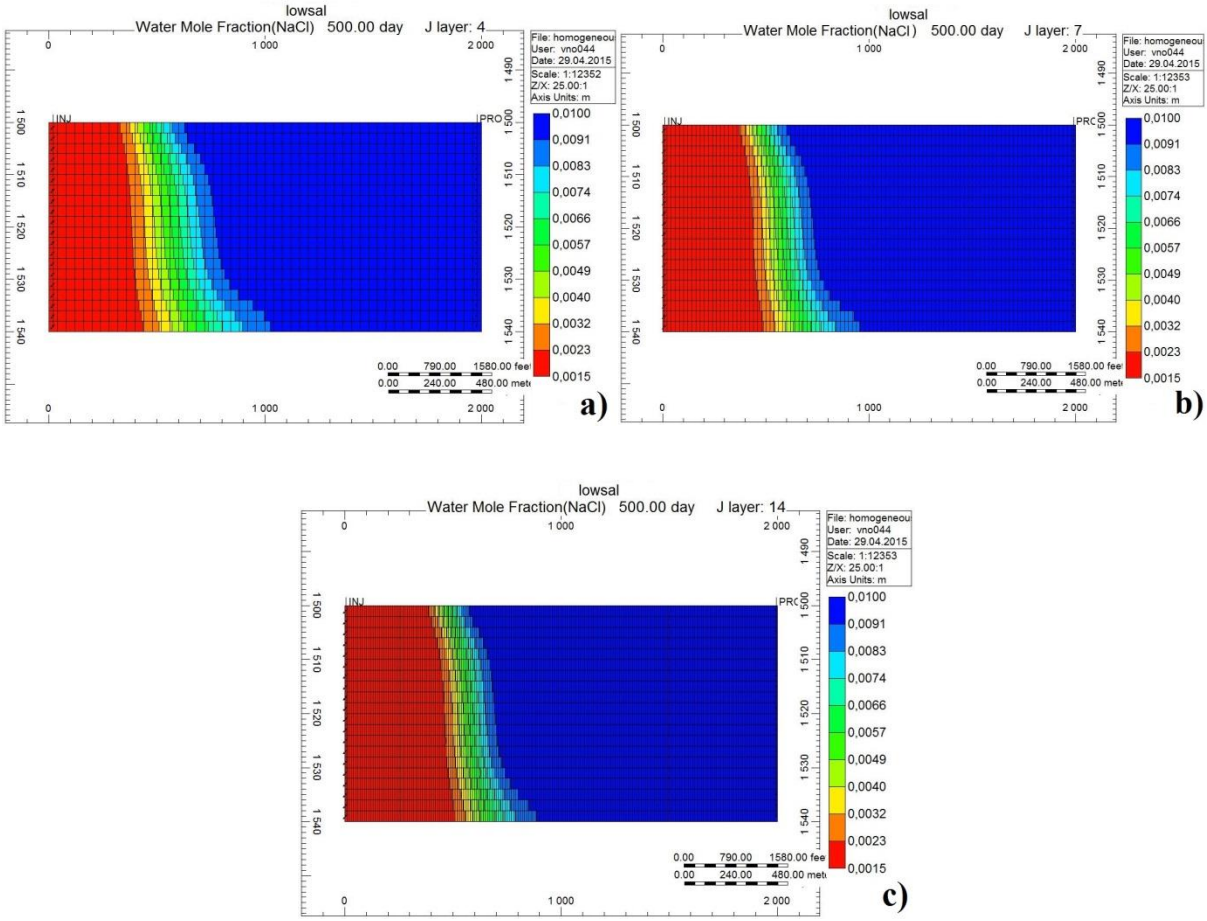

Figure 6-25a,b,c: *Sectional view in XZ-direction of NaCl-concentration after 500 days in coarse, medium, and fine grid, respectively.*

As seen in figures 6-25a,b,c, the salt mixing front is smaller and more stable for the finer grids, due to a smaller numerical dispersion. From Figure 6-14 it is clear that the water breakthrough is delayed, and with a stable salt mixing front the decrease in NaCl-concentration will be slower, initially. This can be seen in Figure 6-26. One can also see that the delayed effect gets smaller for each grid refinement. Each of the finer grid models accounts for a double amount of cells in the X and Y-direction, i.e the medium grid has twice the number of cells in X- and Y-direction than the coarse model and the fine model has four times the number of cells in X- and Y-direction than the coarse model. However, the delay is

larger from the coarse-to medium model than the medium- to fine model. This shows a trend of the smaller the grid block size for each model, the smaller the delay is. The finer the grid block sizes become, there will at some point be no significant change in this delay, meaning the physical dispersion will eventually be equal for the finer grid block sizes.

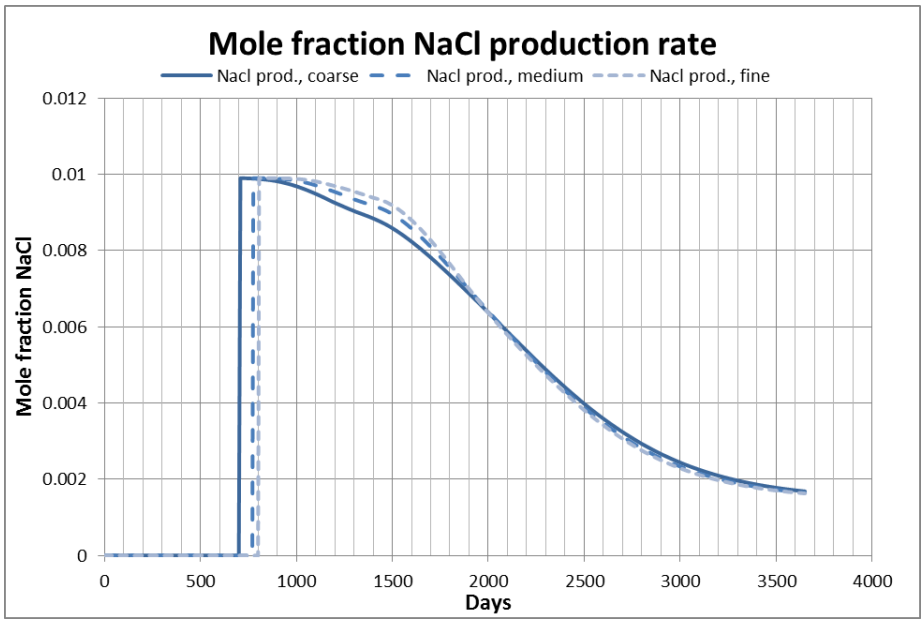

Figure 6-26: P*roduction rate of mole fraction NaCl for the different grid resolutions in lowsal waterflooding.*

By investigating each block individually one can see the difference in dispersion with varying depth. Figure 6-27a,b,c,d show the water saturation and NaCl-concentration in grid blocks in different layers in the reservoir. The grid blocks chosen are located at the dimensionless reservoir coordinates $X_D = 0.8$ and $Y_D = 0.5$, where a value of 1 would imply the end of the reservoir. For layer 15 the saturation starts to increase after 700 days while the NaCl-concentration starts to decrease a bit after. The same scenario occurs in layer 10, with an increase in water saturation before the decrease in NaCl-concentration. In both layer 15 and layer 10, the block water saturation increases before a reduction of salinity occurs, implying a displacement of connate highsal water by the injected lowsal water.

The opposite occurs in layers 5 and 4. There is a salinity reduction before the saturation increase, implying a mixing between the injected and connate water in front of the water bank. Somewhere between layers 10 and 5 there should be an equilibrium point where the salt front progresses at an equal pace as the water front. Figure 6-27a,b,c,d are taken from the fine grid model, and there is a similar trend in the coarse models with the only variation being which point in the reservoir the "equilibrium point" is, due to the grid resolutions effect on the waterfront.

In Figure 6-27c and 6-27d there is a small "pit" in the water saturation curves before they start increasing. These pits show lower water saturation than the S_{wi} utilized in the relative permeability curves, indicating an error or miscalculation of some sort. This error is a result of an erroneous interpolation between the relperm curves, as the NaCl-concentration has already started to decrease. This kind of error also appears in chapter 6.3.2 where a decrease of NaCl-concentration results in a lower S_w. This phenomenon only occurs in the upper parts of the reservoirs where the water is not able to flow, or has a harder time flowing, due to the gravitational pull.

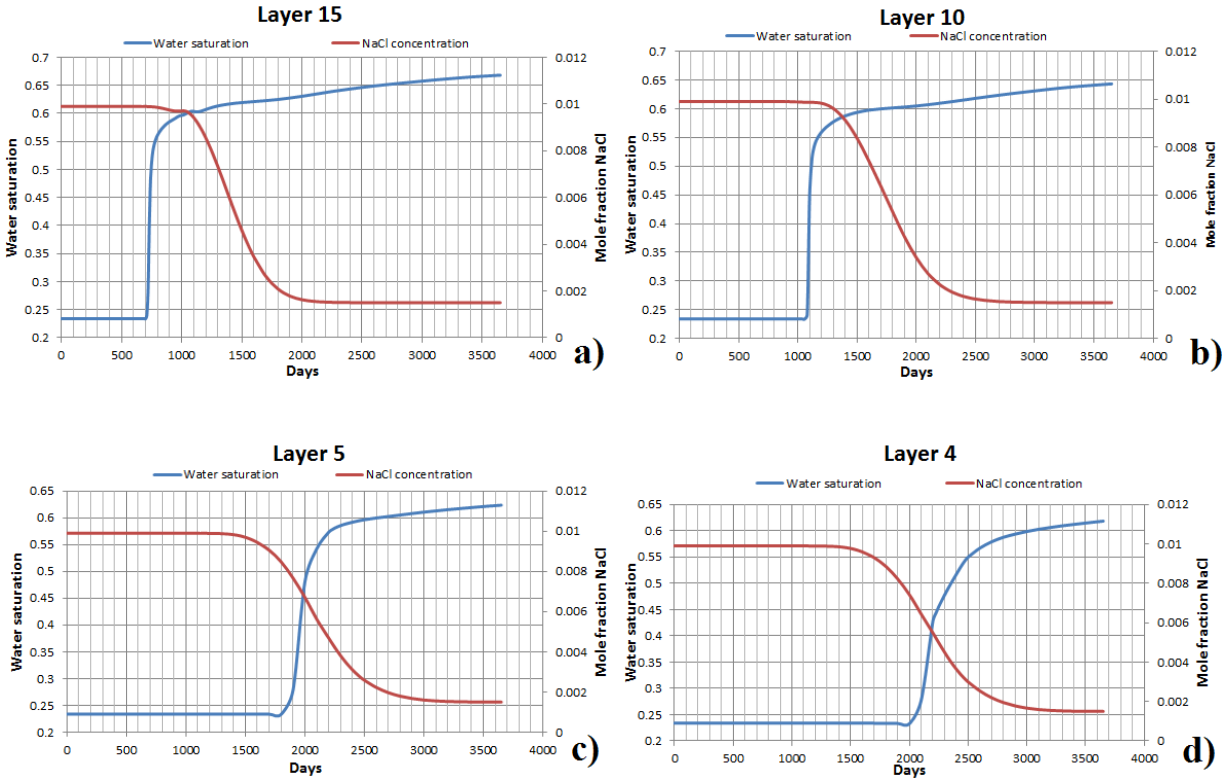

Figure 6-27a,b,c,d: *Water saturation and NaCl-concentration in grid blocks in various layers in the reservoir.*

6.3.2 Tertiary low salinity brine injection

In the tertiary low salinity brine simulation, the reservoir is first flooded with 1 PV of highsal water followed by 1 PV injection of low salinity water. Total production time stretches over 20 years, 10 years with highsal injection followed by 10 years of lowsal injection, with a constant injection rate throughout the whole production period. The results presented in this subchapter can be considered as a continuation of the results in chapter 6.1.

6.3.2.1 Increased oil recovery

Looking at the cumulative production from the highsal-only and highsal-lowsal injection, Figure 6-28, one can see that although the oil production with HS-only injection is stagnating it is still increasing, meaning that the cumulative production could be increased with a longer production period. Therefore, the increased recovery expected from the low salinity water injection is therefore not only due to the lowsal effect but also occurs because of the

increased production period. The same applies for the HSLS graph; given an injection of "only" 1 PV of LS water, recovery would be increased with an increased production period.

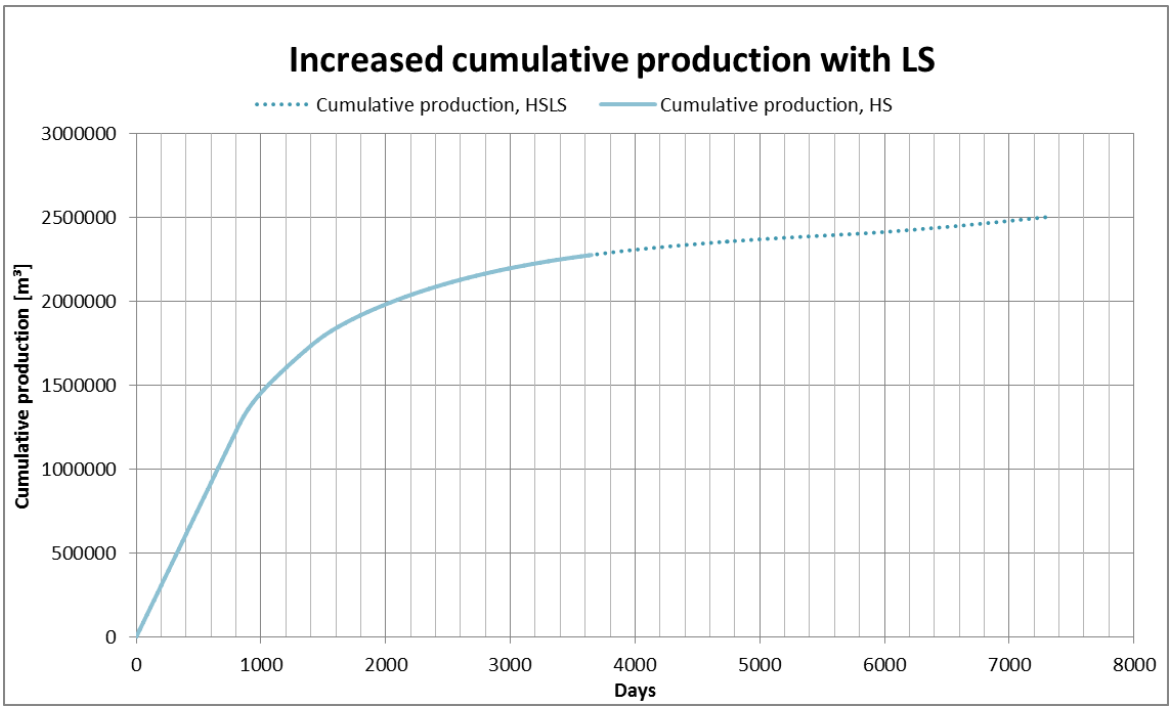

Figure 6-28: *Cumulative oil production in highsal injection, fine grid.*

The HSLS curve continues on the same slope as the HS-curve until the curvature starts increasing around 5500 days, meaning that a noticeable difference in production takes 1850 days as the lowsal injection starts after 3650 days. This could be seen more clearly by looking at the oil production rates for the two cases.

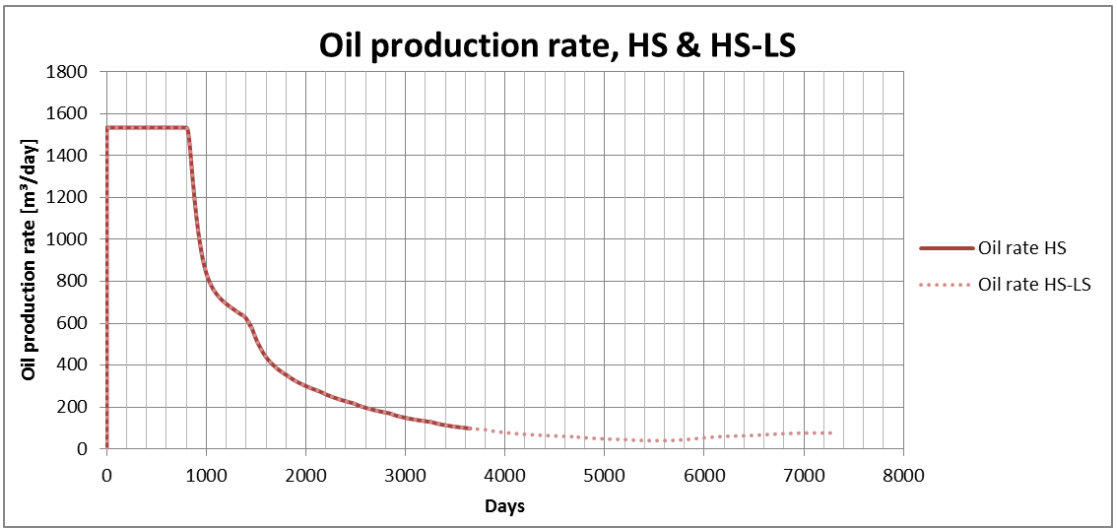

Figure 6-29: *Oil production rates for HS and HSLS in the fine grid.*

As seen in Figure 6-29, the production rate continues decreasing long after the low salinity water initiates. At around 5500 days the production starts to increase again due to the lowsal water causing a reduction of residual oil in the reservoir.

The regional production is not affected to any significant degree in the lower regions (2-4). The oil liberated from the reduction in S_{or} will migrate upwards due to the density difference and is produced from the upper layers in region 1. The layer production in region 1 shows a production increase in layers 1-2 only, see Figure 6-30.

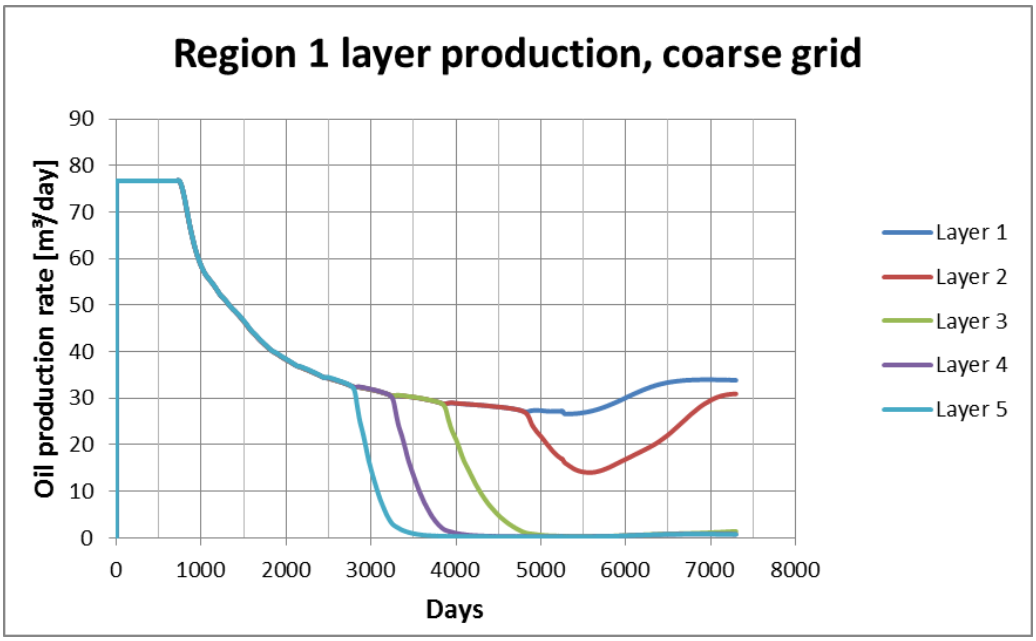

Figure 6-30: *Layer production in region 1, coarse grid.*

As seen in Figure 6-30 there is a marginal increase in production in layers 3-5, and also to a smaller extend in regions 2 and 3 (not shown in Figure 6-30), but the total increase in production comes from the increased production in layer 1 and 2. The increase in layer oil production in the lower layers comes from the liberated oil in the area near the producing well. The larger the distance from a grid cell to the producer, the longer time it takes before the cell`s liberated oil is being produced, and it is thus affected by the density difference over a longer period, resulting in an increased production in the upper layers.

Comparing the production rates in layer 1 and 2 between the grid models shows a slight difference.

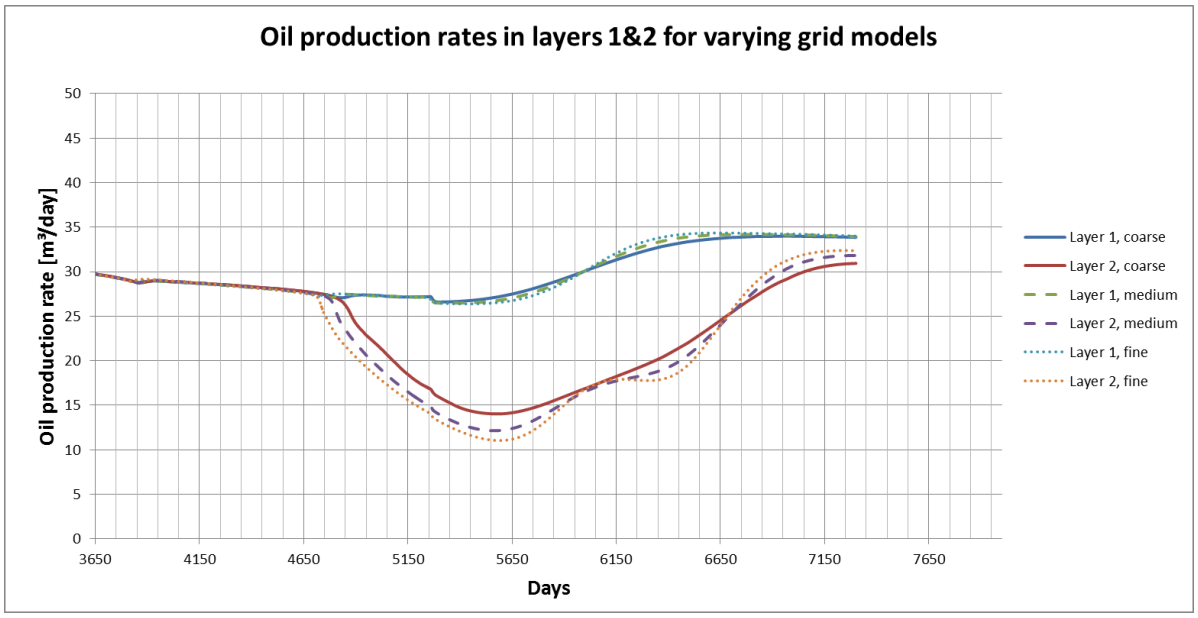

Figure 6-31: *Oil production rates in layer 1&2 in HSLS for the different grid resolutions, from start of LS injection.*

One can see in Figure 6-31 that the production in layer 2 starts to decrease for the fine grid first. As stated earlier the water front tends to be sharper and steeper for the finer grid models, resulting in a delayed water breakthrough. However, at time of water breakthrough the water-cut increases faster for the finer grids due to the steeper waterfronts, and therefore reaching breakthrough in certain layers before the coarser models. Despite of the fine grid reaching water breakthrough first, all the grid models have an equal decrease in production before increasing again.

Another noteworthy result in Figure 6-31 is the shapes of the curves when the production increases in layer 2 for the medium and fine grid. Instead of a steady increase the production increases in an oscillating fashion. This could be an indication of an uneven migration of the liberated oil with varying grid resolution.

Due to there already being a relatively large water-cut when the LS water injection starts, this leads to poorer displacement efficiency in the reservoir leaving the upper layers filled with oil after ended simulation. The injected water flows downwards in the reservoir rather than displace this oil. Figure 6-32a,b shows a comparison of the reservoir after HS and HSLS flooding, respectively.

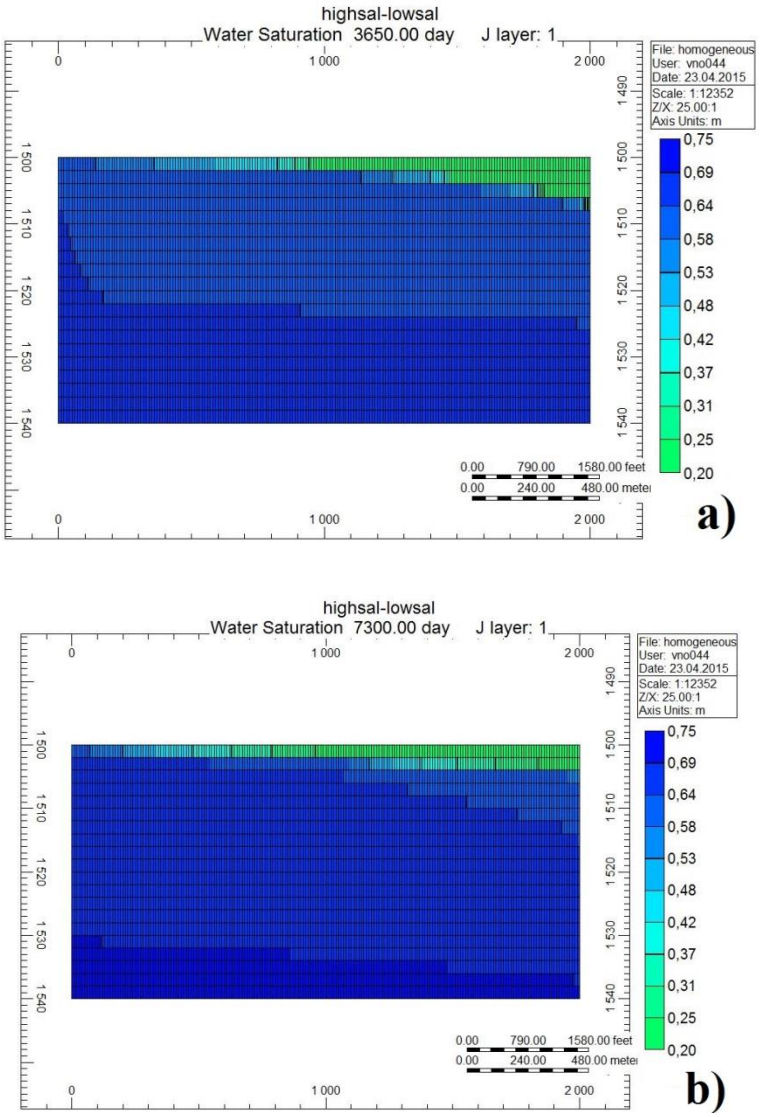

Figure 6-32a,b: *Sectional view in XZ-direction of water saturation in fine grid after highsal flooding and highsal-lowsal flooding, respectively.*

In Figure 6-32a) and Figure 6-32b), the water saturation in layer 1 “withdraws” despite of 1 additional pore volume injected. This shows why the increase in oil production only occurs in the top layers, as seen in Figure 6-31.

When comparing the HS and HSLS production results, naturally the latter simulation provides a higher recovery due to increased production time and the lowsal effect. The results can be found in Table 6-8.

Table 6-8: *Production results for HS and HSLS simulations.*

	HS cum. Prod [m³]	RF HS	HSLS cum. Prod. [m³]	HSLS RF	Increased RF
Coarse grid	$2.2695*10^6$	0.5290	$2.5001*10^6$	0.5828	**5.3745 %**
Medium grid	$2.2750*10^6$	0.5303	$2.5029*10^6$	0.5834	**5.3139 %**
Fine grid	$2.2780*10^6$	0.5310	$2.5037*10^6$	0.5836	**5.2623 %**

As earlier stated, a finer horizontal grid resolution seems to result in a slightly increased recovery. This applies for both the HS and the HSLS simulations. But the increased recovery (shown in green in Table 6-8) seems to contradict this trend by showing a larger increased recovery by a coarsening of the grid, i.e the increased recovery due to the lowsal effect is larger with a coarser grid. This larger increase could be due to the Nacl progressing faster with larger grid blocks, thus interpolating at an earlier time lowering the S_{or} and obtaining the maximum water saturation at an earlier time. But this theory does not comply with the fact that the HSLS simulations have a higher recovery with increased grid resolution. However, the increase in recovery with finer grid models is very small compared to the total recovery, leading to the conclusion that horizontal coarsening of grid blocks does not affect the total recovery.

6.3.2.2 Salt dispersion

As addressed in chapter 3.3, the injected low salinity water will displace the connate water while creating a mixing zone with a decreasing salt concentration for the salt. By the time lowsal injection starts most of the reservoir, except for the upper layers, will be filled with a saturation equal to (or close to) S_{or}. Since the water is defined in a continued phase due to the reservoir being water-wet, the salt is able to advance throughout the reservoir and not

necessarily following the water. The salt dispersion is not affected by the gravitational forces to the same extent as the oil and water but since the salt is dispersed in the water phase, and the water is to a large degree affected by the gravitation, one would expect to see some curvature of the salt concentration front. As with the water front, one would also expect that the salt concentration front is more smeared out with a coarsening of the grid. Figure 6-33a,b,c show the salt concentration fronts for the different grid models after 5000 days.

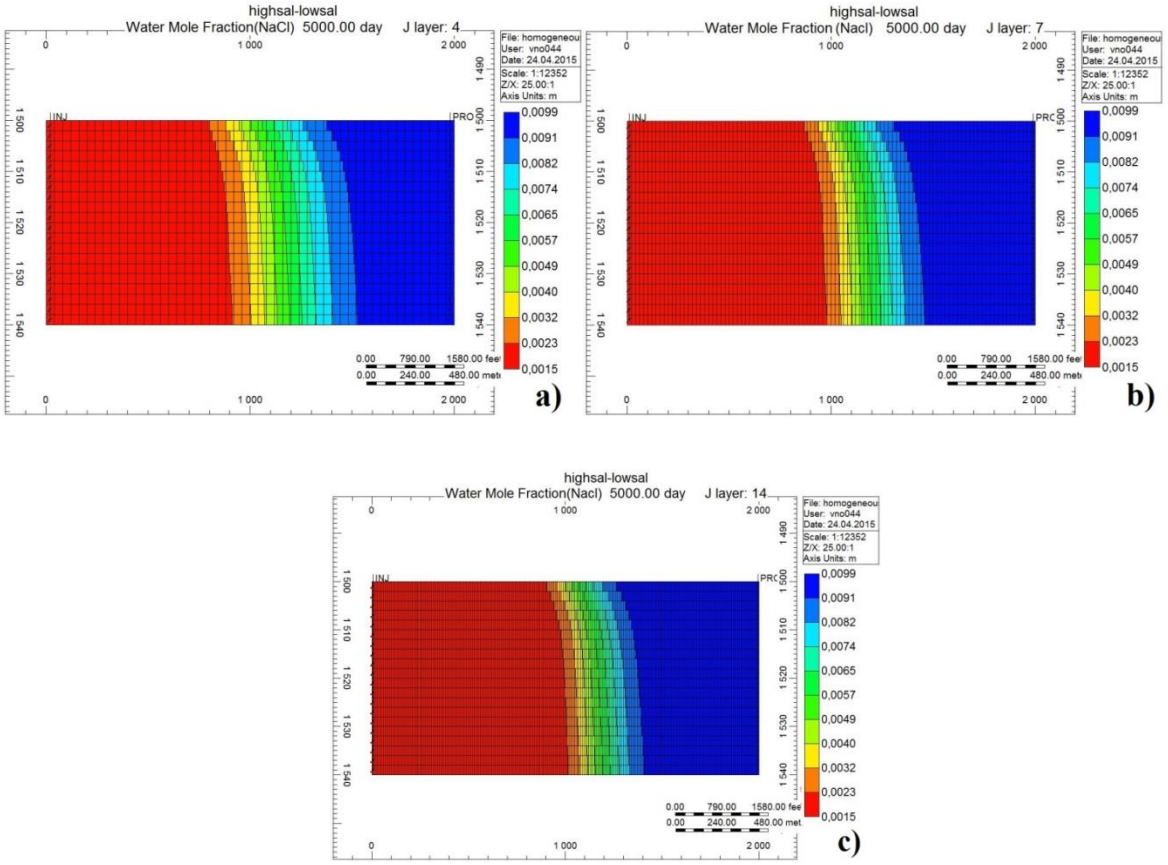

Figure 6-33a,b,c: *Sectional view in XZ-direction of NaCl-concentration after 5000 days for the coarse, medium and fine grid, respectively.*

As expected, there is a clear trend of a sharpening of the front with the finer grid resolutions, and the coarse grid has progressed a bit further. The mixing zones are larger than shown in the figure, but the color scale limits the possibility to observe this more accurate.

If one were to look at the mole fraction NaCl produced over time one could achieve a more accurate description of how the salt mixing zone is spread out in the different grid models. This can be seen in Figure 6-34.

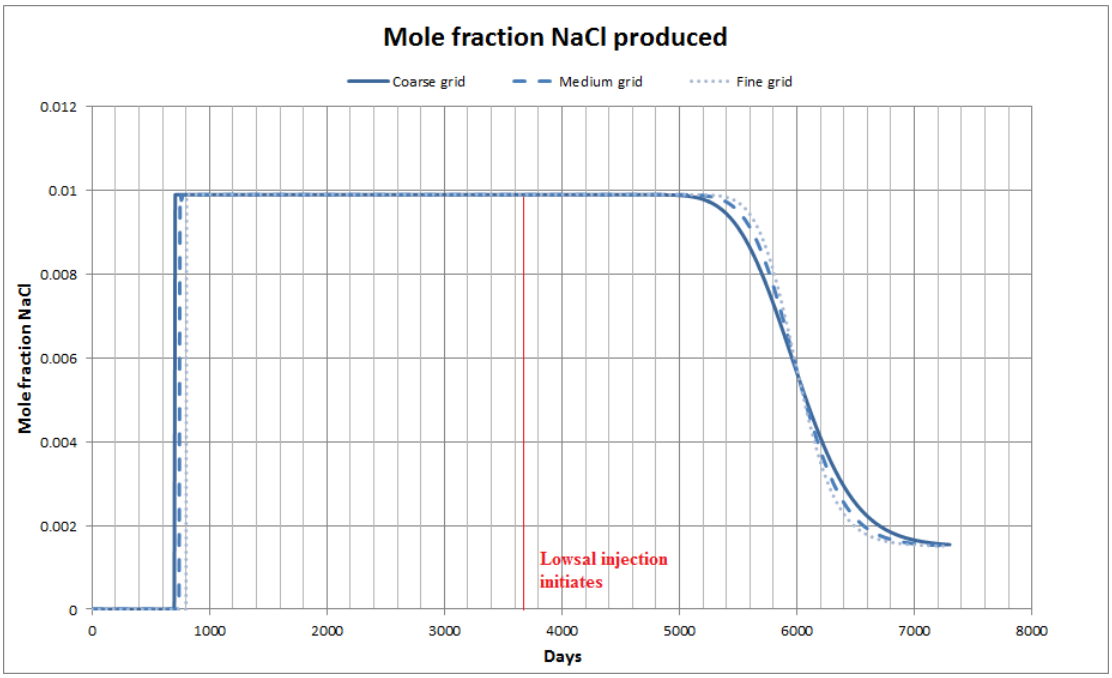

Figure 6-34: *Mole fraction NaCl produced for the different grid models in homogeneous reservoir.*

Figure 6-34 shows an expected relationship between the grid models, with a delayed and sharper curve for the finer grids. Red line indicates start of lowsal injection. The deviation between the grid models is very small, showing that dispersion of salt is not very sensitive to grid resolution and that the deviation observed is mostly due to a decrease of numerical dispersion.

6.3.2.3 Block saturations

Some unpredictable results were found in the grid blocks in the upper layers (layer 1&2) regarding saturations. Due to the water not being able to displace the oil in most of these layers, the oil saturation never decreases. The total dispersion coefficient is defined in keywords *DISPI/*DISPJ/DIPSK*, thus making the salt progress in the layers. Upon salt

entering the grid blocks, an interpolation between the two relative permeability sets occurs and this is when the surprising results present themselves. When the NaCl mole fraction decreases the water saturation decreases also, and the oil saturation increases accordingly, thus having saturations beyond the relative permeability curves utilized, see Figure 6-35.

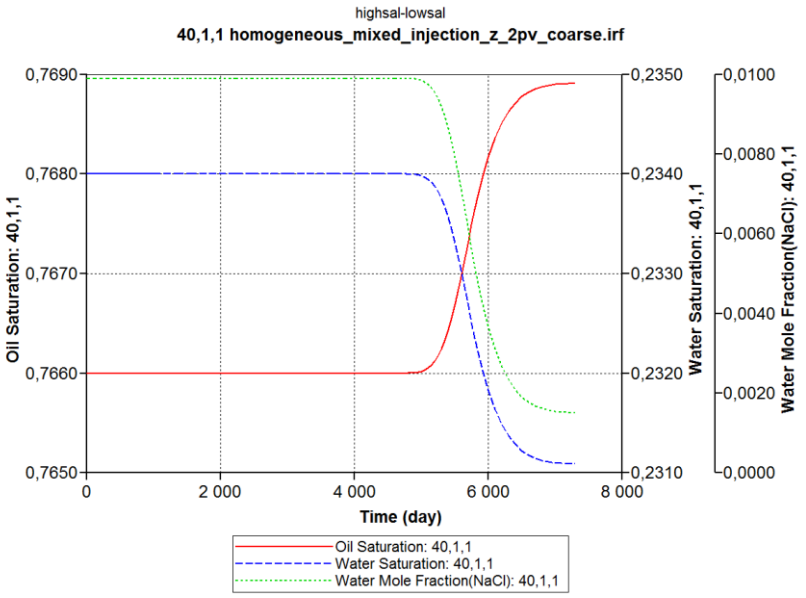

Figure 6-35: *Plot of water &oil saturation, and NaCl mole fraction in grid block in layer 1 in HSLS run.*

Because of the water saturation never increasing, the relative permeability of water never increases above 0, thus making it immobile and therefore not giving any reason as to why water seems to flow out of the grid cell. This problem occurs for all grid resolutions. The most obvious solution is to check if the S_{wi} are equal for the two sets of relperm curves. Should the LS-curves have a lower minimum water saturation it would be logical that the saturation decreases in the grid blocks. However, this is not the cause. There are some other factors which could lead to these results: too large convergence margins, too big timesteps, or an erroneous interpolation scheme.

The interpolation scheme in this simulation is set to be quadratic, using the *QUAD keyword, which define which type of interpolation to be used in the interval between zero and non-zero. However, the quadratic interpolation is the recommended type for this simulation, so this could not be the deciding factor.

The convergence margin is set using the keywords *CONVERGE *TIGHTER. This setting gives the smallest convergence margin error, minimizing the material balance error. It can therefore not be the deciding factor either.

It might be possible that the timesteps were too large, making the calculations too large for each timestep and therefore resulting in a matrix solver failure. The maximum timestep size has in these simulations been set to 10 days, *DTMAX=10. However, the data log file showed 0 matrix solver failures and 0% IMPES (Implicit pressure, explicit saturation) therefore excluding the timestep size being a main cause. Just to confirm, a single simulation with a maximum timestep of 5 days was performed; no significant changes were observed.

6.4 Results in homogeneous reservoir

Table 6-9 shows a comparison of the production results between the HS, LS, and HSLS simulations. A comparison of the HS and HSLS run does not exclusively show the lowsal effect as the injection volume is twice the size in the HSLS run.

Table 6-9: *Comparison of results in homogeneous reservoir*

Simulations	Highsal [RF]	Lowsal [RF]	Highsal-Lowsal [RF]	Increased recovery, %
Coarse	0.5291	0.5483	0.5828	**9.2141**
Medium	0.5303	0.5505	0.5835	**9.1174**
Fine	0.5311	0.5515	0.5837	**9.0114**
		Deviation		
Coarse-medium, [%]	**0.2268**	**0.4012**	**0.1201**	-
Medium-fine, [%]	**0.1509**	**0.1817**	**0.0343**	-
Coarse-fine, [%]	**0.3777**	**0.5829**	**0.1544**	-

The increased recovery column to the right in Table 6-8 shows the additional oil production when 1PV highsal is followed by 1 PV lowsal. The coarse and medium models show a larger increased recovery than the fine model.

Roughly, the LS simulations resulted in a 2% increased production compared to the HS runs. When keeping in mind that these results are after (only) 1 reservoir pore volume injected, there is reason to believe that an increased production period would increase the differences between the two.

When comparing the salt dispersion in the reservoir one needs to look at the HSLS and LS runs. The difference in the water saturation at start of the lowsal injection is expected to make a difference. The injected water will in the LS run displace the oil and thus be much more affected by the gravitational forces than for the HSLS run. This will also have an impact on the salt concentration front as the salt will follow the water. Since large parts of the reservoir is already filled with high salinity water in the HSLS run, the injected lowsal water will have to mix with a much larger volume of connate water, thus hindering the progress of the salt front to some degree. In the LS run, the salt will to a larger degree follow the water as it displaces the oil, and therefore follow the flow pattern of the water as it flows faster in the lower layers. Figure 6-36 shows a comparison between the two runs, with mole fraction NaCl produced over time.

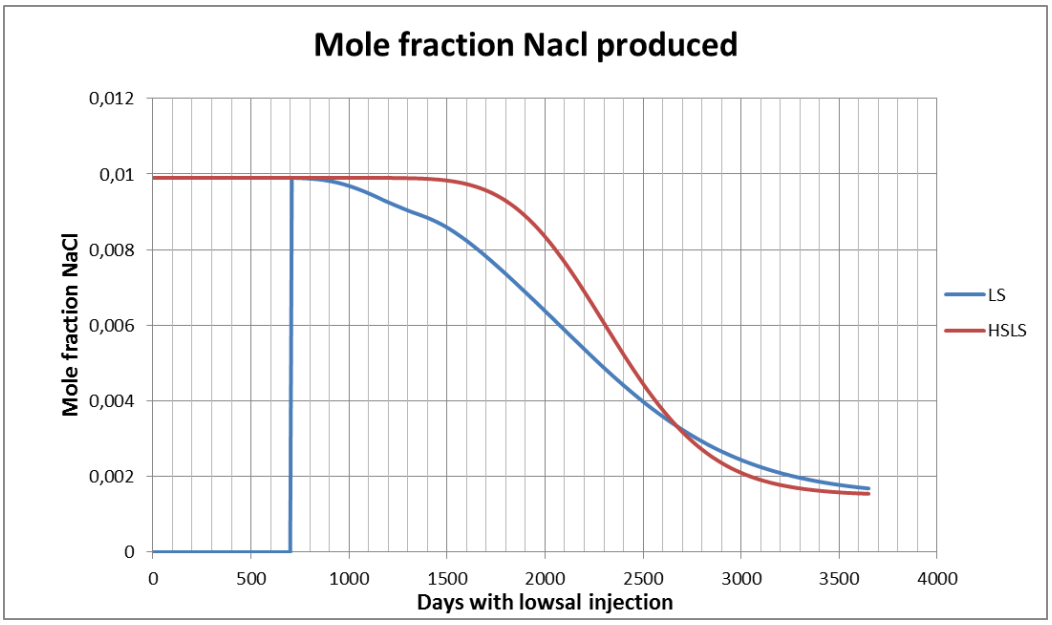

Figure 6-36: *Mole fraction NaCl produced after days of injection lowsal water, coarse grid.*

Figure 6-36 shows the production of mole fraction NaCl as a function of number of days with lowsal injection in the coarse grid. One can see that at the water breakthrough for the LS run, the initial mole fraction is of high salinity, 0.0099, but starts decreasing right after. This indicates a large amount of mixing as the concentration is steadily decreasing after the initial breakthrough. The mixing zone grows larger in the lower zones.

The HSLS curve starts to decline at a later time, around 800 days, due to the higher volume of connate salt in the mixing process. When it starts to decline, the mole fraction NaCl drops faster for the HSLS run than for the LS run, indicating a more stable salt front throughout the reservoir. It is also only the HSLS run that reaches a full low salinity water production before simulation end.

Using the 3D-viewer could give a better explanation on how the salt mixes in the two reservoirs:

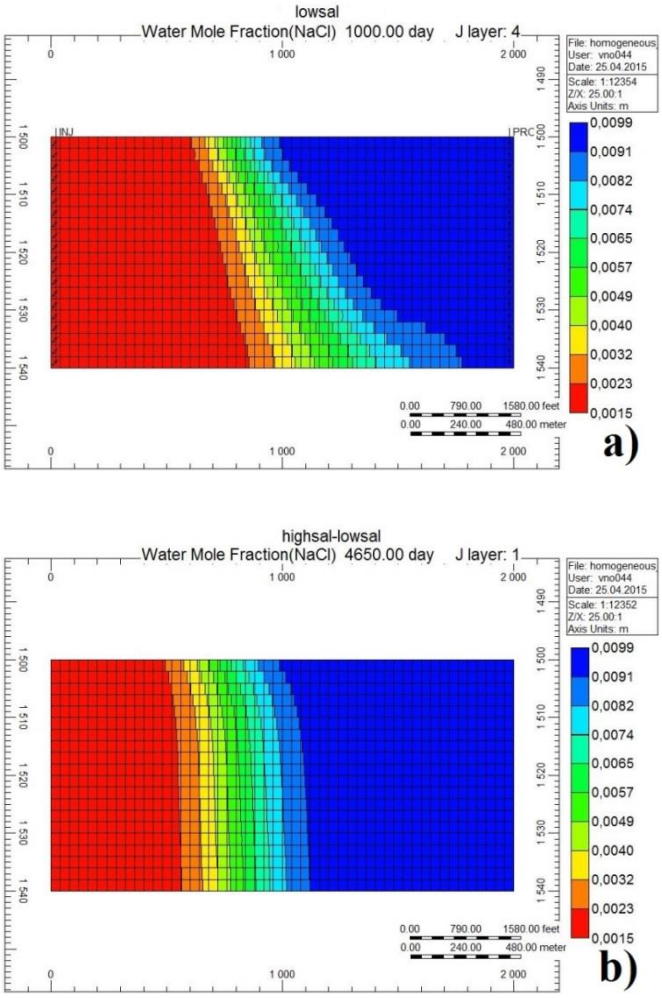

Figure 6-37a,b: *Sectional view in XZ-direction of NaCl fronts in coarse grid for a) LS simulation, and b) HSLS simulation.*

Figure 6-37a,b show the salt fronts in the LS and HSLS runs after 1000 days of lowsal injection. As seen, the LS run is more affected by the gravitational pull on the water, resulting in an advance of the front in the lower layers, and a much larger mixing zone in whole. There is some advance as a function of depth in the HSLS run but not significant. This is because there is equal amount of water saturation at the salt fronts. Since the water is unable to displace the oil in the top layer, the salt mixes with the connate water present in this area, and advances at the approximately same pace. It is worth mentioning that the salt fronts are actually larger than shown in the figures, and that the LS run shown in Figure 6-37a have already started producing water with a lower than initial salinity.

7 Heterogeneous reservoir

The simulations presented so far have been in a homogeneous reservoir with no flow obstructions other than a 10% vertical permeability. The following chapter concerns simulations performed in a more heterogeneous reservoir with a permeability difference between the regions. This permeability difference will affect the preferred flow pattern of the injected water and thus affect the total recovery of the reservoir. The regions are the same regions utilized in the homogeneous reservoir, see table 6.2, with region 1 and 3 now being low-permeable with a permeability of 200mD, and region 2 and 4 maintain the original permeability of 2000mD. Vertical permeability is still 10% of horizontal permeability, i.e 20mD in the low-permeable regions and 200mD in the high-permeable regions.

7.1 Fluid-flow test

In order to be able to interpret the results achieved from the heterogeneous reservoir, it is important to know how the fluids behave in the reservoir. To get information on this, a fluid-flow test has been performed. In this test the injecting and producing wells has only been perforated in the low-permeable region 3. Since the water is injected in the low-permeable layer it is expected that it will directly flow into the adjacent high-permeable regions and progress at a faster pace than in the low-permeable region. The injection will be equal to the other simulations with a rate of 1500 $^{m^3}/_{day}$, and production and pressure will not be monitored, only the preferred fluid paths. This test will only be performed in the fine grid model, with highsal-only and lowsal-only simulation runs. The lowsal-run gives the opportunity to see how the salt dispersion reacts to the low-permeable regions.

7.1.1 Highsal flooding

Figure 7-1a-f shows the water saturation every 100 days during the fluid flow of for the first 600 days of production, and Figure 7-2 shows the water saturation at ended simulation after 1 PV injected. One can see that the water immediately flows upwards and downwards into the high permeable regions and advances there. After 200 days there is already some gravitational segregation within the high-permeable regions with a faster advancement in

the lower layers. Due to the gravitational pull on the water, some water is flowing into the low-permeable region 3 from the high-permeable region 2 above. The saturation in the top layer in region 3 (layer 11) will show advancement over time, as well as the layer beneath (layer 12) to some degree. The water reaches the end of the reservoir after 500 days (Figure 7-1e) and the water starts coning upwards due to production from region 3 only. At 600 days (Figure 7-1f) the water has reached the producing well and the water-cut will increase until end of simulation.

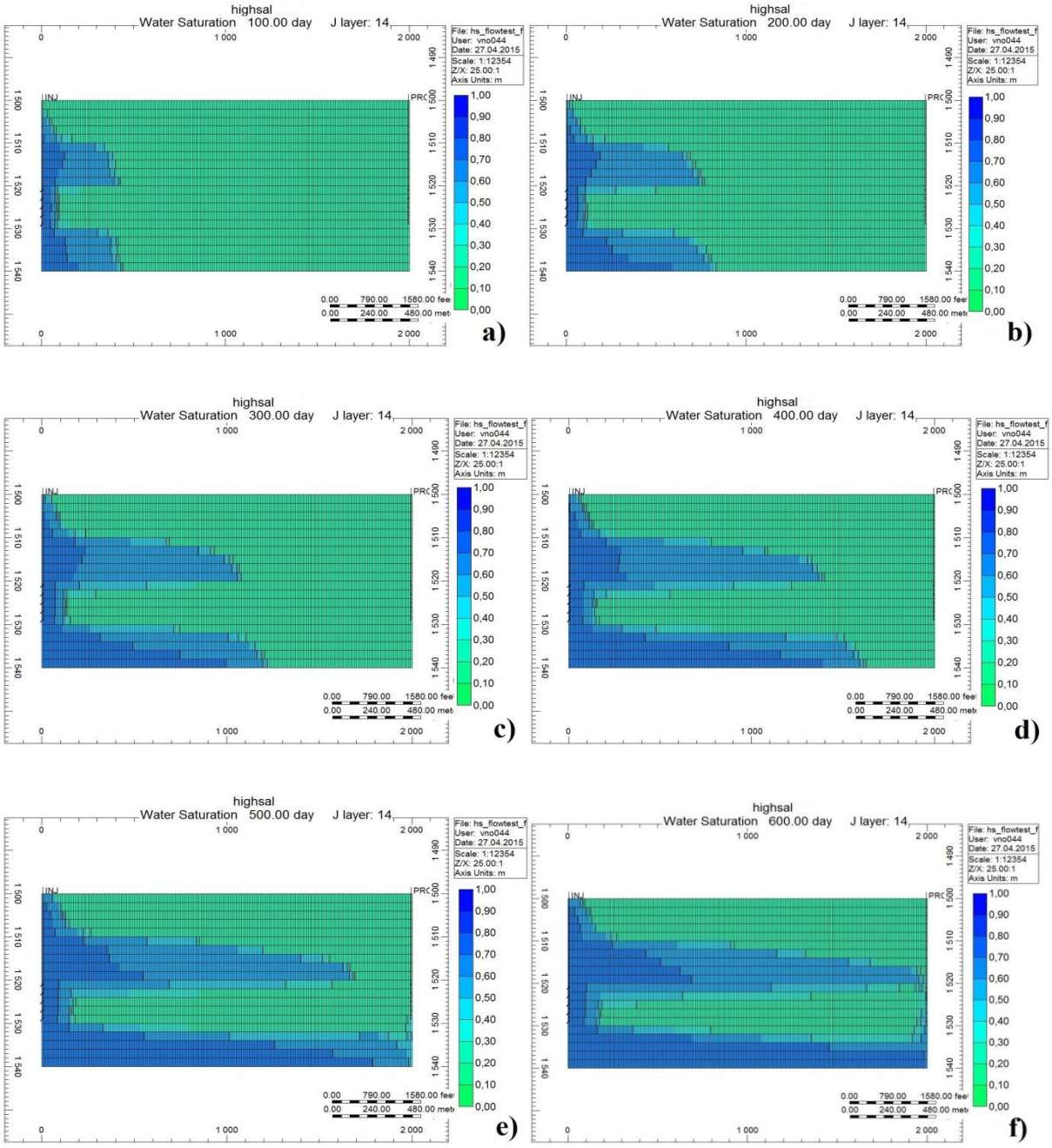

Figure 7-1a,b,c,d,e,f: *Sectional view in XZ-direction of water saturation every 100 days in heterogeneous reservoir during the fluid-flow test.*

When the injecting and producing well is perforated through all 20 layers the outcome will naturally be different. But nonetheless, the fluid-flow test does show the general preferences the water will have in this heterogeneous reservoir and how the permeability difference affects the flow pattern.

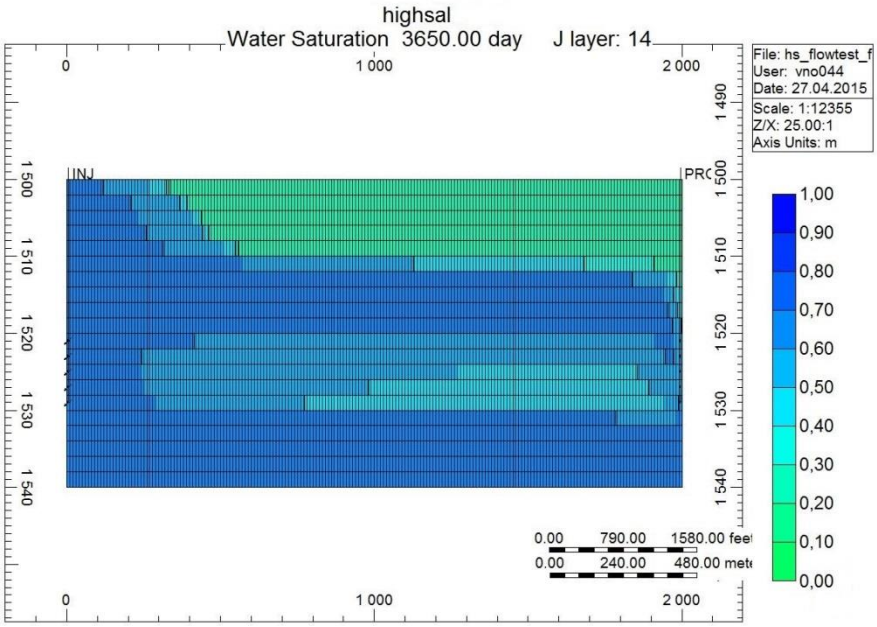

Figure 7-2: Sectional view of water saturation after 1 PV injected highsal water in fluid-flow test.

Figure 7-2 shows the water saturation at simulation end. Most of the upper part of the reservoir, region 1, has been left untouched and region 3 still has a large amount of oil left. However, it is somewhat surprising that the water has advanced this far in region 1 due to the water having to flow upwards *through* the high-permeable region 2 and into the low-permeable region 1, overcoming not only the gravitational force but also the permeability difference between region 1 and 2. This could however be a consequence to the injection rate remaining constant but the area of injection is smaller (20 layers → 5 layers) generating a larger flux movement of water and thus forcing it upwards.

7.1.2 Lowsal flooding

When performing the fluid-flow test with low salinity water we can observe how the salt mixing process is affected by the permeability differences. The flow path of the water will be affected to some degree due to interpolation, but it will not make a big difference. As seen in chapter 6.3.1, the salt mixing front will progress through the reservoir despite the water being unable to flow through the areas because the water is defined as a continuous phase in the grid blocks, and the salt can therefore move through it by diffusion. One would therefore also expect the salt to advance through region 1 without injected water present. When comparing the HS and LS fluid-flow tests, the LS flooding showed a faster advancement of water in region 2 than for the HS flooding, and vice versa in region 4. Due to the water phase density is to some degree dependent by the NaCl-concentration, this makes the connate highsal water slightly denser than the lowsal water. This is probably the reason for the advancement in the different regions. But the overall flow patterns are very much alike for both the highsal and lowsal fluid-flow tests with a preferred water flow path in the high permeable regions above and underneath region 3.

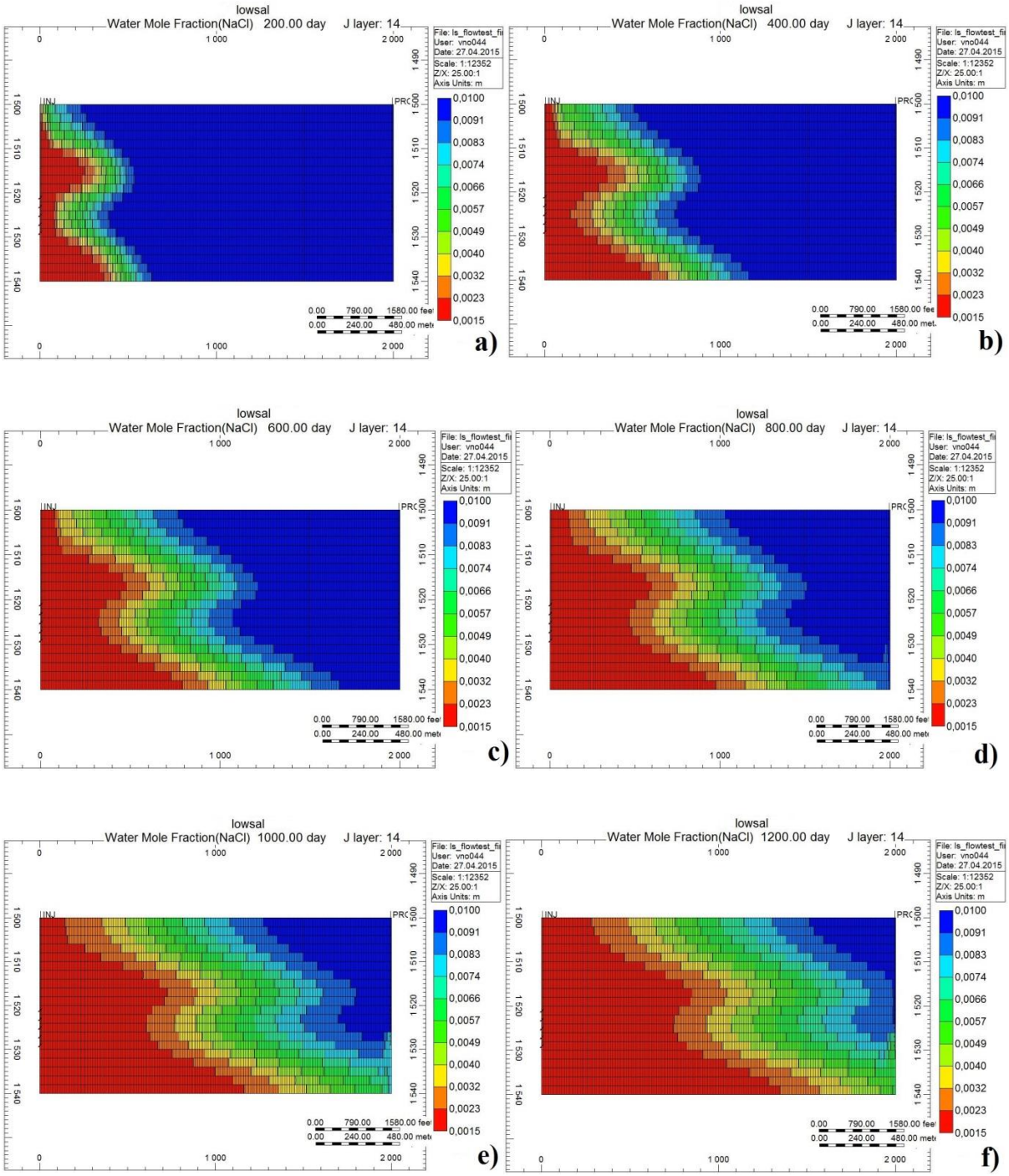

Figure 7-3a,b,c,d,e,f: Sectional view in XZ-direction of NaCl-concentration at every 200th day, LS fluid-flow test.

Figure 7-3a-f show the NaCl-concentration every 200th day for the first 1200 days of lowsal injection in. The salt front advances faster in the high-permeable regions, and in the lower layers of these regions, but there is also a clear advancement in the low-permeable regions.

The low-permeable region 3 is “trapped” between the two high-permeable regions 2 and 4, and it is therefore a large amount of salt mixing in this region. Due to the spreading of the injected water the salt mixing zone gets larger as it advances through the reservoir, and at some point stretching over half of the reservoir length in the upper layers.

The results presented in subchapter 7.1.1 and 7.1.2 can be considered as “background knowledge” when performing the other simulations in the heterogeneous reservoir. They will naturally differ to some extent, but the fluid flow and salt dispersion will to some degree be based on the results above.

7.2 High-salinity waterflooding

As with chapter 6.1, 1 reservoir pore volume of high-salinity brine with a mole fraction of 0.0099 NaCl is injected in the reservoir over a 10 year period. All fluid and reservoir properties are equal to the ones utilized in 6.1 except for a lowered permeability in region 1 and 3, vertical permeability included.

7.2.1 Production results

The production results from the highsal waterflooding in the heterogeneous reservoir showed almost no variations with a varying grid resolution. The cumulative production followed the trend of slightly higher recovery with a finer grid, but the production rate showed almost no change, seen in Figure 7-4. The oil rate drops right before 500 days indicating water breakthrough in region 4, and after around 600 days. There is also a “dip” in production rate after 2600 days, as this marks the water breakthrough in layer 16.

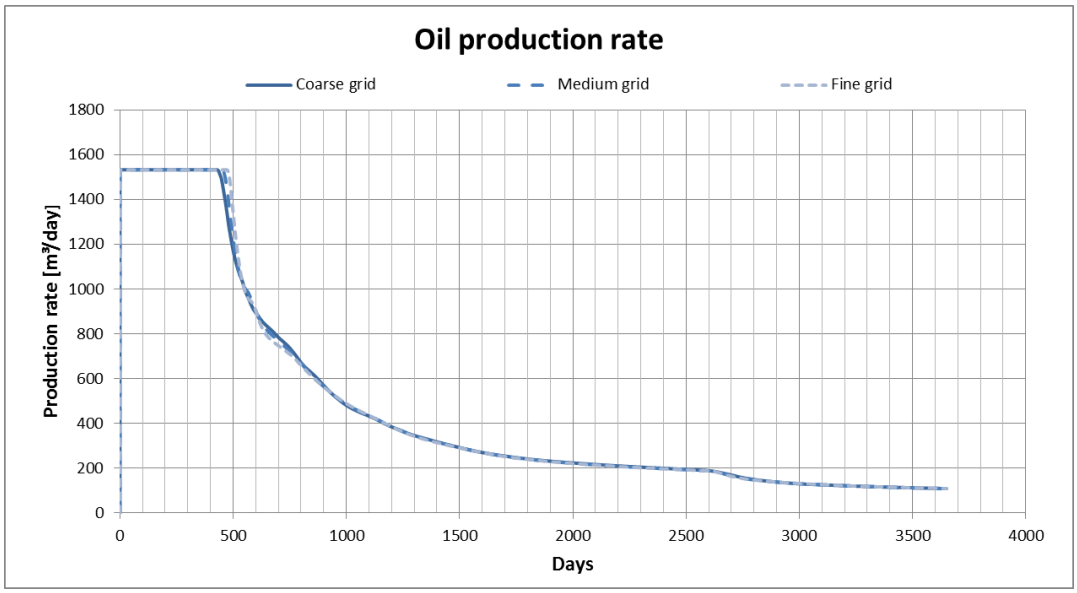

Figure 7-4: *Oil production rate with highsal waterflooding in heterogeneous reservoir.*

Besides from the slightly delayed water breakthrough, no significant variation is observed. Inspecting the regional production rates for the different grid models did not show any specific variation either. This lack of variation, which has been seen in nearly all the homogeneous simulations, is due to the regional differences with high permeable regions. It seems that the "thief-zone" effect on the production results is larger than the grid resolutions effect, therefore showing little to no variation with varying grid resolutions.

Inspecting the displacement in each layer shows a rapid displacement in the high permeable regions 2 and 4 and a slow advancement of water in the low-permeable regions. We know from chapter 6 that the gravitational forces on the water pulls it down thus making displacement poor in region 1 but it was unexpected that region 3 showed such poor displacement. Figure 7-5a,b,c show the water saturation at breakthrough time for the different grid models, and one can clearly see that the progression in region 3 (layer 11-15) is barely present. It seems that almost all of the water injected in layers 1-20 tends to flow directly into the high-permeable regions. It is no surprise that the water prefers to flow in the high-permeable region 2 and 4 over the low-permeable regions 1 and 3 but it is surprising that the difference is to such a large extent. The low-permeable regions have a permeability of 200mD and the high-permeable 2000mD, making the difference one order of magnitude. While this difference is notable, it was not expected for it to have such a large

effect given that an absolute permeability of 200mD is still a reasonable condition for water to flow.

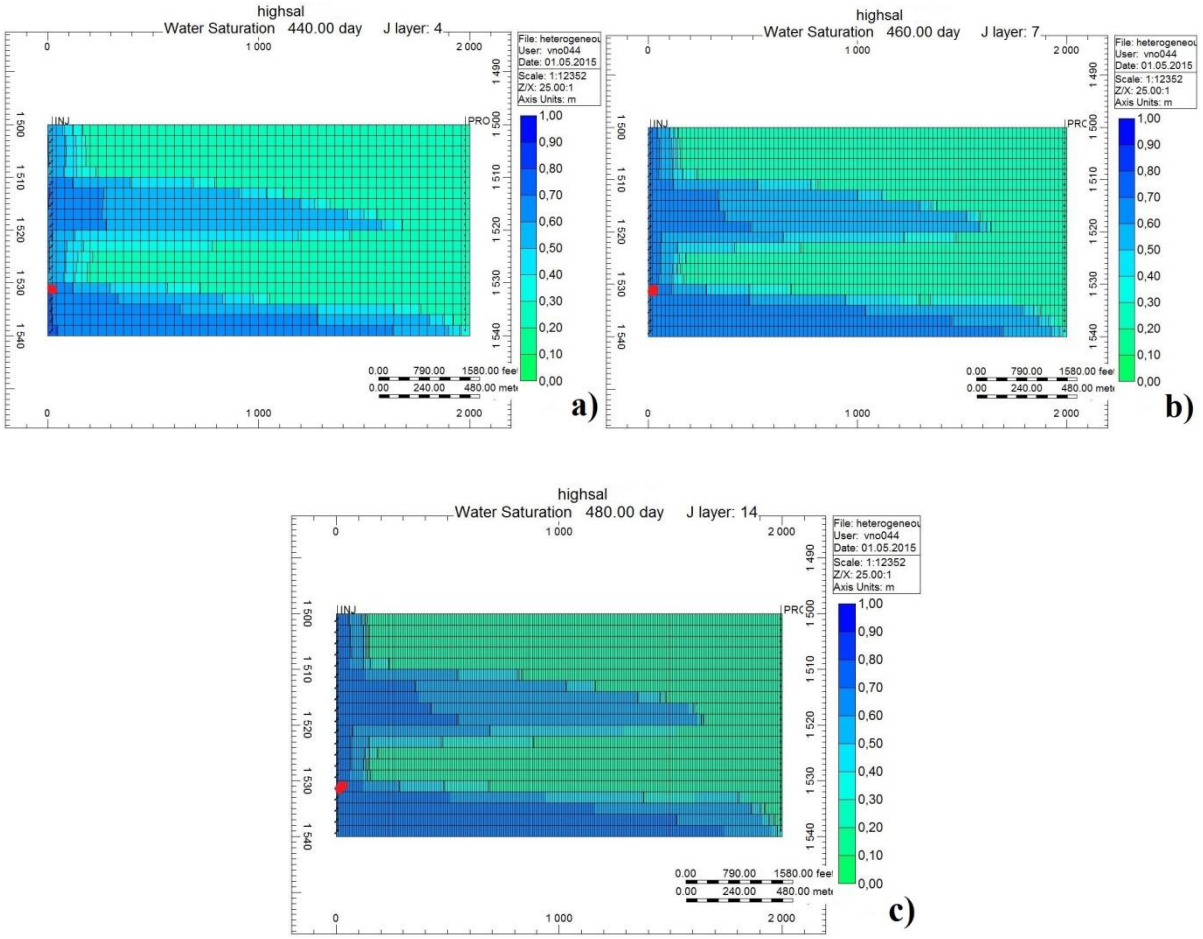

Figure 7-5a,b,c: *Sectional view of water saturation in highsal flooding of heterogeneous reservoir at time of water breakthrough.*

Even within the high-permeable layers the displacement is unstable. The red dots in Figure 7-5a,b,c marks layer 16 which is the top layer in region 4. At WBT the water this layer has not advanced half the distance to the producer even. This in itself is not very unusual given that such behavior is often seen with reservoir flooding, but when all layers in region 2 (which is located higher up in the reservoir) have progressed further it is worth mentioning. Especially since one would expect the bottom layers to fill up with water before the upper layers.

The rapid advancement in region 2 and 4 can be explained when investigating the injection rate within the individual layers and regions. The injection rate is initially set to be 1500 $^{m^3}/_{day}$ for the injection well. For the simulations in the homogeneous reservoir this resulted in an equal injection rate throughout all the 20 layers. With the heterogeneous reservoir, it seems that the permeability difference affects the distribution of the injected water, injecting a higher volume in the high-permeable layers.

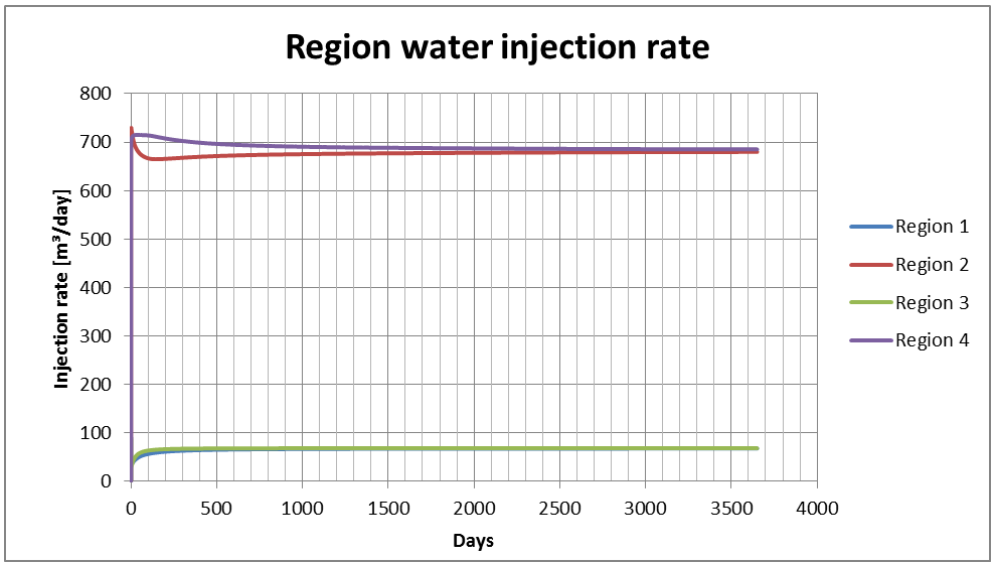

Figure 7-6: *Regional water injection rates in heterogeneous reservoir.*

Figure 7-6 shows the regional injection rates, and one can see that the injection rates for the high-permeable regions 2 and 4 are much higher than for the low-permeable regions 1 and 3. Under closer inspection, the injection difference is about 10 times larger for the high-permeable layers, which follows the Dykstra-Parson method:

$$Q_i = \frac{k_i h_i}{\sum_{i=1}^{n} k_i h_i} \qquad (7.1.1)$$

Where Q_i is flux flow of water in layer *i,* k_i is permeability in layer *i,* and h_i is the height of layer *i.* Given that all the cells are of the same height and the permeability is 10 times higher for the high-permeable layers than the low-permeable layers (200mD → 2000mD), this explains why the injection rate is higher in the high-permeable layers.

7.3 Low-salinity waterflooding

7.3.1 Secondary low salinity brine injection

Secondary injection of low-salinity water should lead to an increased recovery compared to highsal injection due to the lowered S_{or}. However, with the occurrence of interpolation from highsal- to lowsal relative permeability curves the oil permeability gets lowered instantly and thus lowering the flow abilities of the oil. This could have an effect on the oil production rates, when compared to the highsal injection. This comparison will be presented in chapter 7.4.

7.3.1.1 Production results

A variation in grid block size did not show any significant variation in total recovery, only the regular small increase with a finer grid. The production rates showed a small variation with a delayed water breakthrough time and minor differences around after 600-700 days, but other than that no difference. This can be seen in Figure 7-7.

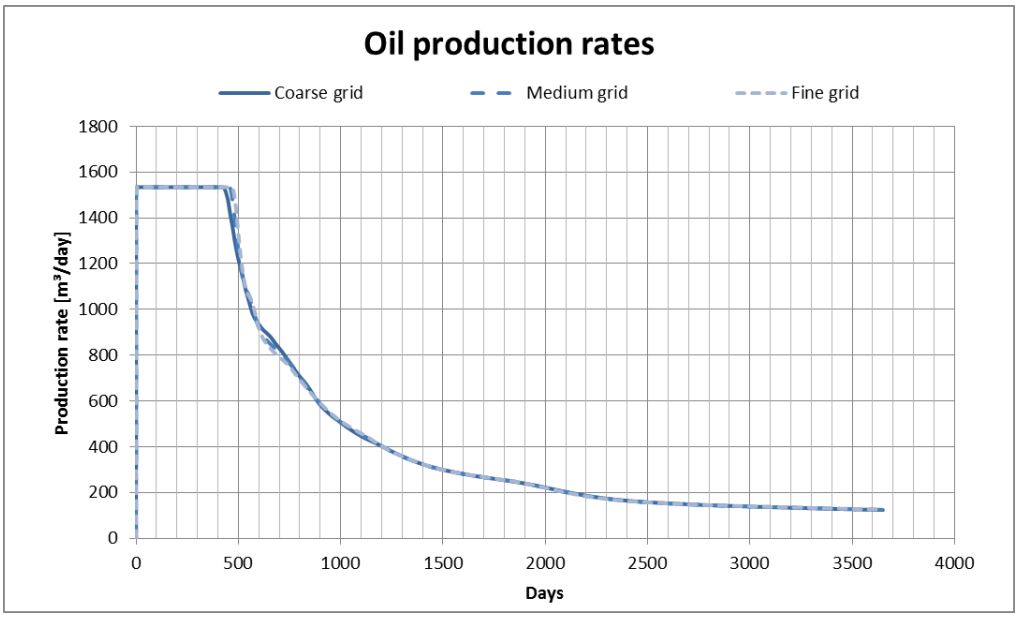

Figure 7-7: *Oil production rate for low salinity waterflooding, heterogeneous reservoir.*

When comparing results in Figure 7-7 to the lowsal injection scheme performed in the homogeneous reservoir (Figure 6-22) one can see that the variation in between the grid models is much smaller in the heterogeneous reservoir than in the homogeneous reservoir. The earlier breakthrough in the heterogeneous reservoir is self-explanatory as most of the water pushes through high-permeable channels (region 2&4), but production rates are almost identical in the heterogeneous reservoir while they differ more in the homogeneous reservoir. It seems that the high-permeable regions affects the waterflood to such a degree that the variations observed in the homogeneous reservoir does not appear, at least not in the same extent.

Studying the water front in region 4, one can see a similar “bump” as observed in chapter 6.2.1.1 with the high-viscosity oil, where the water is flowing upwards as the grid resolution gets finer. This is shown in Figure 7-8a,b,c. Note that the color scale has been changed to give a better view of the saturation differences within the layers, with a darker and more red-ish color indicating higher water saturation.

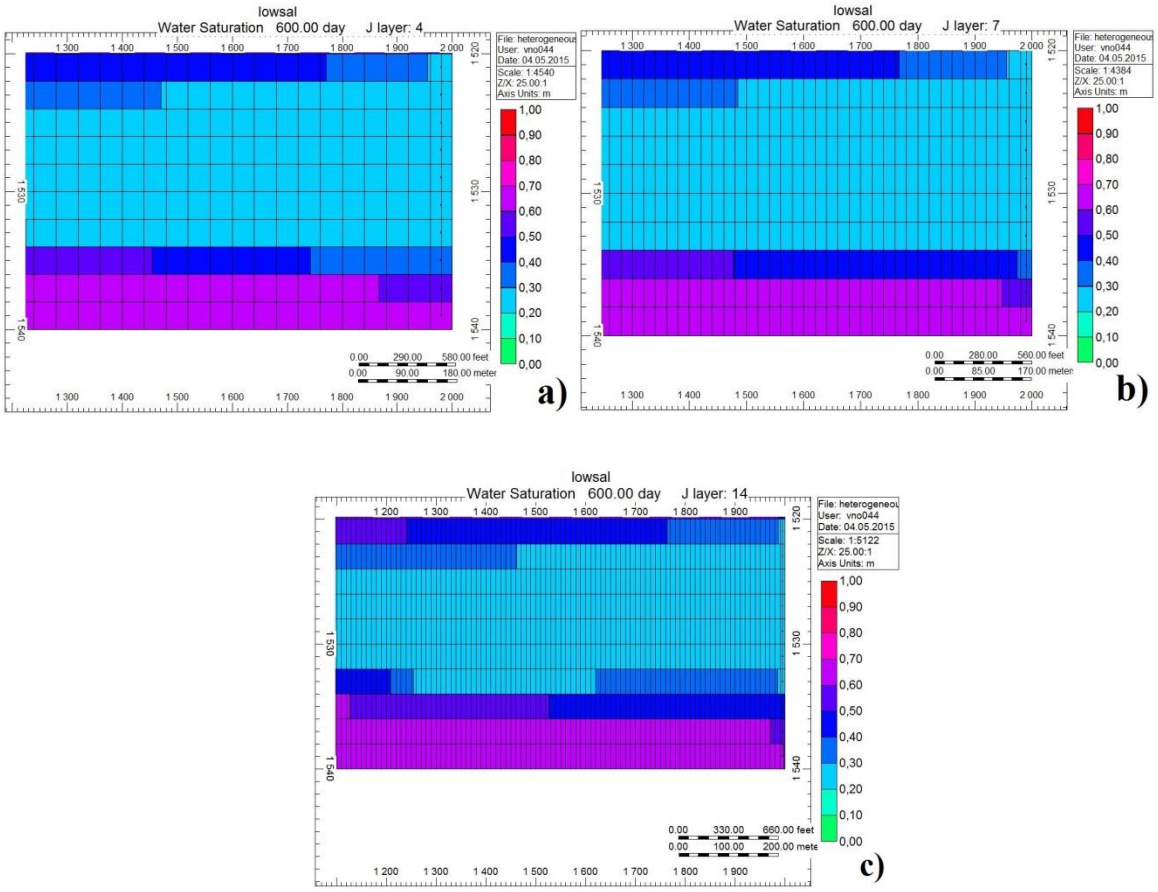

Figure 7-8a,b,c: *Sectional view in XZ-direction of water saturation in layer 11-20 near producing well after 600 days.*

We know from earlier simulations presented in this thesis that the finer grids tend to produce a more stable, higher water front, and this can also be seen in these figures. However, the phenomenon of the water rising can be seen in Figure 7-8c whereas in layer 17 (4^{th} from the bottom) there is a decrease in saturation before it increases again near the producing well. This *could* be due to a "suction-effect" from the producing well, where the water experiences a high drag force as it approaches the producing well and is therefore drawn upwards towards the producer. But since this is not observed in either the medium or coarse grid models, it is not very likely.

Inspecting the water production in each layer revealed some surprising results with some irregularities. It was initially expected to see this in layer 17, given the results in Figure

7-8a,b,c, but layer 18 showed more “extreme” results. Figure 7-9 shows the water production rate for layer 18, and there is an increasing spike with a finer grid resolution.

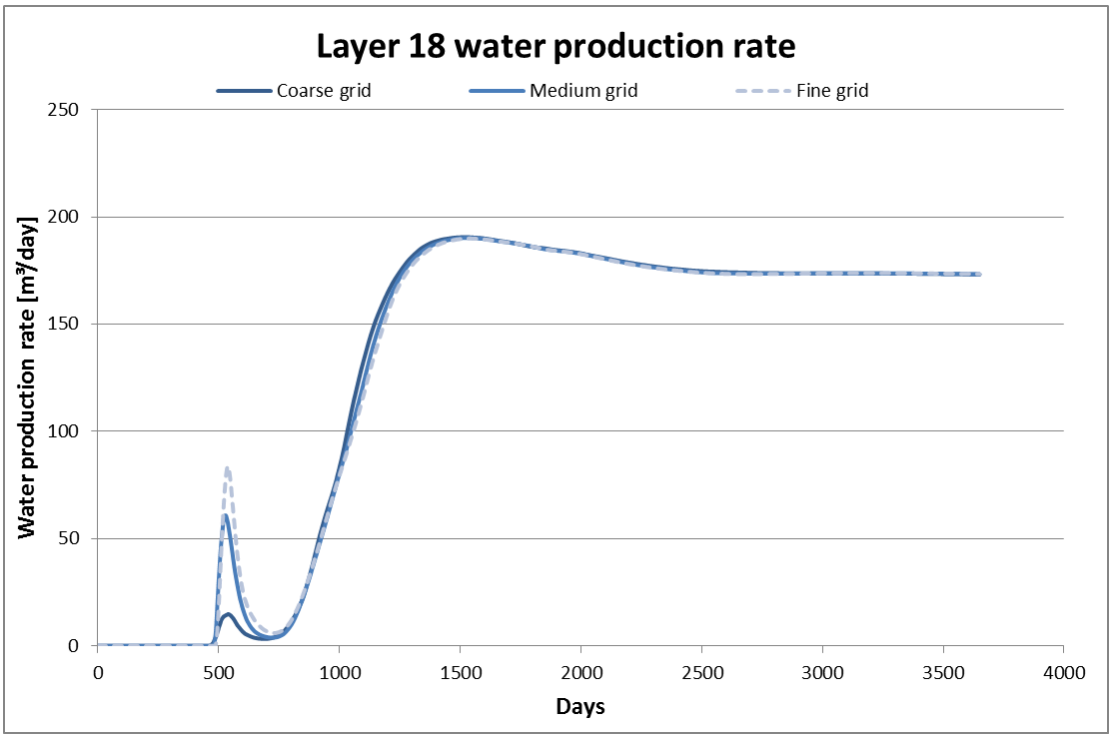

Figure 7-9: *Water production in layer 18 in heterogeneous reservoir with low-salinity waterflooding.*

This increasing spike with finer grids can to some degree also be observed in layer 17. The spike in itself may not be so surprising, taken in consideration that the producing well is controlled by a maximum liquid production rate value which could limit the production in certain layers to compensate for an increased production in other layers. However, the increasing trend with finer grid resolution indicates a difference in the fluid displacement, which could be caused by viscosity differences (see chapter 6.2.1).

7.3.1.2 Salt dispersion

As seen in chapter 6.3, a grid coarsening results in a larger mixing zone in the homogeneous reservoir. This is also applicable for the heterogeneous reservoir where the salt front is more compact with less spreading at fine grid resolution. When comparing the salt dispersion to the results from the fluid-flow test in chapter 7.1.2 one notices it is very much alike. In both cases the salt mixing occurs ahead of the water front, indicating a displacement and mixing of connate water with the injected low salinity water. The water injected in the lowsal fluid-flow test flows straight into the high-permeable regions 2 and 4. The same can be seen in the heterogeneous reservoir when the injector is perforated in all 20 layers, as shown in Figure 7-6. The main difference between these two scenarios is in the upper region where more water is flowing with a full injection.

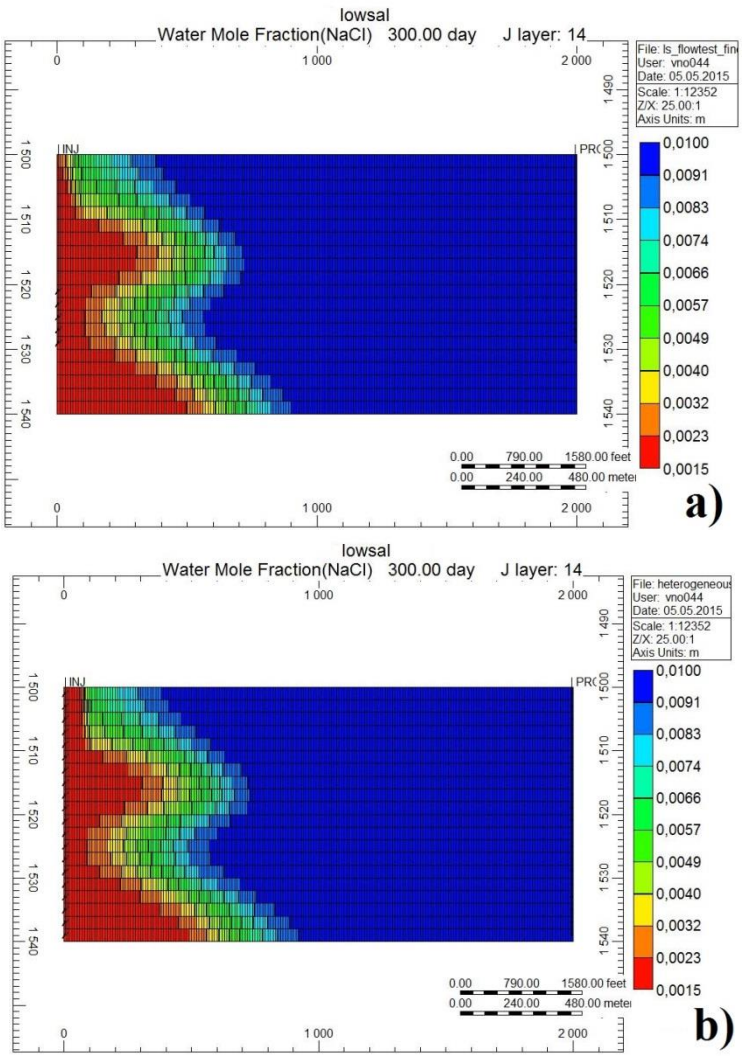

Figure 7-10: *Sectional view in XZ-direction in fine grid model of NaCl concentration in* **a)** *Lowsal fluid-flow test, and* **b)** *Secondary lowsal injection.*

As seen in Figure 7-10a,b, the salt dispersion is very much alike, with a faster progression in the high-permeable regions 2 and 4 and slower in 1 and 3, with region 3 being “trapped” in between the high-permeable regions and therefore experiencing some degree of cross-flow and salt-mixing thereafter. This is somewhat surprising when considering that Figure 7-10a) is injection in region 3 only.

The fast salt progression in region 2 makes up a big contrast compared to the progression in region 1. Since dispersion of salt is defined through keywords DISPI/DISPJ/DISPK, some of the salt will flow upwards into the low-permeable layers through diffusion. This leads to an uneven salt progression in some of the upper layers, where it seems that lower saline water

flows upwards in the layers. Figure 7-11a,b,c,d show the development of the upwards flowing low-salinity water in layer 3. This phenomenon could only be observed in the fine grid resolution and was not observed in the lowsal fluid-flow test, which had an equal grid resolution. The interesting part about this is that the occurrence of the lower saline area corresponds with the water advancement of the water front, i.e. the shape of the low salt concentration which appears in Figure 7-11b) is similar to the water front.

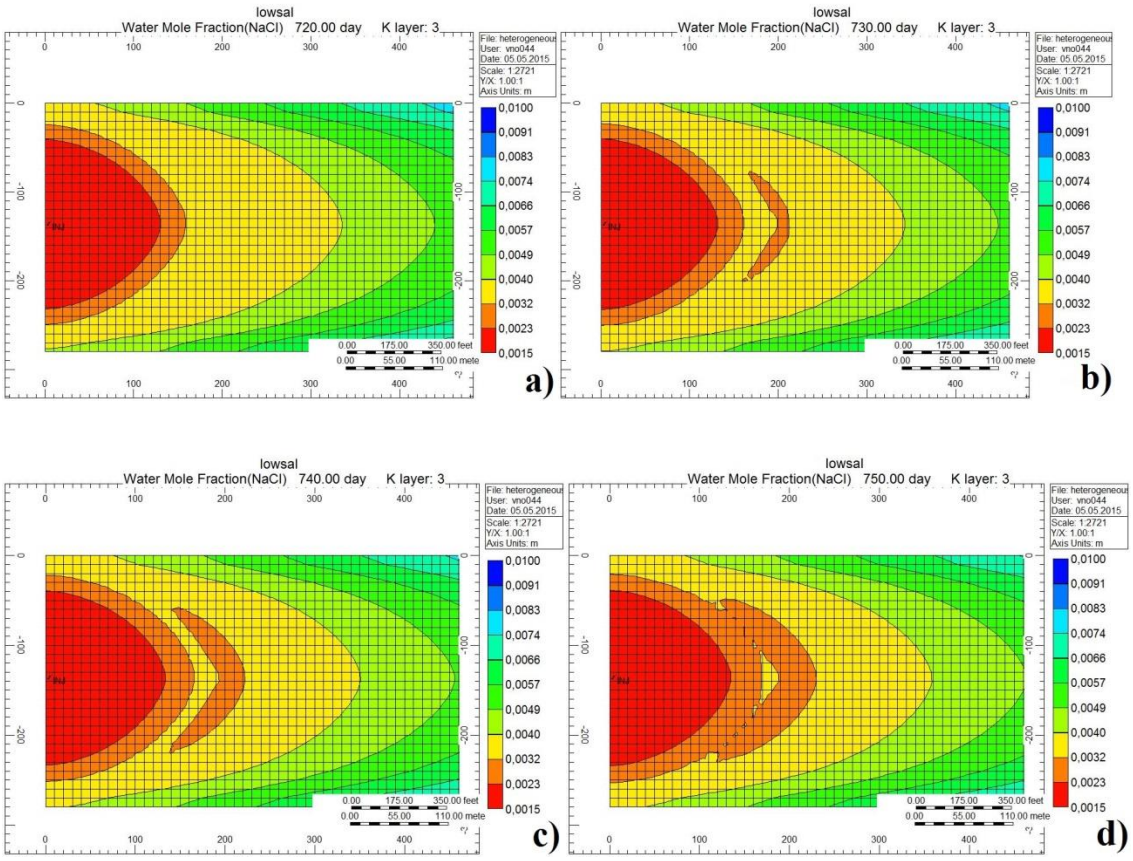

Figure 7-11a,b,c,d: *Progression of NaCl in layer 3 in fine grid after 720 days.*

Again, it is worth mentioning that the concentration differences observed in Figure 7-11a,b,c,d could be over-exaggerated due to the color scale. The concentration in the occurring lower salt area is 0.00319 NaCl and the yellow area between the two fronts contains a concentration of 0.0033 NaCl. This difference is not crucial and does not affect the final results in any particular manner, however it is still worth mentioning.

7.3.2 Tertiary low salinity brine injection

With the tertiary lowsal injection, 1 pore volume of highsal is first injected followed by 1 pore volume of lowsal water. In the tertiary lowsal injection in the homogeneous reservoir, presented in chapter 6.3.2, the increased recovery is partly due to the lowsal effect, but also because of the increased injection period. The latter reason is less applicable in the heterogeneous reservoir, where the reservoir sweep is poorer and thus the high-permeable regions are already relatively well recovered. The increased recovery is therefore mostly a result of the lowsal effect.

7.3.2.1 Production results

As with the other simulations performed in the heterogeneous reservoir, the production results did not show any significant variation with varying grid resolution, neither the total oil production rate nor the regional production rates. This confirms further that the reservoir heterogeneity has a bigger effect on flow patterns than the grid resolutions.

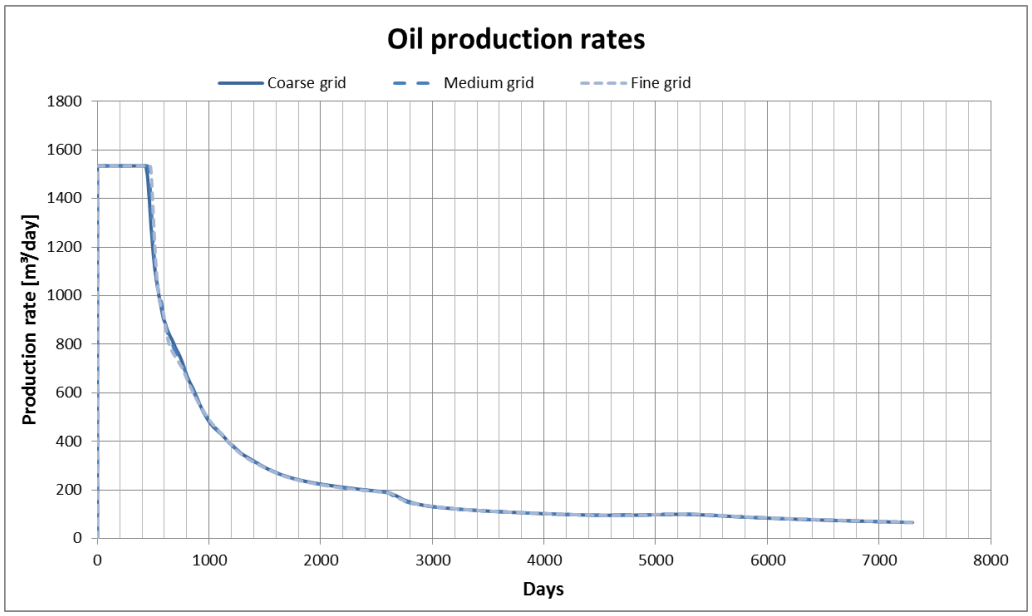

Figure 7-12: *Oil production rates for HSLS injection in heterogeneous reservoir.*

The lowsal injection starts at 3650 days and the production curves stagnates sometime after that and increases a bit until dropping again after ~5400 days. When comparing to the tertiary lowsal injection for the homogeneous reservoir, in Figure 6-29, one notices that the increased recovery from the lowsal effect is larger for the homogeneous reservoir than for the heterogeneous. This is because of the water`s poor sweeping ability in the low-permeable layers, making the lowsal-effect only “half as effective” as a result.

One can see in Figure 7-12 above that the production rates for the different grid models have a small variation upon water breakthrough time in the highsal injection-period, but other than that no significant difference. Even after the lowsal injection at 3650 days the production rates are equal for the grid models, meaning that the liberated oil upon interpolation between the relperm curves behaves the same way regardless of grid resolution. For the tertiary lowsal injection in the homogeneous reservoir, the increased recovery was most notable in the top layers, meaning that the liberated oil after lowsal water displacement flowed upwards due to density differences. This is also applicable in the heterogeneous reservoir where a lowsal effect only can be observed in regions 1 and 2. The production increase in region 2 is not very visible in Figure 7-13b), but there is a slight production increase between 4800-5200 days. The reason for why the increased production is observed also in region 2 instead of it being exclusive for region 1 is probably because of permeability differences hindering upwards flow of oil.

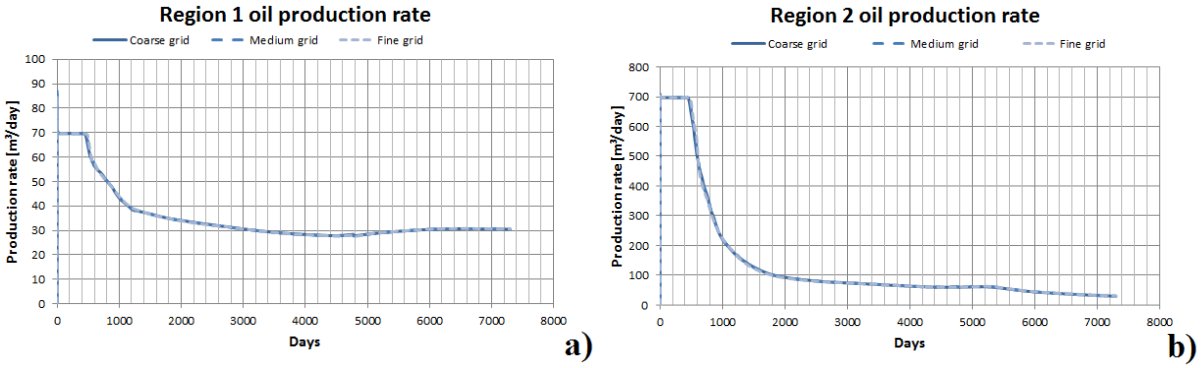

Figure 7-13a,b: *Regional production rates in region 1 and 2 for HSLS injection in heterogeneous reservoir.*

Figure 7-13a,b show the regional production in regions 1 and 2. Note that the fall in oil production occurs at the same time, but it does not represent a water breakthrough in region 1 as the water does not displace the oil in the top layers of the reservoir. The fall in oil production in region 1 occurs in order to maintain the total liquid rate in the producing well, as regions 2 and 4 have reached water breakthrough. Also notable is the production difference between the two regions, where region 2 produces at 10 times the rate as region 1.

The effect of the lowsal is shown after 4500 days where the production rate slowly increases. The increase in both regions is not very significant but it helps maintain a certain production rate for a while longer. Note that the production rates are constantly equal for the different grid resolutions.

7.3.2.2 Salt dispersion

The salt mixing zone is as expected more stable with the finer grid resolutions and with a smaller spread within the layers. But despite of this the produced mole fraction of NaCl showed little variation between the grid resolutions, with the only variation being the time when the decrease in NaCl starts. Most parts of the decline curves are equal for all grid models, see Figure 7-14.

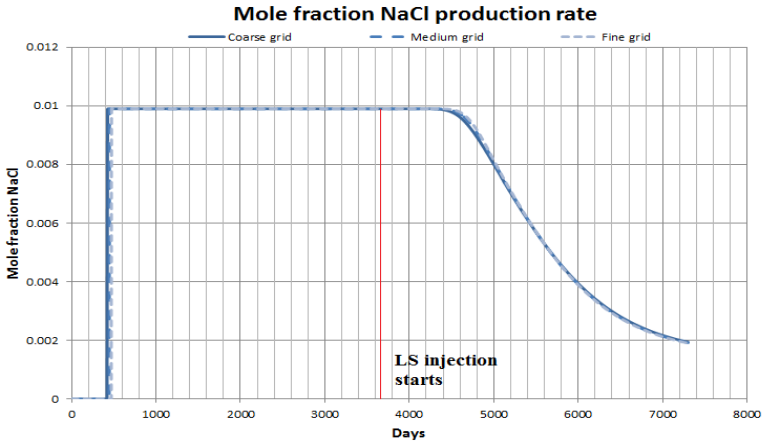

Figure 7-14: *Mole fraction NaCl production rate for the HSLS runs.*

Compared to the secondary lowsal injection presented in chapter 6.3, the salt front is less affected by the gravitational forces, making the fronts in the high-permeable layers more stable. The advancement of the mixing zone is also slower due to a larger volume of high-salinity water present in the reservoir at injection start.

The fine grid showed some irregularities in the salt concentration front in region 1, with low salinity water rising up within the mixing layer, following the same trend as shown in chapter 7.3.1.2 where it follows the water saturation. Figure 7-15a,b,c,d shows the salt mixing zone every 50th day in the upper region.

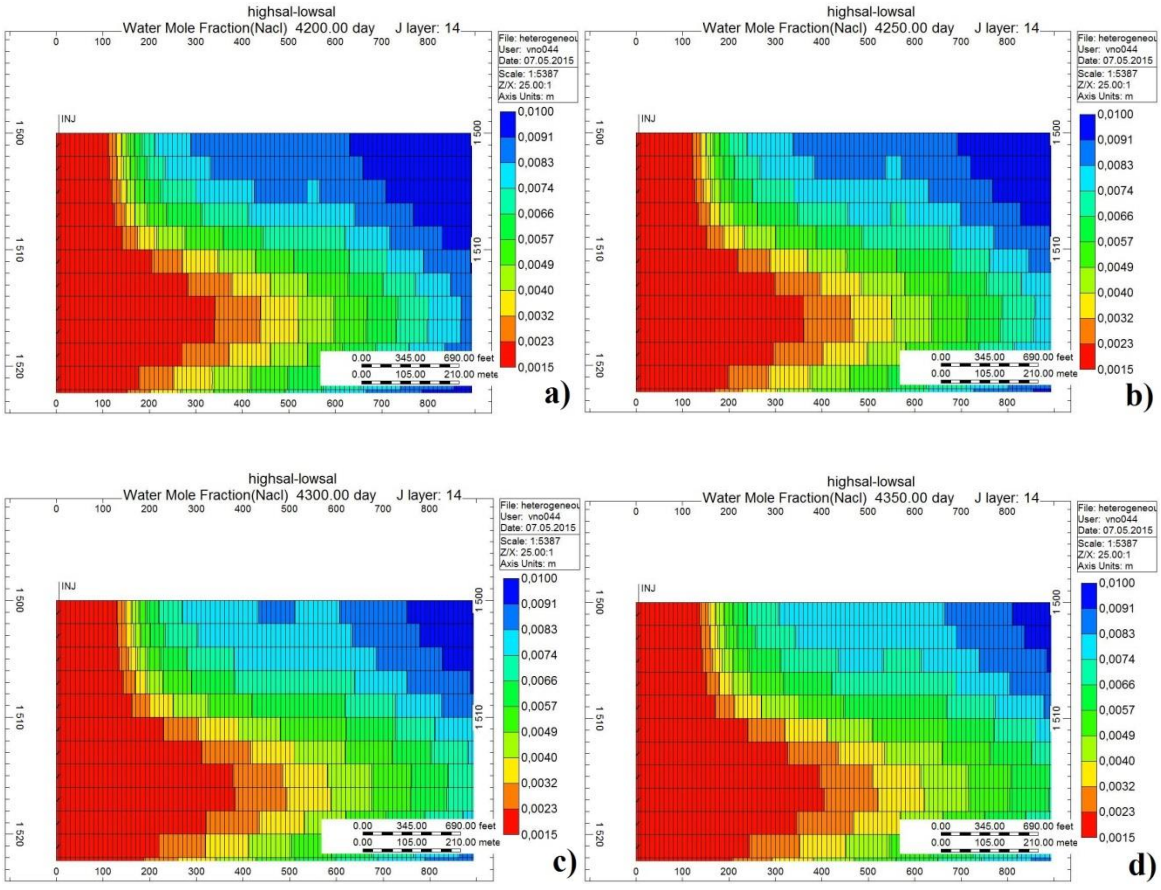

Figure 7-15a,b,c,d: *Salt concentration behavior in upper layers in fine grid between 4200-4350 days.*

It is unsure to what degree this phenomenon affects the final production results. The interpolation occurs between NaCl-concentrations of 0.0099-0.0015 and the variation in concentration is roughly ± 0.0003, so it is uncertain if the relperm-curves are affected in any significant manner and thus affecting the water flow. Nonetheless, it is noteworthy that this only occurs in the fine grid with 10m*10m*2m dimensions.

7.4 Results in heterogeneous reservoir

As predicted, the oil recovery from the heterogeneous reservoir is substantially lower than for the homogeneous reservoir. Table 7-1 shows the total production results for the simulations performed with the heterogeneous reservoir. It also shows the deviation in production results between the coarse and the fine grid.

Table 7-1: *Comparison of results in heterogeneous reservoir.*

Grid resolution	Highsal, RF	Lowsal, RF	Highsal-Lowsal, RF	Increased recovery, %
Coarse	0.3962	0.3995	0.4720	**16.0593**
Medium	0.3967	0.4006	0.4730	**16.1311**
fine	0.3969	0.4012	0.4733	**16.1420**
		Deviation		
Coarse-medium [%]	**0.1260**	**0.2746**	**0.2114**	-
Medium-fine [%]	**0.0504**	**0.1495**	**0.0634**	-
Coarse-fine [%]	**0.1764**	**0.4241**	**0.2748**	-

One can assume that the production results are stable with varying grid resolution, given a small difference in cumulative production, under 1 %. The difference seems to be largest in the lowsal-only simulations which is reasonable due to the grid block size not only affecting the water flow, but also the salt dispersion, which in turn gives a higher recovery. When injecting an additional 1 PV of lowsal water after the highsal injection, a relatively large

production increase of 16 % is obtained. This increase gets marginally larger with a finer grid, contradicting the trend observed in the homogeneous reservoir where a finer grid resulted in a *smaller* increased recovery with additional 1PV lowsal injected.

Also, the production difference between highsal and lowsal simulations is smaller than for the equivalent simulations in the homogeneous reservoir, and the increase with the mixed HSLS injection is larger. This is probably because the lowsal-effect is influencing a smaller volume, excluding low-permeable regions, and there is therefore less additional recovery due to a smaller volume of the reservoir being affected by a lowered S_{or}. Since oil displacement by water occurs in a larger portion of the reservoir volume in the homogeneous reservoir, the saturations in some parts will not exceed the S_{or} for the high-salinity relperm curves and an increased production due to the lowsal water lowering this S_{or} will not be attained.

The salt dispersion in the LS and HSLS seems to be fairly equal with a somewhat equal salt front and mixing zone in the upper 3 regions. The salt front seems to be more gravitationally stable in the HSLS runs, probably due to a larger volume of highsal water. Figure 7-16 shows NaCl-concentration after 700 days of lowsal injection, and one can see that the fronts are fairly equal in the top 3 regions. The salt in region 4 is more advanced, and it is clear that the salt follows the water flow to a larger extent in the LS run than in the HSLS.

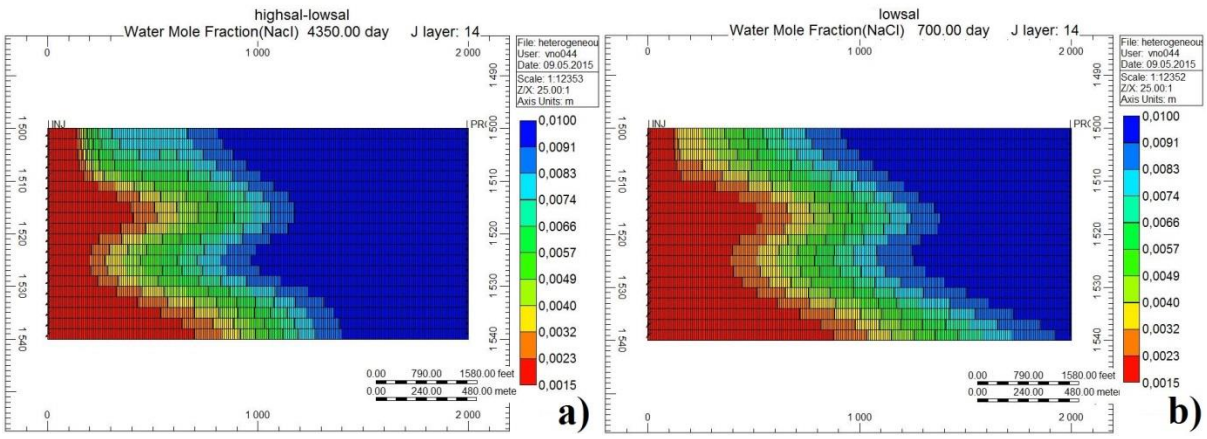

Figure 7-16a,b: *Sectional view in XZ-direction of NaCl concentration in HSLS and LS runs, after 700 days of lowsal injection.*

Figure 7-16a shows the upflowing lowsal water in region 1 mentioned in the last chapter which is occurring at the same pace as the water front is advancing in that region. This same phenomenon also occurs in the LS simulation (not shown in Figure 7-16b) to a smaller extent. It seems that it is the heterogeneity of the reservoir that entices this phenomenon since it is not occurring in either of the lowsal homogeneous simulations. It is also only occurring with a fine grid resolution.

From the figures shown above, one would assume that the decline in NaCl-production starts earlier and is less steep for the LS simulation. This is somewhat correct as the produced water salinity does in fact start decreasing earlier, but as the HSLS run reaches a decreasing NaCl-production the decrease slope is fairly equal for the two, see Figure 7-17. This implies that the salt mixing zones are fairly equal with maybe the mixing zone for LS being slightly longer.

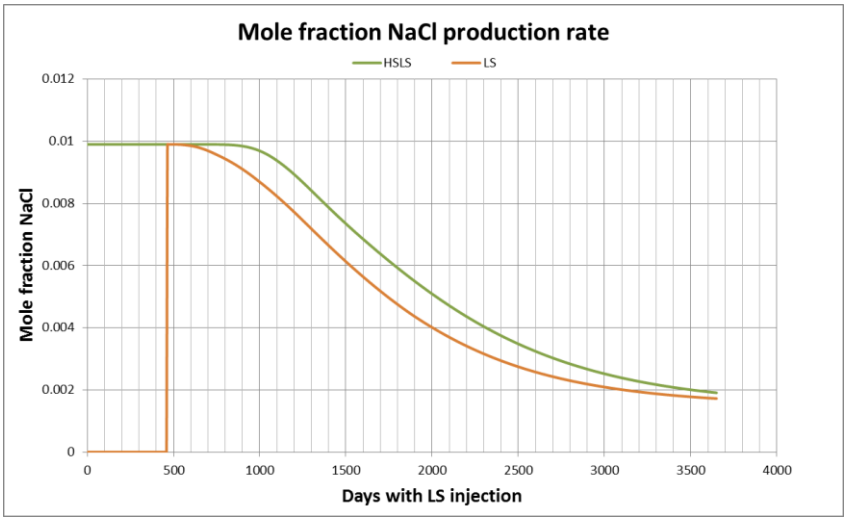

Figure 7-17: *Mole fraction NaCl production rates for LS and HSLS simulations in fine grid as function of days of LS injection.*

8 Polymer injection

With regular waterflooding in the heterogeneous reservoir there are large parts of the reservoir left untouched and therefore affects total recovery. Polymers are long molecule chains which can be added to the water phase to raise the water phase viscosity. An increase of water phase viscosity will lower the mobility in the high-permeable regions and therefore force the injected water to flow in the low-permeable regions, thus lead to an increased production. When combining polymer injection with lowsal flooding a smaller fraction of polymer is needed compared to polymer injection with highsal water, one third or less (Mohammadi and Jerauld, 2012). This fact, in combination with the proposed mechanism of wettability change by an effect of lowsal injection, makes it very attractive to use it as a recovery method.

Earlier published papers (Wang et al., 2002) have estimated an increased recovery up to 15% with polymer flooding, partly due to an increased displacement efficiency. Laboratory experiments as well as field polymer tests have shown a potential for a similar increase in viscous oil reservoirs with following conditions (Alzayer and Sohrabi, 2013) :

- Reservoir temperature < 200°F
- Reservoir permeability > 20mD
- S_o > 30%
- μ_o < 100cP
- Total reservoir thickness > 10 ft

Except for maybe oil saturation being slightly lower than 30% in the high-permeable regions, the other criteria are met upon polymer injection.

This chapter will present a highsal-lowsal-lowsal&polymer injection performed in the heterogeneous reservoir and investigates how the polymer injection affects the production results and how it varies with grid resolution. The total injected volume will be equal to the HSLS simulations, approximately 2 reservoir pore volumes, injected at a constant rate over 20 years. The 6 first years will be highsal injection, followed by 7 years of lowsal injection and 7 years of lowsal-polymer injection, hereafter abbreviated as LS&P. The effectiveness of the polymer injection, or all EOR processes in general, are always dependent on the time of implementation. It is generally believed that an earlier implementation of EOR-methods will

lead to a higher and more cost-effective benefit. This will not be taken into account in this thesis, and polymer injection will occur as a tertiary recovery method only.

Due to a long computational runtime and limited computational resources, results from the fine grid were not attainable. This chapter will therefore only present results from the coarse and medium grid, with the assumption that the results follow an equal trend with a fine grid resolution.

8.1 Polymer simulation

To include a polymer in the simulations, it must first be defined as a new component in the data file, see Table 8-1 for polymer properties.

Table 8-1: *Properties of polymer utilized in heterogeneous reservoir.*

Component	CMM [kg/gmol]	MASSDEN [kg/m³]	AVISC [cP]	Injection concentration
Polymer	6000	1000	10	$1.50491*10^{-9}$

Mass density of the polymer has been set to 1000, equal to the water component, so that the only depending property is viscosity. The Molecular weight is very high compared to the water component, which is 0.018, but this will not have any additional effect on water flow due to the very low polymer concentration.

For a polymer to act realistically in a waterflood certain behavioral properties must be defined:

- Water phase viscosity upon polymer injection
- Concentration-dependent viscosity
- Velocity-dependent viscosity / shear rate
- Polymer`s effect on relative permeability curves

- Polymer adsorption
- IPV (Inaccessible pore volume)
- RRF (Residual resistance factor)

The viscosity of the water phase with full polymer concentration has been chosen to be 10cP to ensure a lower mobility rate and to investigate the effect when introduced to the heterogeneous reservoir. This is defined through *AVISC. The keywords *VSMIXCOMP and *VSMIXENDP were used to choose the endpoints of polymer concentration so that water phase viscosity increases linearly with increasing polymer concentration until it reaches maximum concentration and equals the viscosity value used in keyword *AVISC.

Upon injection in field-scale, the velocity is usually very high and so the shear rate affects the polymer viscosity, “thinning it out” and thus lowering the viscosity. Due to technical challenges this has not been included in the simulations presented in the following subchapters. See chapter 8.4 for further details.

An inclusion of polymer to the water phase would usually affect the relative permeability of the water phase. This could be done by creating a new set of relative permeability curves through *RPT->*INTCOMP->*SWT and by that include a new interpolation set dependent on polymer concentration. This has for simplification purposes not been done in the simulations presented in this thesis, but it is considered to be recommended in order for the simulation to produce the most accurate result. Since a new set of relative permeability curves is not defined for polymer, it will continue to follow the interpolation based on NaCl-concentration.

The reservoir rock will react chemically with the polymer and will therefore have some degree of polymer adsorption. This adsorption will be considered irreversible due to a very slow desorption. STARS accounts for adsorption of polymers to the rock through a Langmuir isotherm correlation. This adsorption will in these simulations not affect the absolute permeability in the reservoir. Due to this only being a random polymer, the adsorption values and Langmuir constants have been picked randomly to represent a plausible adsorption scenario with a low adsorption.

The amount of polymer adsorbed follows the Langmuir adsorption isotherm which is expressed as

$$ad = \frac{(tad1 + tad2 * x_{nacl}) * ca}{(1 + tad3 * ca)} \quad (8.1.1)$$

Where *tad1*, *tad2* and *tad3* are parameters in the Langmuir expression, *ca* is polymer concentration, and xnacl is mole fraction of salt. Values used in these simulations can be found in Table 8-2.

Table 8-2: *Parameter input for polymer adsorption*

Parameters	Value
tad1	2 [gmol/m^3]
tad2	0 [gmol/m^3]
tad3	$8 * 10^9$

Inaccessible pore volume, IPV, is a phenomenon that occurs due to the large size of polymer molecules. This will cause some pore volume to be unavailable for the polymer and will therefore act as an opposite of retention whereas the polymer solution will accelerate through the medium. IPV is usually between 1-30% and can be defined in STARS through keyword *PORFT.

Polymer dispersion is included through the keyword *DISPI /*DISPJ /*DISPK. The same total dispersion coefficient as the NaCl was first tried ($0.01 {}^{m^2}/_{day}$) but this resulted in a very fast progression in the low-permeable regions. It was decided that this was somewhat unrealistic because the polymer will not mix in the same degree as the NaCl. The dispersion coefficient was therefore reduced to 0.001 in order for the polymer to follow the water flow to a larger degree.

Besides the new polymer component and its properties and a new injection scheme, no additional changes have been done to the data files. Addition of a new component that

introduces a viscosity change in the water phase, and therefore a change in the flow regime, surely has an effect on computational performance. Simulation runtime has increased significantly, e.g. the medium grid resolution runtime has increased from ~10 minutes in the HSLS run to 7hr 23mins for the HS-LS-LS&P, when total production period is equal with 7300 days (20 years). There was an occurrence of timestep cuts with the polymer injection, which did not occur with the other simulations. These cuts did not appear immediately after polymer injection, but occur after a few years of production. However, despite these convergence failures causing timestep cuts no matrix failures were reported, 0% IMPES occurred and a low material balance error was recorded, < 1%. All three parameters could be crucial to the simulation. As mentioned in chapter 3.5.1: if timestep cutting occurs more often than every 2nd or 3rd timestep, it should be investigated as it could affect the production results. This is discussed in further chapter 8.2.

8.2 Production results

Initial production results from the coarse grid showed irregularities in the results. Convergence problems occur when the Newtonian iterations do not converge within the given timesteps. The large amount of timestep cuts, which indicates convergence problems, showed unexpected results in terms of an oscillating water production when polymer was included to the water phase. As a possible solution to this the maximum timestep size was reduced, using the *DTMAX keyword, from 10 to 5 days. Results can be seen in Figure 8-1.

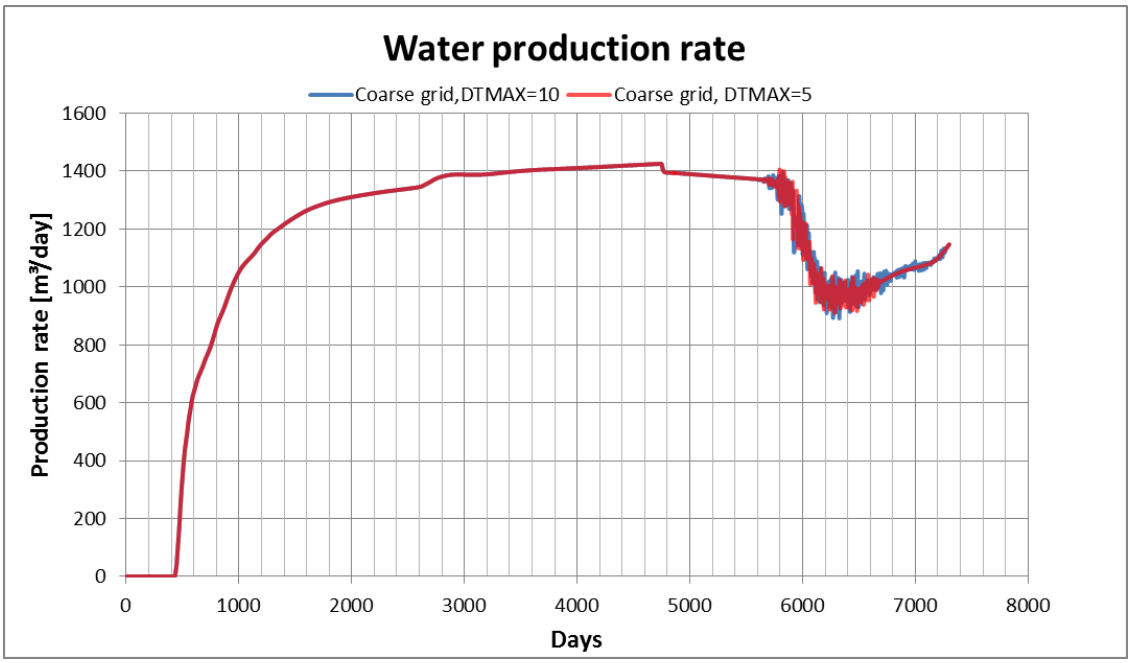

Figure 8-1: *Water production rate for in coarse grid with maximum timestep size of 10 and 5 days.*

One can see that after approximately 5800 days, water production starts declining due to an increased oil production, confirming the polymer`s effect on reservoir displacement efficiency. The fact that the curves are oscillating indicates calculation errors by STARS, and even though the simulation with a reduced timestep size (shown in red) somewhat lowers this oscillation to some degree, it is still a sign of convergence problems. The same trend can be seen when comparing the produced mole fraction of polymer, see Figure 8-2.

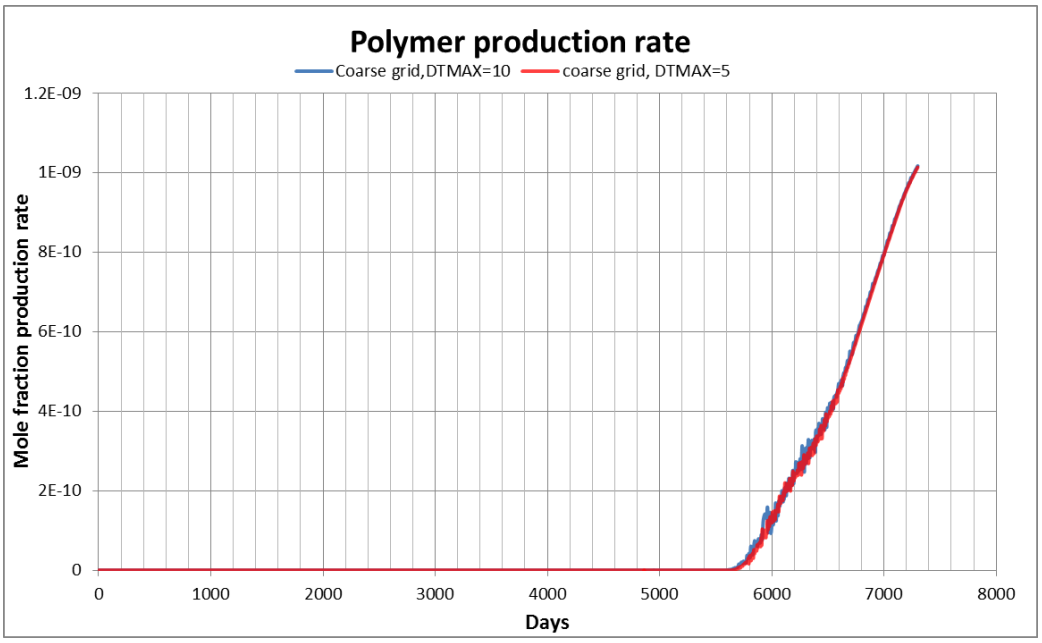

Figure 8-2: *Polymer mole fraction production rate in coarse grid with maximum timestep size of 10 and 5 days.*

Again, a lower maximum timestep size lowers the oscillating tendency of the production curves, but it is still erroneous in the sense of not being a realistic production curve.

Looking at Figure 8-1 and Figure 8-2, one can see that the oscillating production curves occur at the start of polymer production. To handle this, *DTMAX was reduced from 5 to 2.5 days from 5500 days until end of production.

The reduction in DTMAX removed all timestep cuts from the simulation and the production curves were no longer oscillating. The simulation runtime was also reduced by 50%, meaning that STARS handles smoother with more timesteps and less iterations per timestep than with fewer, large timesteps with many iterations.

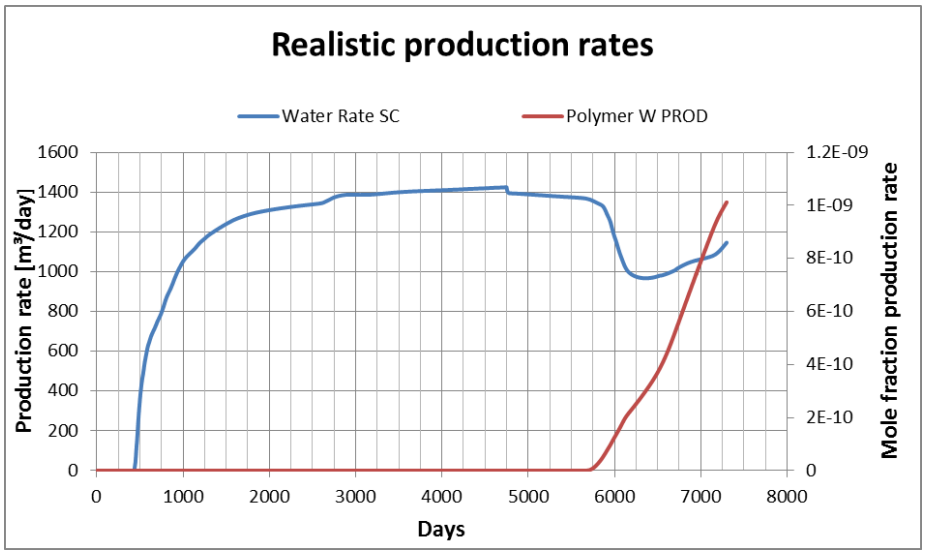

Figure 8-3: *Realistic water and polymer production rates after lowering DTMAX to 2.5.*

Figure 8-3 shows the final production results from the coarse grid, without any oscillating tendencies. Due to convergence failures causing timestep cuts the results could not only be oscillating, but also vary substantially. The production curves presented thus far in this subchapter are, except from the oscillating tendency, equal.

The polymer injection plugging the high-permeable regions will lead to an increased displacement in the low-permeable regions and thus increasing oil production significantly. Figure 8-4 shows the oil production rates, and one can see there is a clear increase in oil production after 5800 days. Due to a larger dispersion in the coarse grid, the increased production occurs earlier in the coarse grid, and with a lower production peak. The fine grid would presumably show a longer delay and steeper production increase than the coarse and medium grid.

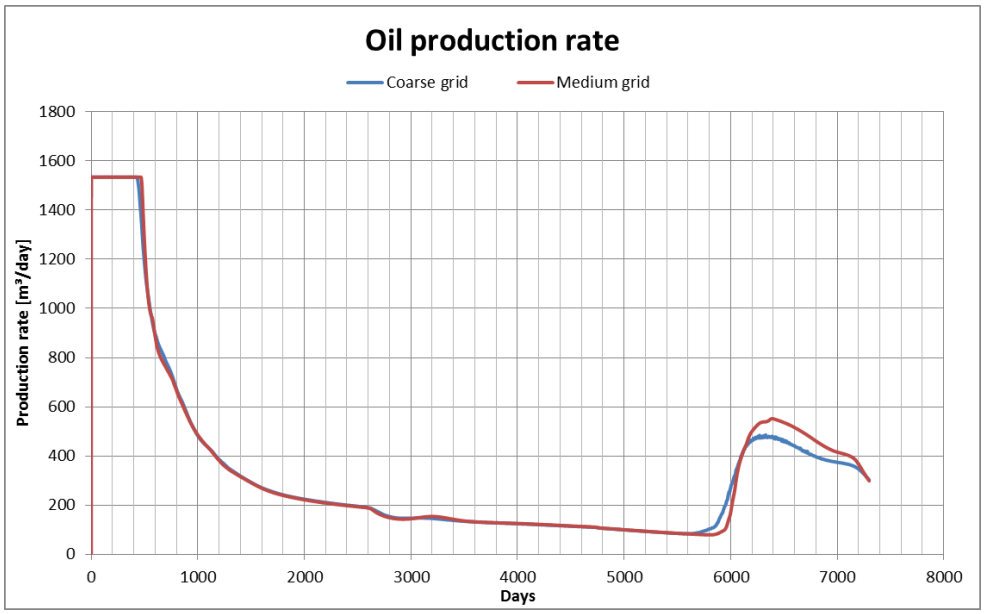

Figure 8-4: *Oil production rate for coarse and medium grid, HS-LS-LS&P.*

When studying the regional production, there is a significant increase in oil production in all regions. Especially in region 1 which has shown very poor displacement efficiency, the polymer injection will have a large effect. Also, due to the density difference much of the displaced oil will flow upwards before reaching the producer. This is shown by a larger increase in oil production in the upper regions, and a small increase in production in region 4, see Figure 8-5a,b,c,d. One would presume that most of the oil in region 4 would already be produced, but due to the gravitational segregation of water the displacement in the upper layers is poor. Per volume, the increase in region 4 is larger than in region 3, but the percentage-wise production increase is larger in region 3.

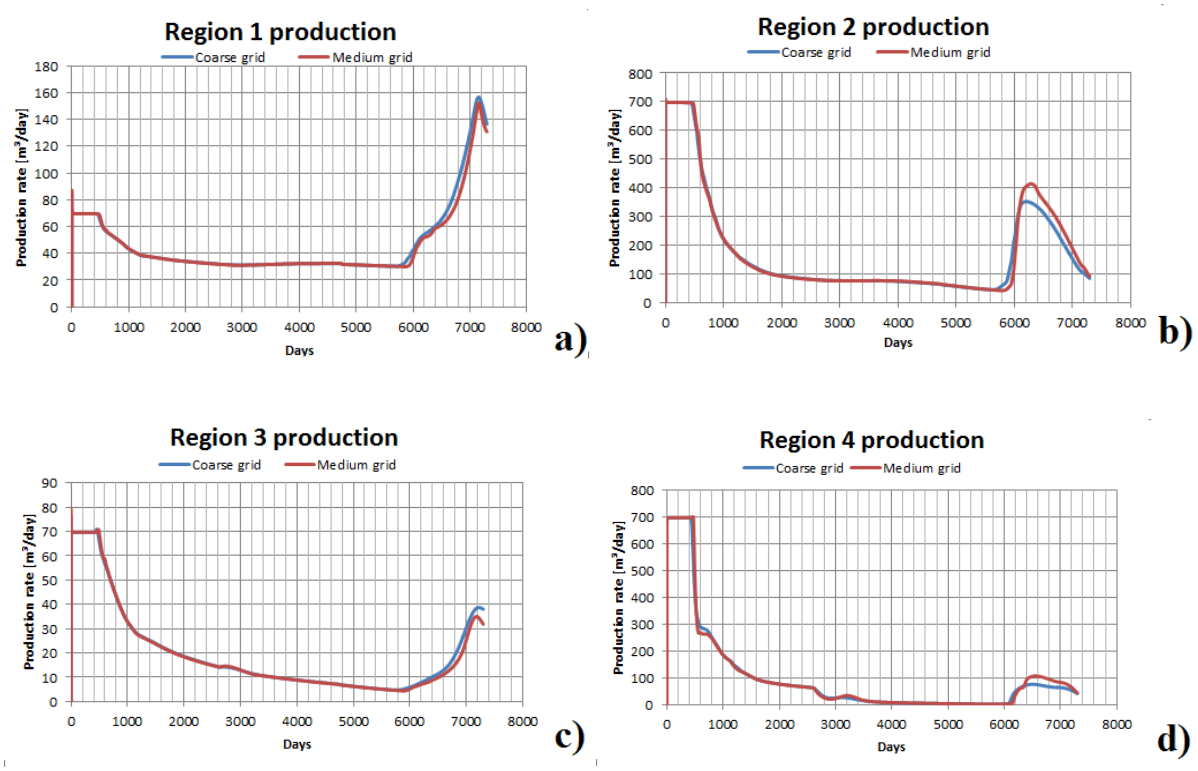

Figure 8-5a,b,c,d: *Regional oil production for coarse and medium grid resolution, HS-LS-LS&P.*

One can see in Figure 8-5a that production increases to over twice of initial production, with the coarse grid model having a slightly higher production rate. It seems that the low-permeable regions give a higher production rate for the coarse grid model, and vice versa with the high-permeable regions. This is probably due to increased polymer dispersion in the coarse model. One can also see that the increase is by far larger in the upper 2 regions than the lower 2, showing that even though the density difference between oil and water is not major, it is still enough to lead to an extensive upflowing of oil.

The regional production rates seem to have different peaks, with the high-permeable regions 2 and 4 peaking relatively early, and a later peak for the low-permeable regions 1 and 3. The peaks are also sharper in the high-permeable regions. The pressure increase after introduction of polymers in the reservoir would probably start to drop again after these peaks, but this can not be confirmed due to the pressure values beeing unreliable, see chapter 8.4.

Table 8-3 shows the cumulative production results from the coarse and medium grid model. Except for a higher production with polymer injection, a deviation of 1% between the grid models is large compared to the highsal-lowsal simulations. Especially when considering that a fine grid model would probably show an even higher production, resulting in an even larger deviation between the coarse and fine grid model. However, this increase from medium-fine grid would probably be smaller than the increase between coarse-medium.

Table 8-3: *Production results from polymer injection.*

	Cumulative Production [m^3]	**RF**
Coarse grid	$2.5113*10^6$	0.5859
Medium grid	$2.5556*10^6$	0.5958
-	**Deviation**	
Coarse-medium [%]	**1.0169**	-

This could mean that while the highsal-lowsal simulation results showed stable production results with varying grid resolutions, an introduction of other fluids or chemicals (such as polymers, surfactants, etc.) could show a larger deviation in results. Different injection schemes such as slug injections or multiple wells could also show a deviation with a varying grid sensitivity.

8.3 Block behavior

As with the case in chapter 6.3.2.3, the tertiary low salinity injection in the homogeneous reservoir, where the water saturation went below the S_{wi} utilized in the relperm-curves, a similar phenomenon occurs with the polymer injection. Endpoint saturations are defined by interpolation with NaCl-concentration, and the added polymer should therefore have no effect on this. However, when introducing polymer to the water phase, water saturation in certain grid blocks goes above the maximum saturation defined in the relative permeability curves, see Figure 8-6.

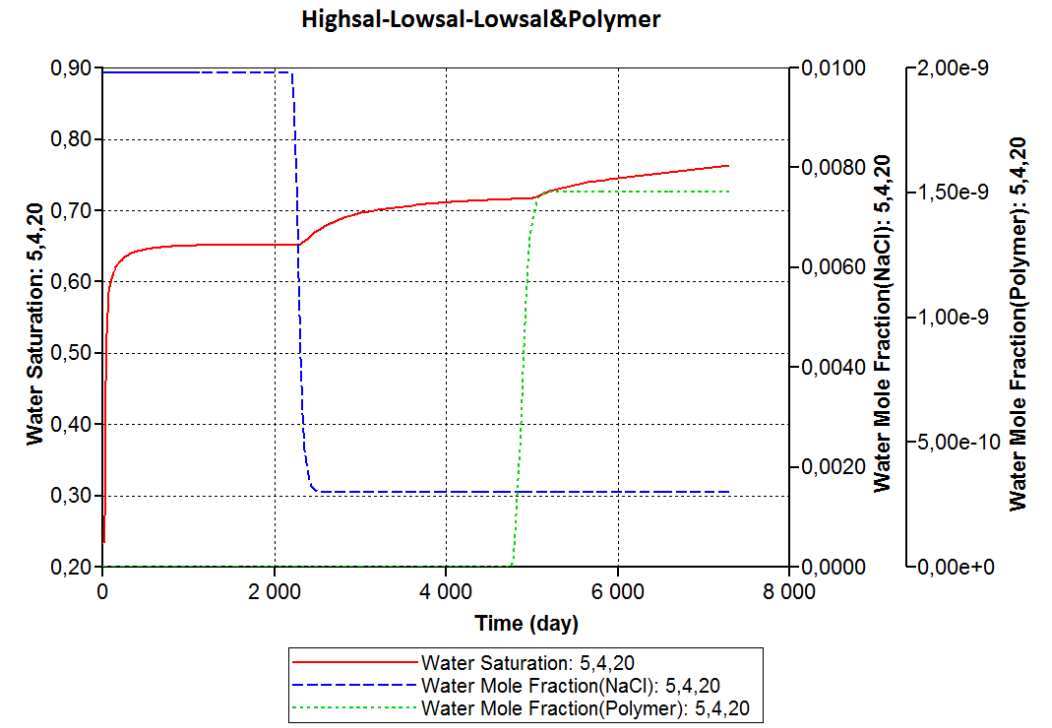

Figure 8-6: *Plots of water saturation and mole fraction NaCl and Polymer in grid block in layer 20.*

Figure 8-6 shows plots taken from a grid block in the bottom layer, but similar plots can be found in all grid blocks near the injecting well. Since the water saturation is still increasing towards the end of LS injection (4750 days), it is possible that it would have eventually reached S_{or}. But at time of polymer injection there is a sudden increase in water saturation which increases until simulation end. Water endpoint saturation (red graph) is 0.763, which clearly violates the endpoint water saturation in the relperm curves, which is 0.744. Since it is still increasing at simulation end, it is possible that the saturation would have increased even further with continued injection. This erroneous phenomenon occurs in all grid models in the area near producer. Increased viscosity in the water phase is not affecting the relative permeability (water relperm is at constant maximum value, 0.18) so this is not an interpolation issue. There is a reason to believe that this is not simply a near-well phenomena but rather a problem with how STARS handles phase calculations. Thus, some of

the increased recovery from polymer injection is due to faulty, increased displacement of oil in these near-well grid blocks.

8.4 Pressure

The introduction of the polymer into the reservoir increases the water phase viscosity. By a direct consequence of the multiphase derivative of Darcy`s law, an increase in the viscosity will lead to an increase in reservoir pressure. Due to the water phase viscosity increasing by a factor of 20 (0.5cP-10cP) the reservoir pressures will be greatly affected.

However, the initial run gave an enormous response in higher pressure with unrealistic values. The increased water phase viscosity resulted in an average reservoir pressure almost twice the amount of initial pressure, see Figure 8-7.

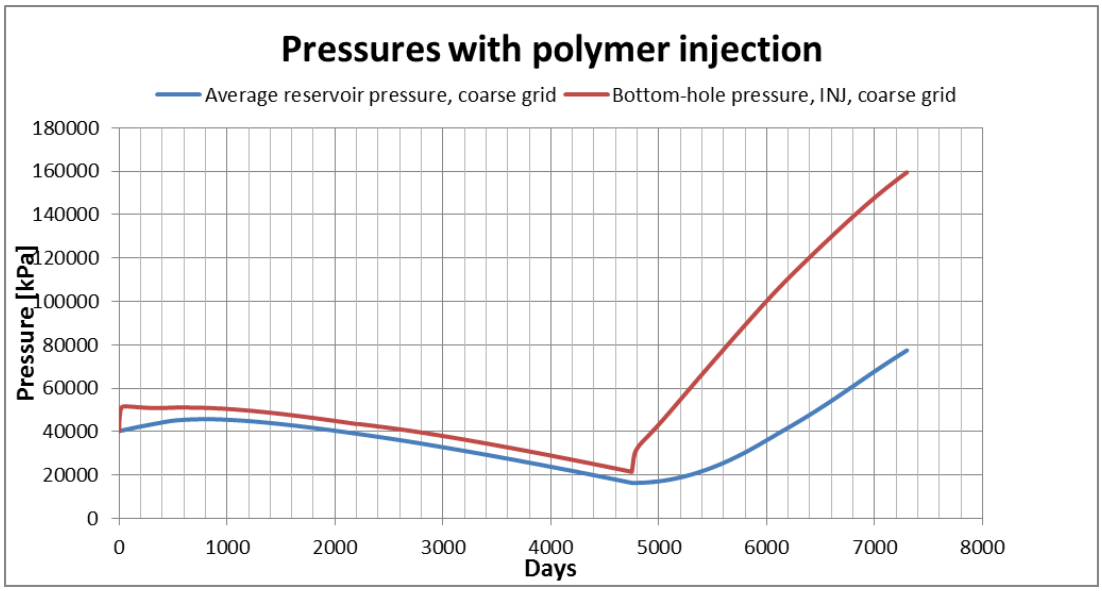

Figure 8-7: *Average reservoir pressure and bottom-hole pressure for injecting well, in initial run with polymers.*

As seen in Figure 8-7, the bottom-hole pressure for the injector starts to increase rapidly at start of polymer injection after 4750 days. This increase does not stop until simulation end. This large increase in bottom-hole pressure travels throughout the reservoir and thus affects

the average reservoir pressure. Initially, the reservoir pressure increases until it reaches a maximum at ~800 days before decreasing again. When the polymer injection starts at 4750 days the pressure increases until simulation end. This pressure at simulation end is above initial pressure and would therefore have to be dealt with.

A solution to this could be to include a negative skin factor in the injecting well to compensate for the very high pressure increase. A negative skin factor would indicate a cracking of reservoir rock in the near-well area which would lead to a higher permeability and thus lower the pressure in the injection well. To include this, an equivalent proportionality factor, or a well index, is developed to accustom for an appropriate pressure drop through the cracked zone. The well factor is expressed as:

$$f_{cwell} = \frac{2\pi * ff}{\ln\left(\frac{r_w}{r_e}\right)+S} \tag{8.2}$$

Where ff is the well fraction, which is 1 if the well is going through the center of a grid block. Rw is well radius and re is effective radius in a cell grid block, and is given by

$$r_e = CC * \sqrt{\frac{\Delta x^2+\Delta y^2}{f\pi}} \tag{8.3}$$

CC is the “geofac” defined through keyword *GEOMETRY in the recurrent data section, Δx and Δy are block sizes in perpendicular planes to the well.

In equation (8.2), f_{cwell} needs to be a positive number for the simulation to work. In order to utilize a negative skin factor some adjustments must therefore be made to either the well radius or the well placement in the grid block. Due to the polymer injection being performed in different grid sizes, the skin factor value must therefore be altered accordingly.

A skin factor was included for each of the grid models in the polymer injection simulations, but very little change was observed, due to not being able to include a sufficiently large negative skin, see Table 8-4.

Table 8-4: *Calculated skin-factor for the grid models.*

	dX [m]	dY [m]	Rw [m]	Re [m]	Skin-factor
Coarse grid	40	40	0.1	7.50	**-4.3**
Medium grid	20	20	0.1	3.75	**-3.6**
Fine grid	10	10	0.1	1.87	**-2.9**

A negative skin factor of -4.3 for the coarse grid did not show any significant difference in pressure increase. One could increase the negative skin factor by reducing the well radius but this will in turn increase the injection pressure in the grid block, which is not the preferred result.

One could also try to increase permeability in well perforated grid blocks in order to increase the pressure drop in the injecting grid blocks. This would lead to a lower average reservoir pressure. A simulation was performed where the permeability in the injection blocks was increased to 10 Darcy, to see how/if this would have any significant effect. While the bottom-hole pressure for the injecting well decreased to some degree, results showed no difference in average reservoir pressure, thus maintaining an unrealistic pressure value.

Water phase viscosity have this far been defined through polymer concentration only. Though it is right that the viscosity increases with concentration, it does not fully describe the non-newtonian behavior of polymers, where the water phase viscosity could decrease due to a high Darcy velocity upon injection. The near-well phenomenon occurring in real-life offshore processes is therefore not defined. Since this is not defined in STARS, the recorded viscosity upon injection is too high, and the reservoir pressure will therefore be much higher than in a realistic scenario.

STARS has an option where one can define shear thinning and thickening effects by using a power law relation using the keywords *SHEARTHIN and/or *SHEARTHICK. The user would have to define a reference Darcy velocity and a dimensionless power in the viscosity shear thinning equation, ranging from 0.1 to 0.99. Alternatively, one could specify the shear effects using tabular input data in a table through the keyword *SHEARTAB. This table would exist

of velocity or shear-rate values which each would correspond to a chosen viscosity value. This keyword cannot coexist with *SHEARTHIN/*SHEARTHICK keywords, meaning one would have to choose between the two methods. It is useful to utilize *SHEARTAB when the viscosity-versus-velocity relation is specified by laboratory data or when a simple power law relation should not be sufficient.

Both methods mentioned were tried in this simulation, but the computational needs were substantial, even with reduced a timestep size to DTMAX=1. The simulation advancement was in both cases greatly reduced down to $5 * 10^{-3}$ days for each timestep, indicating a requirement of 200 timesteps to be performed for each day of simulation, for the coarse grid only. The simulations were therefore terminated since it would have taken weeks or months to finish, and because the shear rate effects on polymers is not the main focus in this thesis.

8.5 Polymer dispersion and adsorption

Due to the dispersion coefficient for polymer being set to 0.001 it will follow the water flow path to a larger degree than what the salt does, thus seeing a larger difference in polymer advancement in the high- and low-permeable regions. Naturally, there will be a faster advancement in the high-permeable regions with an increased spread in the polymer concentration as it advances through the reservoir. Figure 8-8a,b,c,d shows the progression of the polymer concentration as it flows through the reservoir, and there is a clear difference between the regions.

Region 1 will have the slowest progression due to gravitational pull, but will over time experience an increase in flux movement of water due to the lower region 2 being plugged, forcing the injected water into other regions. The low-permeable region 3 experiences cross-flow from both regions 2 and 4, mostly from the above-laying region 2 due to gravitational forces pulling the water down.

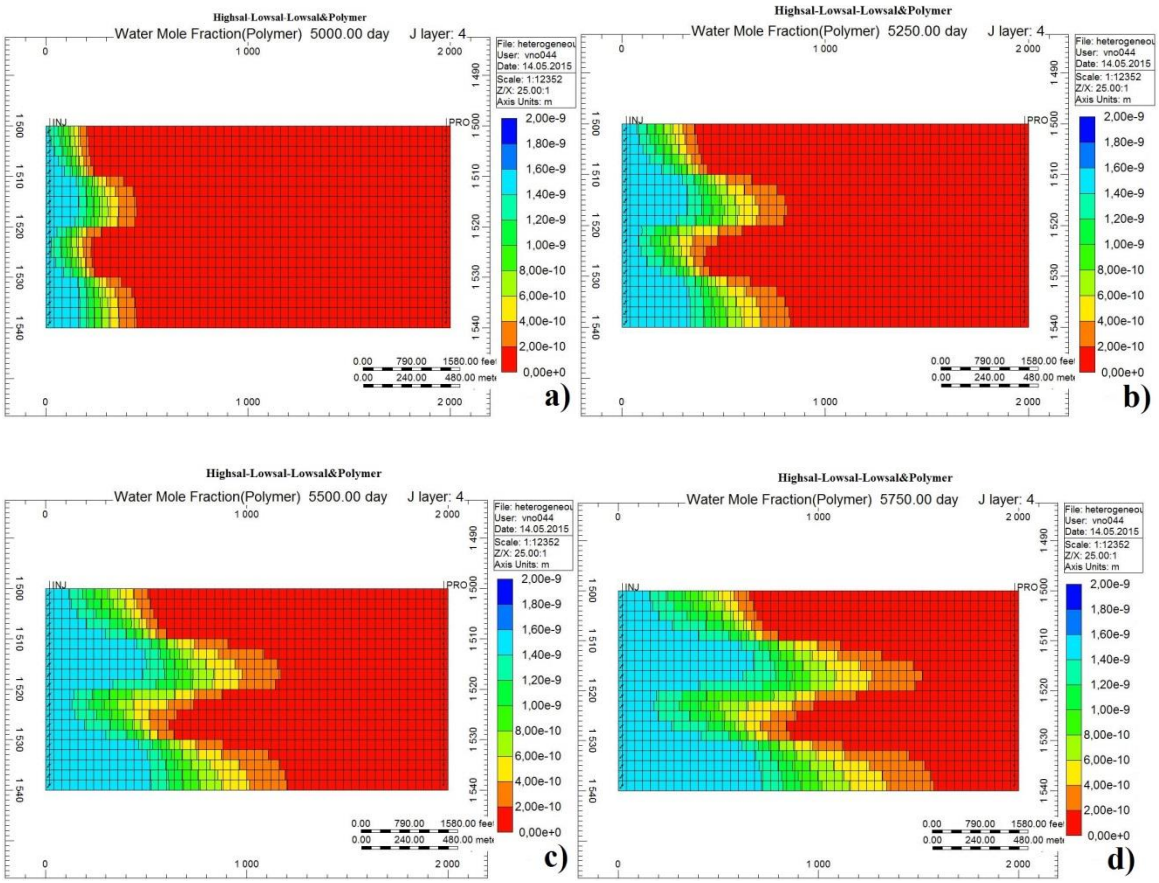

Figure 8-8a,b,c,d: *Sectional view in XZ-direction of polymer concentration after 5000,5250,5500, and 5750 days, respectively.*

When investigating polymer concentration in layer 11, which is the neighboring layer to the high-permeable region 2, it is clear that there are some irregularities in the polymer progression. At a certain time during polymer injection, one would expect that the polymer concentration decreases as a function of length from the injecting well, in a shape of an “S-shaped” curve. As seen in Figure 8-9, the polymer concentration actually increases in the center part before decreasing again. This area with increased polymer concentration travels over time.

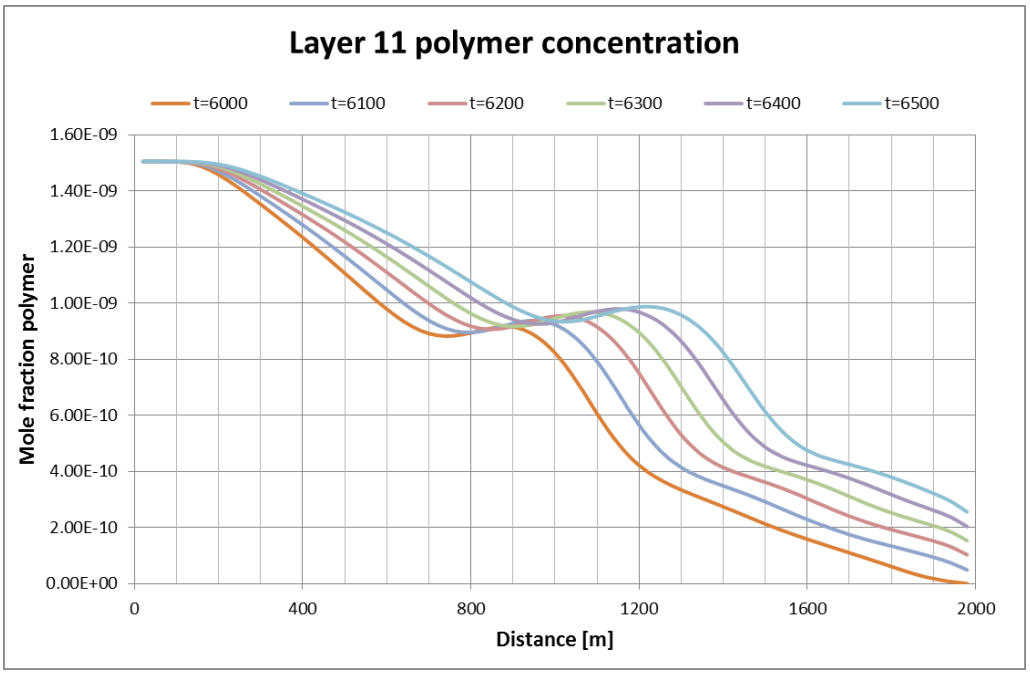

Figure 8-9: *Mole fractions of polymer over distance every 100th day after 6000 days, coarse grid.*

Upon further investigation as to why this occurs, it was found that not only did the polymer concentration increase in the center section, but also the water- and oil saturation accordingly. As with the polymer, the water saturation also travels over time, indicating a "snap-off"-like process with a portion with higher water saturation breaking off, see Figure 8-10a,b,c. It was first assumed that this was due to higher water viscosity lowering the mobility of the water, but the viscosity increases steadily from the water front shown in Figure 8-10a towards the injection well. It could also occur due to injected water in layer 10 flowing downwards into layer 11, but this would lead to an increase of water saturation rather than a decrease.

At a later time, this phenomenon also occurs in layers 12 and 13 below, as if there was some sort of flow obstruction in the layers, causing an uneven downflowing of water.

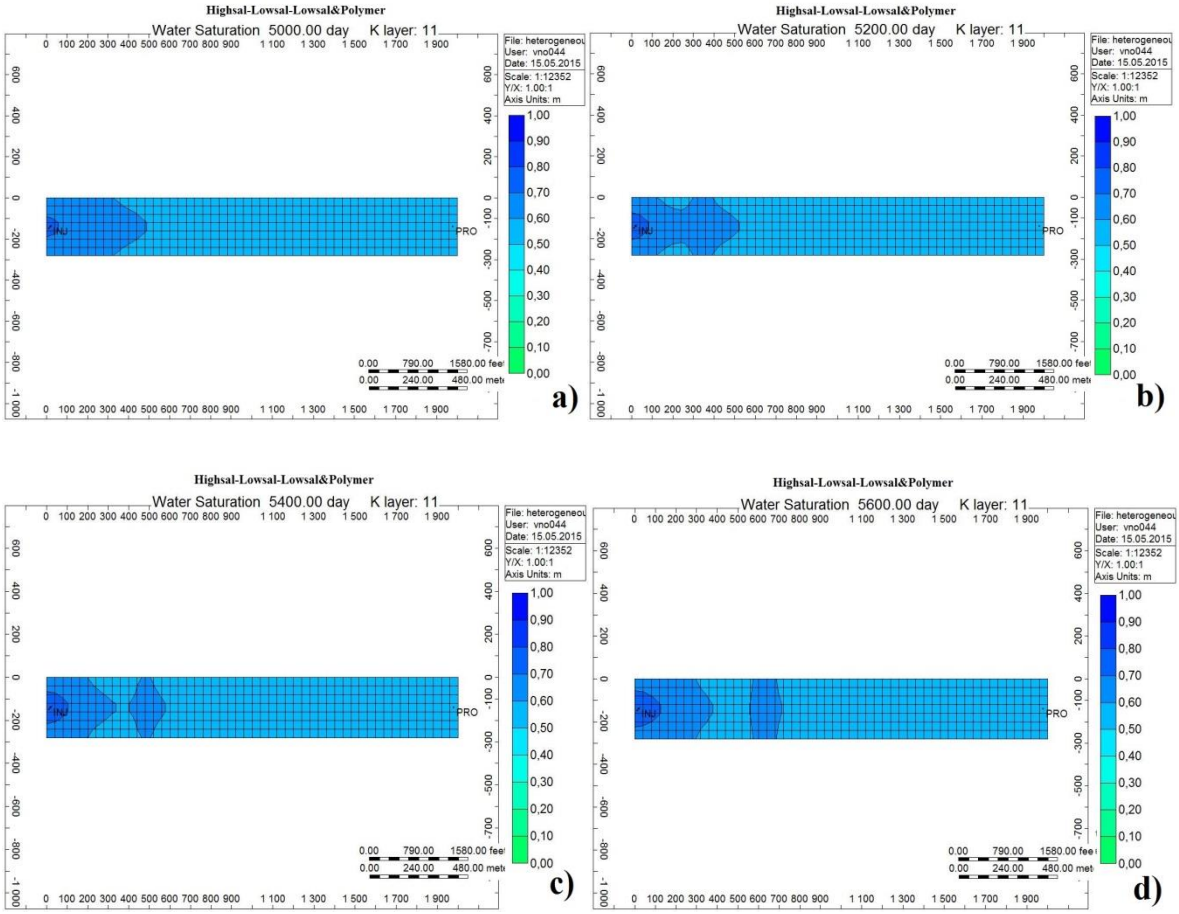

Figure 8-10a,b,c,d: *Sectional view in XY-direction in layer 11 of the «snap-off»-effect, every 200th day at 5000 days.*

Figure 8-11 shows production rate of polymers in mole fraction, and one can see the “usual” delay of breakthrough with a finer grid. While the coarse grid show an almost linear increase with only a slight deviation of curvature, the medium grid shows a more fluctuating increase in production rate. Unfortunately, it is not possible to inspect the mole fraction of polymer produced for each individual layer, since STARS does not provide a specific keyword for this. Upon inspecting the polymer concentration as it reaches the producing well, it looks like the fluctuation is caused by the (more) stable polymer front in the high-permeable region 2 since it reaches producing well at a later time. The fine grid would presumably show an even larger fluctuation in a plot of polymer production rate.

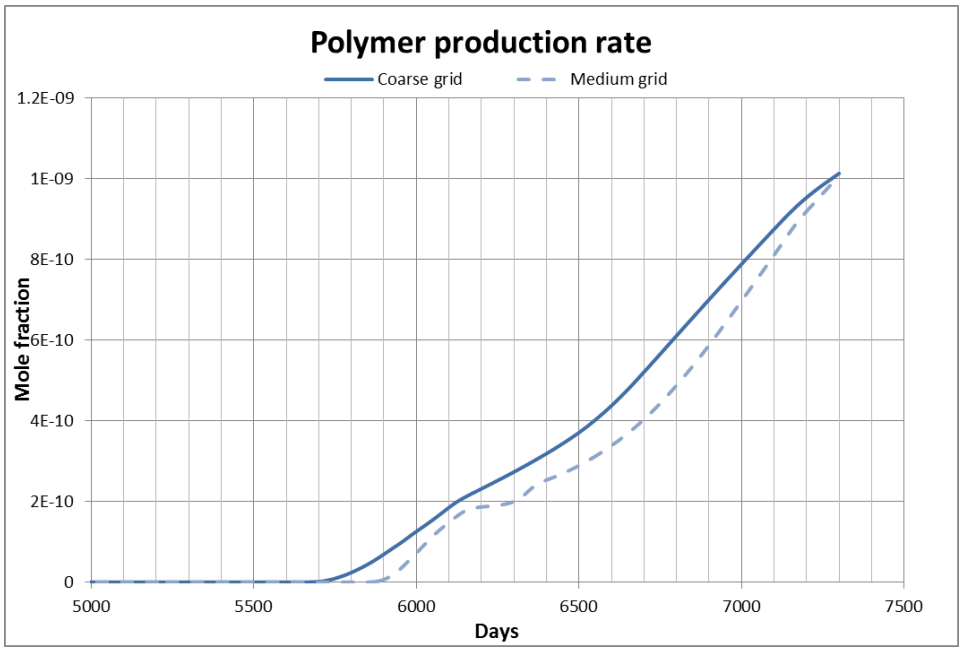

Figure 8-11: Polymer production rate, mole fraction, for coarse and medium grid. X-axis starts at 5000 days.

Figure 8-12a,b shows the polymer concentration for the coarse and medium grid models at 5500 days. As with salt, the polymer dispersion seems to be smaller with a finer grid resolution, again showing that a smaller grid block size results in smaller numerical dispersion.

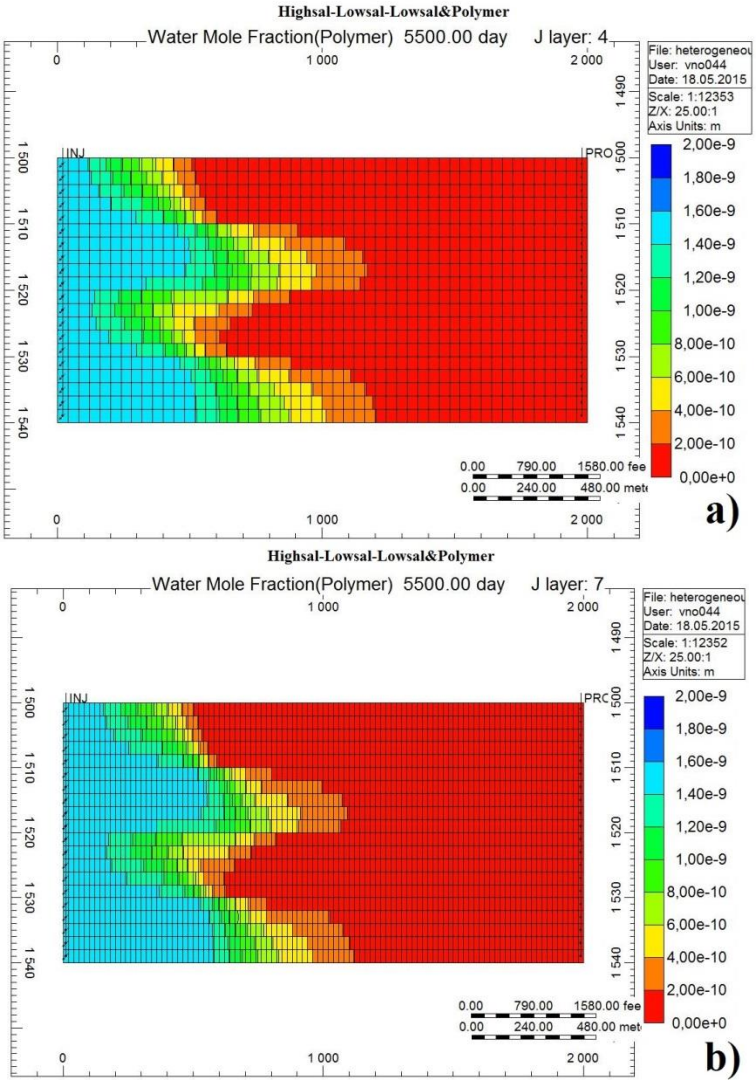

Figure 8-12a,b: *Sectional view in XZ-direction of polymer concentration at 5500 days, in coarse and medium grid models.*

The polymer adsorption was observed for both the coarse and medium grid model. As with dispersion, the adsorption will take longer time to reach maximum adsorption level further away from injection point compared to closer cells. Also, the medium grid showed a steeper adsorption curve than the coarse model, showing that the rate of adsorption is a direct consequence of component dispersion. Figure 8-13a,b shows adsorption for two grid resolutions and one can see that it follows the same trend as with dispersion with a less spread out front with a finer grid resolution.

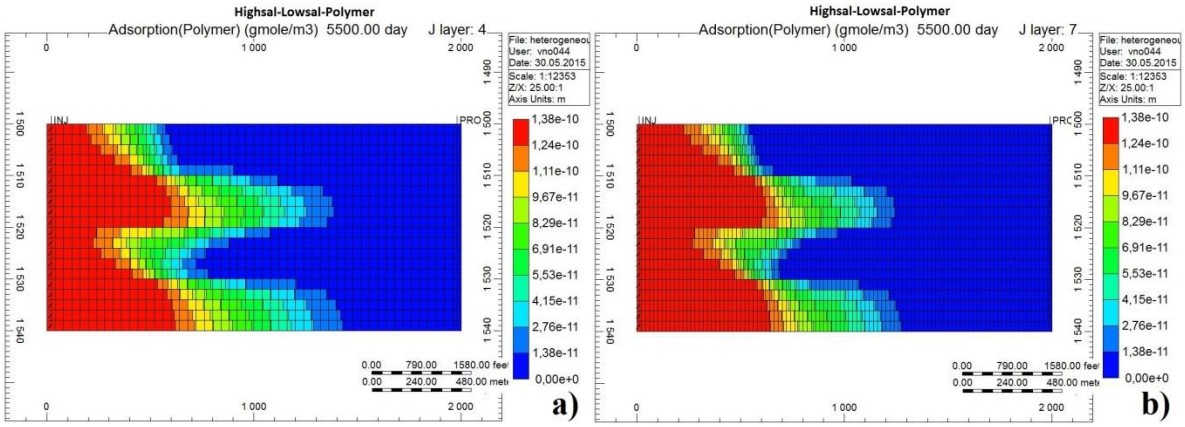

Figure 8-13 a,b: *Sectional view of polymer adsorption in coarse and medium grid at 5500 days.*

9 Conclusion

From the simulations performed with high- and low-salinity water, results from both the homogeneous and heterogeneous reservoir point towards a stable recovery with varying grid block size. The heterogeneous reservoir showed a smaller deviation with a varying grid size, probably due to the smaller recovery in general. For both reservoirs, the secondary low-salinity injection showed the highest deviation of the three injection schemes with highsal/lowsal. While total recovery may be stable for different grid resolutions, investigation of production rates in layers could show larger differences between the grid models. Upon interpolation which leads to liberation of oil due to a lower S_{or}, the upflowing of oil due to density differences acts differently for the varying grid models.

A smaller grid block size will "delay" the dispersion and make the dispersion fronts more stable and less spread out, thus showing that finer grid resolution reduces numerical dispersion. This accounts for both injected fluids such as water, and other components dispersed in the water. This results in a slower advancement and could, for example, be seen as a delayed water breakthrough for the finer grids. This delay was larger between coarse-medium grid resolution than for medium-fine, which could indicate a finite limit to how fine a grid resolution could become before no further change in dispersion is seen. The deviations in production between the grid models were also larger between coarse-medium than for medium-fine.

Several numerical discrepancies could be seen in the heterogeneous reservoir, where it appears that the regional permeability difference combined with poor oil displacement by water affects the salt dispersion in the upper region. It is unknown to which degree these irregularities affects the production results, but it is unlikely to have a major impact on the results.

Polymer injection showed the most interesting results. Firstly, realistic pressure values were not attainable in the simulations performed due to the water phase viscosity not being modeled as non-Newtonian. Furthermore, the variation in recovery with alternating grid resolution is noteworthy, with a 1% increase in production from coarse to medium grid model. The fine grid model would probably show an even larger recovery.

Irregularities were also observed with water saturations in grid blocks, going both above and beneath the saturation boundaries given in the relperm curves. This was observed upon salt mixing in cells with only connate water present, and with polymer injection.

The reservoirs in this thesis are very small compared to real-life oil fields, and the grid block sizes accordingly. It is common in the industry to operate with a grid block size of 100m*100m up to even 1km*1km in horizontal resolution, due to the large size of the reservoirs. There is reason to believe that such large reservoirs will show a much higher sensitivity to grid resolution and would therefore show a more precise estimate with a finer grid model, but this boils down to computational demands since simulations at such large dimensions could often imply millions of grid blocks.

10 Further work

Although some conclusions have been drawn in this thesis there is a lot of potential for further research to be performed regarding grid-sensitive simulations, and field-scale simulations in general.

Firstly, the amount of heterogeneity can be included further with larger and more often occurring permeability differences, flow barriers, and rock types. The heterogeneity included is in thesis showed some irregularities regarding dispersion so it could be interesting to see how grid sensitivity varies more advanced geology.

The polymer injection showed a sensitivity to grid resolution, but it proved hard to produce realistic pressure results. This could be researched further with emphasis of the effect shear-rate would have in field-scale reservoirs.

Other hybrid EOR techniques such as lowsal-surfactant or even lowsal-polymer-surfactant injection could be investigated, as it is probable that it would also show a sensitivity to grid resolution.

Lastly, further work regarding grid sensitivity could be further upscaled with larger reservoirs and larger grid block sizes since there is reason to believe that deviation between grid models become larger with a larger grid block size.

The following appendixes show a selection of some of the data files used in this thesis. Since several of the data files are very similar with only small differences distinguishing them, only one data file per “different” simulation has been included. Note that almost all timesteps have been removed for simplification purposes, and therefore only show the first and last timestep following or preceding a change in injection.

Appendix A- B7 History match data file

```
** ============== INPUT/OUTPUT CONTROL ============================

TITLE1 'B7 History match'
INUNIT LAB

INTERRUPT *STOP
WSRF WELL 1
WSRF GRID TIME
WSRF SECTOR TIME

OUTSRF SPECIAL DELPBLK 2 1 1     119 1 1
OUTSRF SPECIAL DELPBLK 1 1 1      120 1 1
OUTSRF SPECIAL DELP 'INJ' 'PRODN'
OUTSRF SPECIAL MOLEFRAC 'PRODN' 'SALT'
OUTSRF SPECIAL MASSFRAC 'PRODN' 'SALT'
OUTSRF GRID ALL
OUTSRF WELL LAYER NONE

WPRN GRID 0
OUTPRN GRID POREVOL
OUTPRN RES NONE
WPRN ITER 1
OUTPRN ITER NEWTON

PARTCLSIZE 1e-017

** ============== GRID AND RESERVOIR DEFINITION =================
GRID CART  120  1  1
KDIR DOWN
DI                    0.01 118*0.0672  0.01
DJ ALL    120*3.297
DK ALL   120*3.297
NULL CON 1
POR 0.999 118*0.25 0.999

PERMI ALL
160470 118*585.5  20470
PERMJ EQUALSI
```

```
PERMK EQUALSI

PINCHOUTARRAY CON     1  **No pinchout cells. all cells are active
END-GRID

** ================== COMPONENT PROPERTIES ======================

MODEL 3 3  3 2
COMPNAME        'WATER'             'SALT'      'DEAD_OIL'
CMM              0.018   0.058   0.4
PCRIT           0 0 0
TCRIT           0 0 0
CP              0   0   1.2E-6
MASSDEN         0.001000      0.001900     0.0008784
AVISC           1  5  13.8
BVISC           0  0  0

VSMIXCOMP 'SALT'
VSMIXENDP 0.0015 0.0099
VSMIXFUNC 0.006183 0.014736 0.023174 0.031498 0.039713 0.04782 0.055822 0.063723 0.071525 0.07923
0.086841

SOLID_DEN  'SALT'   0.0182482  0  0

PRSR  2528.25
TEMR  31
PSURF 101
TSURF 31


** ==================  ROCK-FLUID DATA  ================== **
ROCKFLUID
RPT 1 WATWET

INTCOMP 'SALT' WATER
** Set #1: High-sal. water injection
** ------------------------------------------------
KRINTRP 1
DTRAPW 0.0099
SWT
 SMOOTHEND QUAD
          ** sw             krw             kro
          0.234            0               1
          0.25             5.99125E-06     0.996106325
          0.27             7.17668E-05     0.983370779
          0.29             0.000284647     0.962240268
          0.31             0.000751088     0.932331782
          0.349979192      0.002986857     0.844899047
          0.37             0.005101713     0.787347713
          0.41             0.012403842     0.648763729
```

0.43	0.018114779	0.57098451
0.45	0.025575898	0.490610345
0.47	0.035063181	0.410326485
0.49	0.046809721	0.332832661
0.510160267	0.061085553	0.260030946
0.5428828	0.089414723	0.158222176
0.556943893	0.103345501	0.12185257
0.565259814	0.111991956	0.102580085
0.571303904	0.118436683	0.089630648
0.580425203	0.128373266	0.071779123
0.587468028	0.136180827	0.059382728
0.593179822	0.142573833	0.050210539
0.597861826	0.147840806	0.043275877
0.601594746	0.152049684	0.038120791
0.612666845	0.164528103	0.024757607
0.619487584	0.172165403	0.017940839
0.624500453	0.177730961	0.01361028
0.628429651	0.182056045	0.01061618
0.641291499	0.195909585	0.003287684
0.647129118	0.202006703	0.001252063
0.65	0.204954075	0.000572556
0.655	0.21	0

** Set #2: Low-sal. water injection
** ---

*KRINTRP 2
*DTRAPW 0.0015
SWT
SMOOTHEND QUAD

** sw	krw	kro
0.234	0	1
0.25	0.000936841	0.918442297
0.27	0.003265858	0.846816847
0.29	0.006521471	0.7808626
0.31	0.010580916	0.716878935
0.349979192	0.020840615	0.591561006
0.37	0.02695018	0.530118338
0.41	0.040851329	0.412039763
0.43	0.048542824	0.356489747
0.45	0.056651524	0.304060013
0.47	0.065115374	0.255292317
0.49	0.073869215	0.21063927
0.510160267	0.082918082	0.170134401
0.5428828	0.097903718	0.114504745
0.556943893	0.104392132	0.094480411
0.565259814	0.108228334	0.083717782
0.571303904	0.111012407	0.076390308
0.580425203	0.11520267	0.066106011
0.587468028	0.118425197	0.058788422

0.593179822	0.121028159	0.053243022
0.597861826	0.123153582	0.04895182
0.601594746	0.124842209	0.045691595
0.612666845	0.1298152	0.036838472
0.619487584	0.132848481	0.031972105
0.624500453	0.135061164	0.028669878
0.628429651	0.136784891	0.026239206
0.641291499	0.14235533	0.019209789
0.647129118	0.14484363	0.016465237
0.65	0.146057409	0.015212537
0.655	0.148154899	0.013178367
0.671148956	0.154773722	0.007808585
0.696129084	0.164461177	0.002635241
0.702348709	0.166749773	0.001843751
0.709204197	0.16920569	0.001164154
0.711132705	0.169882989	0.00100659
0.71348691	0.170701198	0.000832972
0.714273393	0.17097237	0.000779413
0.715830505	0.171505938	0.000679737
0.716743827	0.171816809	0.000625119
0.716968417	0.171893012	0.000612115
0.717165112	0.171959672	0.000600864
0.717338681	0.172018432	0.000591042
0.717754543	0.172158983	0.00056791
0.717968047	0.172231011	0.000556253
0.718060613	0.172262212	0.000551245
0.718145311	0.172290746	0.000546687
0.718223155	0.172316958	0.000542518
0.718294799	0.172341073	0.000538698
0.718422413	0.172384001	0.000531936
0.718479455	0.172403178	0.00052893
0.718532562	0.172421028	0.000526141
0.718672156	0.172467919	0.000518852
0.718787849	0.172506751	0.000512859
0.718854547	0.172529126	0.000509423
0.718885243	0.172539421	0.000507846
0.73	0.176129464	0.000115883
0.74	0.179037491	4.98189E-06
0.744	0.18	0

DISPI_WAT 'SALT' *CON 0.01
DISPJ_WAT 'SALT' *CON 0.01
DISPK_WAT 'SALT' *CON 0.01

** ================= INITIAL CONDITIONS ====== ============== **
INITIAL
VERTICAL OFF

INITREGION 1
PRES CON 1724.5515

```
TEMP CON          31

SW ALL
 1 118*0.234 1

MFRAC_OIL 'DEAD_OIL'  CON  1.0
MFRAC_WAT 'SALT'      CON  0.0099
MFRAC_WAT 'WATER'     CON  0.9901

** ================= NUMERICAL CONTROL ====================== **

NUMERICAL
TFORM SXY
ISOTHERMAL

** =================  RECURRENT DATA  ====================== **

RUN

TIME 0
DTWELL 0.001

WELL 'INJ'
INJECTOR UNWEIGHT 'INJ'
INCOMP WATER   0.9901   0.0099  0
OPERATE MAX STW 0.1 CONT
GEOMETRY  K  0.01  0.249  1.    0.
PERF TUBE-END 'INJ'
1 1 1  1.  OPEN    FLOW-FROM  'SURFACE'

WELL  'PRODN'
PRODUCER 'PRODN'
OPERATE  MIN  BHP  1722.25  CONT
GEOMETRY  K  0.01  0.249  1.    0.
PERF  TUBE-END  'PRODN'
120 1 1  1.  OPEN    FLOW-TO  'SURFACE'

TIME 1
TIME 1440

WELL 'INJ'
INJECTOR UNWEIGHT 'INJ'
INCOMP WATER   0.9985   0.0015  0
OPERATE MAX STW 0.1 CONT

TIME 1450
TIME 3840

STOP
```

Appendix B- Highsal data file, fine, homogeneous reservoir

```
** ==============  INPUT/OUTPUT CONTROL  ======================= **

RESULTS SIMULATOR STARS 201210
INTERRUPT STOP

TITLE1 'highsal'
TITLE2 'Only dead oil and water'

INUNIT *SI

OUTPRN GRID *PRES *SW *SO *SG *TEMP *X *W *OBHLOSS *ADSORP
           *MASDENO *MASDENG *MASDENW *KRINTER *IFT
           *MASFR
OUTPRN WELL ALL
OUTSRF WELL DOWNHOLE
OUTSRF WELL DOWNHOLE
OUTSRF SPECIAL DELP  'INJ' 'PROD'
OUTSRF SPECIAL MOLEFRAC  'PROD' 'NaCl'
OUTSRF SPECIAL AVGVAR PRES
OUTSRF WELL LAYER ALL

WRST 100
WPRN *GRID 100
WPRN *ITER 100
OUTSRF WELL COMPONENT ALL
OUTSRF GRID ALL

OUTSRF SPECIAL DELPBLK 1,14,1 200,14,1
OUTSRF SPECIAL DELPBLK 1,14,5 200,14,5
OUTSRF SPECIAL DELPBLK 1,14,6 200,14,6
OUTSRF SPECIAL DELPBLK 1,14,10 200,14,10
OUTSRF SPECIAL DELPBLK 1,14,11 200,14,11
OUTSRF SPECIAL DELPBLK 1,14,15 200,14,15
OUTSRF SPECIAL DELPBLK 1,14,16 200,14,16
OUTSRF SPECIAL DELPBLK 1,14,20 200,14,20




**$  Distance units: m
RESULTS XOFFSET         0.0000
RESULTS YOFFSET         0.0000
RESULTS ROTATION         0.0000  **$  (DEGREES)
RESULTS AXES-DIRECTIONS 1.0 -1.0 1.0

** ============ GRID AND RESERVOIR DEFINITION =============== **

RANGECHECK OFF

GRID VARI 200 28 20
KDIR DOWN

DI IVAR
 200*10
DJ JVAR
```

```
 28*10
DK ALL
 112000*2

DTOP
 5600*1500

NULL CON 1

POR CON
0.25

PERMI
112000*2000
PERMJ EQUALSI
PERMK
112000*200

PINCHOUTARRAY CON          1

RANGECHECK ON

** ==================  COMPONENT PROPERTIES  ============== **

MODEL 3 3 3 2
COMPNAME        'WATER' 'NaCl' 'DEAD_OIL'
CMM             0.018   0.058  0.4
PCRIT           0   0  0
TCRIT           0  0  0
CP              0   0    1.2E-6
MASSDEN         1000      2165     750
AVISC           0.5  0.5  8
BVISC           0    0    0

VSMIXCOMP 'NaCl'
VSMIXENDP 0.0015 0.0099

SOLID_DEN  'NaCl'   2165  0  0


PRSR 10110
TEMR 75
PSURF 101
TSURF 31

** ==================  ROCK-FLUID DATA  ================== **

ROCKFLUID
RPT 1 STONE1 WATWET
INTCOMP 'NaCl' WATER
KRINTRP 1
DTRAPW 0.0099
SWT
 SMOOTHEND QUAD
          **  sw              krw               kro

          0.234           0                 1
```

0.25	5.99125E-06	0.996106325
0.27	7.17668E-05	0.983370779
0.29	0.000284647	0.962240268
0.31	0.000751088	0.932331782
0.349979192	0.002986857	0.844899047
0.37	0.005101713	0.787347713
0.41	0.012403842	0.648763729
0.43	0.018114779	0.57098451
0.45	0.025575898	0.490610345
0.47	0.035063181	0.410326485
0.49	0.046809721	0.332832661
0.510160267	0.061085553	0.260030946
0.5428828	0.089414723	0.158222176
0.556943893	0.103345501	0.12185257
0.565259814	0.111991956	0.102580085
0.571303904	0.118436683	0.089630648
0.580425203	0.128373266	0.071779123
0.587468028	0.136180827	0.059382728
0.593179822	0.142573833	0.050210539
0.597861826	0.147840806	0.043275877
0.601594746	0.152049684	0.038120791
0.612666845	0.164528103	0.024757607
0.619487584	0.172165403	0.017940839
0.624500453	0.177730961	0.01361028
0.628429651	0.182056045	0.01061618
0.641291499	0.195909585	0.003287684
0.647129118	0.202006703	0.001252063
0.65	0.204954075	0.000572556
0.655	0.21	0

** Set #2: Low-sal. water injection
** ---
KRINTRP 2
DTRAPW 0.0015
SWT
SMOOTHEND QUAD

** sw	krw	kro
0.234	0	1
0.25	0.000936841	0.918442297
0.27	0.003265858	0.846816847
0.29	0.006521471	0.7808626
0.31	0.010580916	0.716878935
0.349979192	0.020840615	0.591561006
0.37	0.02695018	0.530118338
0.41	0.040851329	0.412039763
0.43	0.048542824	0.356489747
0.45	0.056651524	0.304060013
0.47	0.065115374	0.255292317
0.49	0.073869215	0.21063927
0.510160267	0.082918082	0.170134401
0.5428828	0.097903718	0.114504745
0.556943893	0.104392132	0.094480411
0.565259814	0.108228334	0.083717782
0.571303904	0.111012407	0.076390308
0.580425203	0.11520267	0.066106011

0.587468028	0.118425197	0.058788422
0.593179822	0.121028159	0.053243022
0.597861826	0.123153582	0.04895182
0.601594746	0.124842209	0.045691595
0.612666845	0.1298152	0.036838472
0.619487584	0.132848481	0.031972105
0.624500453	0.135061164	0.028669878
0.628429651	0.136784891	0.026239206
0.641291499	0.14235533	0.019209789
0.647129118	0.14484363	0.016465237
0.65	0.146057409	0.015212537
0.655	0.148154899	0.013178367
0.671148956	0.154773722	0.007808585
0.696129084	0.164461177	0.002635241
0.702348709	0.166749773	0.001843751
0.709204197	0.16920569	0.001164154
0.711132705	0.169882989	0.00100659
0.71348691	0.170701198	0.000832972
0.714273393	0.17097237	0.000779413
0.715830505	0.171505938	0.000679737
0.716743827	0.171816809	0.000625119
0.716968417	0.171893012	0.000612115
0.717165112	0.171959672	0.000600864
0.717338681	0.172018432	0.000591042
0.717754543	0.172158983	0.00056791
0.717968047	0.172231011	0.000556253
0.718060613	0.172262212	0.000551245
0.718145311	0.172290746	0.000546687
0.718223155	0.172316958	0.000542518
0.718294799	0.172341073	0.000538698
0.718422413	0.172384001	0.000531936
0.718479455	0.172403178	0.00052893
0.718532562	0.172421028	0.000526141
0.718672156	0.172467919	0.000518852
0.718787849	0.172506751	0.000512859
0.718854547	0.172529126	0.000509423
0.718885243	0.172539421	0.000507846
0.73	0.176129464	0.000115883
0.74	0.179037491	4.98189E-06
0.744	0.18	0

```
DISPI_WAT 'NaCl' *CON 0.01
DISPJ_WAT 'NaCl' *CON 0.01
DISPK_WAT 'NaCl' *CON 0.01

** ================= INITIAL CONDITIONS ====== ============== **

INITIAL
INITREGION 1
VERTICAL DEPTH_AVE
REFDEPTH  1500
REFPRES 40110
SW ALL
112000*0.234
MFRAC_OIL 'DEAD_OIL' CON          1
```

```
MFRAC_WAT 'WATER' CON      0.9901
MFRAC_WAT 'NaCl' CON      0.0099

** ================= NUMERICAL CONTROL ====================== **

NUMERICAL
TFORM ZT
ISOTHERMAL
NORTH 300
ITERMAX 300
CONVERGE TOTRES TIGHTER

** ================  RECURRENT DATA  ====================== **

RUN
TIME 0
DTWELL 0.1
DTMAX 10

WELL 'INJ'
INJECTOR UNWEIGHT 'INJ'
INCOMP WATER 0.9985 0.0015 0
OPERATE MAX STW 1500 CONT
GEOMETRY  K  0.1  0.0199  1.0  0.0
PERF  GEO  'INJ'
1 14 1:20  1.0  OPEN    FLOW-FROM  'SURFACE'  REFLAYER

WELL 'PROD'
PRODUCER 'PROD'
OPERATE MAX STL 1534 CONT
OPERATE MIN BHP 10110
GEOMETRY  K  0.1  0.0199  1.0  0.0
PERF  GEO  'PROD'
200 14 1:20  1.0  OPEN    FLOW-TO  'SURFACE'  REFLAYER

TIME 1
TIME 3650

STOP

RESULTS SPEC 'Permeability J'
RESULTS SPEC SPECNOTCALCVAL -99999
RESULTS SPEC REGION 'All Layers (Whole Grid)'
RESULTS SPEC REGIONTYPE 'REGION_WHOLEGRID'
RESULTS SPEC LAYERNUMB 0
RESULTS SPEC PORTYPE 1
RESULTS SPEC EQUALSI 0 1
RESULTS SPEC SPECKEEPMOD 'YES'
RESULTS SPEC STOP
```

Appendix C- Highsal-Lowsal data file, medium, heterogeneous reservoir

```
** ==============  INPUT/OUTPUT CONTROL  ====================== **

RESULTS SIMULATOR STARS 201210
INTERRUPT *STOP

TITLE1 'highsal-lowsal'
TITLE2 'Only dead oil water'
INUNIT *SI

OUTPRN GRID *PRES *SW *SO *SG *TEMP *X *W *OBHLOSS *ADSORP
          *MASDENO *MASDENG *MASDENW *KRINTER *IFT
          *MASFR
OUTPRN WELL ALL

OUTSRF WELL DOWNHOLE
OUTSRF WELL DOWNHOLE
OUTSRF SPECIAL DELP  'INJ' 'PROD'
OUTSRF SPECIAL MOLEFRAC  'PROD' ' NaCl '
OUTSRF SPECIAL AVGVAR PRES
OUTSRF WELL LAYER ALL

WRST 100
WPRN *GRID 100
WPRN *ITER 100
OUTSRF WELL COMPONENT ALL
OUTSRF GRID ALL

OUTSRF SPECIAL DELPBLK 1,7,1 100,7,1
OUTSRF SPECIAL DELPBLK 1,7,5 100,7,5
OUTSRF SPECIAL DELPBLK 1,7,6 100,7,6
OUTSRF SPECIAL DELPBLK 1,7,10 100,7,10
OUTSRF SPECIAL DELPBLK 1,7,11 100,7,11
OUTSRF SPECIAL DELPBLK 1,7,15 100,7,15
OUTSRF SPECIAL DELPBLK 1,7,16 100,7,16
OUTSRF SPECIAL DELPBLK 1,7,20 100,7,20

**$  Distance units: m
RESULTS XOFFSET         0.0000
RESULTS YOFFSET         0.0000
RESULTS ROTATION         0.0000  **$  (DEGREES)
RESULTS AXES-DIRECTIONS 1.0 -1.0 1.0

** ============ GRID AND RESERVOIR DEFINITION =============== **

RANGECHECK OFF
GRID VARI 100 14 20
KDIR DOWN

DI IVAR
 100*20
DJ JVAR
 14*20
```

```
DK ALL
 28000*2

DTOP
 1400*1500

NULL CON 1
POR CON
0.25

PERMI
7000*200
7000*2000
7000*200
7000*2000
PERMJ EQUALSI
PERMK
7000*20
7000*200
7000*20
7000*200

PINCHOUTARRAY CON          1
RANGECHECK ON

** ==================  COMPONENT PROPERTIES  ============== **

MODEL 3 3 3 2
COMPNAME 'WATER' 'NaCl' 'DEAD_OIL'
CMM               0.015   0.058  0.4
PCRIT             0   0  0
TCRIT             0  0  0
CP                0   0    1.2E-6
MASSDEN           1000      2165     750
AVISC             0.5  0.5  8
BVISC             0    0    0

VSMIXCOMP 'NaCl'
VSMIXENDP 0.0015 0.0099

SOLID_DEN  'NaCl'   2165  0  0

PRSR 10110
TEMR 75
PSURF 101
TSURF 3


** ==================  ROCK-FLUID DATA  ================== **

ROCKFLUID
RPT 1 STONE1 WATWET
INTCOMP ' NaCl ' WATER
KRINTRP 1
DTRAPW 0.0099
SWT
SMOOTHEND QUAD
```

**	Sw	krw	kro
	0.234	0	1
	0.25	5.99125E-06	0.996106325
	0.27	7.17668E-05	0.983370779
	0.29	0.000284647	0.962240268
	0.31	0.000751088	0.932331782
	0.349979192	0.002986857	0.844899047
	0.37	0.005101713	0.787347713
	0.41	0.012403842	0.648763729
	0.43	0.018114779	0.57098451
	0.45	0.025575898	0.490610345
	0.47	0.035063181	0.410326485
	0.49	0.046809721	0.332832661
	0.510160267	0.061085553	0.260030946
	0.5428828	0.089414723	0.158222176
	0.556943893	0.103345501	0.12185257
	0.565259814	0.111991956	0.102580085
	0.571303904	0.118436683	0.089630648
	0.580425203	0.128373266	0.071779123
	0.587468028	0.136180827	0.059382728
	0.593179822	0.142573833	0.050210539
	0.597861826	0.147840806	0.043275877
	0.601594746	0.152049684	0.038120791
	0.612666845	0.164528103	0.024757607
	0.619487584	0.172165403	0.017940839
	0.624500453	0.177730961	0.01361028
	0.628429651	0.182056045	0.01061618
	0.641291499	0.195909585	0.003287684
	0.647129118	0.202006703	0.001252063
	0.65	0.204954075	0.000572556
	0.655	0.21	0

** Set #2: Low-sal. water injection
** ---
*KRINTRP 2
*DTRAPW 0.0015
SWT
SMOOTHEND QUAD

	** sw	krw	kro
	0.234	0	1
	0.25	0.000936841	0.918442297
	0.27	0.003265858	0.846816847
	0.29	0.006521471	0.7808626
	0.31	0.010580916	0.716878935
	0.349979192	0.020840615	0.591561006
	0.37	0.02695018	0.530118338
	0.41	0.040851329	0.412039763
	0.43	0.048542824	0.356489747
	0.45	0.056651524	0.304060013
	0.47	0.065115374	0.255292317
	0.49	0.073869215	0.21063927
	0.510160267	0.082918082	0.170134401
	0.5428828	0.097903718	0.114504745
	0.556943893	0.104392132	0.094480411
	0.565259814	0.108228334	0.083717782

0.571303904	0.111012407	0.076390308
0.580425203	0.11520267	0.066106011
0.587468028	0.118425197	0.058788422
0.593179822	0.121028159	0.053243022
0.597861826	0.123153582	0.04895182
0.601594746	0.124842209	0.045691595
0.612666845	0.1298152	0.036838472
0.619487584	0.132848481	0.031972105
0.624500453	0.135061164	0.028669878
0.628429651	0.136784891	0.026239206
0.641291499	0.14235533	0.019209789
0.647129118	0.14484363	0.016465237
0.65	0.146057409	0.015212537
0.655	0.148154899	0.013178367
0.671148956	0.154773722	0.007808585
0.696129084	0.164461177	0.002635241
0.702348709	0.166749773	0.001843751
0.709204197	0.16920569	0.001164154
0.711132705	0.169882989	0.00100659
0.71348691	0.170701198	0.000832972
0.714273393	0.17097237	0.000779413
0.715830505	0.171505938	0.000679737
0.716743827	0.171816809	0.000625119
0.716968417	0.171893012	0.000612115
0.717165112	0.171959672	0.000600864
0.717338681	0.172018432	0.000591042
0.717754543	0.172158983	0.00056791
0.717968047	0.172231011	0.000556253
0.718060613	0.172262212	0.000551245
0.718145311	0.172290746	0.000546687
0.718223155	0.172316958	0.000542518
0.718294799	0.172341073	0.000538698
0.718422413	0.172384001	0.000531936
0.718479455	0.172403178	0.00052893
0.718532562	0.172421028	0.000526141
0.718672156	0.172467919	0.000518852
0.718787849	0.172506751	0.000512859
0.718854547	0.172529126	0.000509423
0.718885243	0.172539421	0.000507846
0.73	0.176129464	0.000115883
0.74	0.179037491	4.98189E-06
0.744	0.18	0

DISPI_WAT ' NaCl ' *CON 0.01
DISPJ_WAT ' NaCl ' *CON 0.01
DISPK_WAT ' NaCl ' *CON 0.01

** ================= INITIAL CONDITIONS ====== ============== **

INITIAL
INITREGION 1
VERTICAL DEPTH_AVE
REFDEPTH 1500
REFPRES 40110

SW ALL

```
28000*0.234

MFRAC_OIL 'DEAD_OIL' CON           1
MFRAC_WAT 'WATER' CON      0.9901
MFRAC_WAT ' NaCl ' CON      0.0099

** ================= NUMERICAL CONTROL ====================== **

NUMERICAL
TFORM ZT
ISOTHERMAL
NORTH 300
ITERMAX 300
CONVERGE TOTRES TIGHTER

** ================  RECURRENT DATA  ====================== **

RUN
TIME 0
DTWELL 0.1
DTMAX 10

WELL 'INJ'
INJECTOR UNWEIGHT 'INJ'
INCOMP WATER 0.9901 0.0099 0
OPERATE MAX STW 1500 CONT
GEOMETRY  K  0.1  0.0199  1.0  0.0
PERF  GEO  'INJ'
 1 7 1:20  1.0  OPEN    FLOW-FROM  'SURFACE'  REFLAYER


WELL 'PROD'
PRODUCER 'PROD'
OPERATE MAX STL 1534 CONT
OPERATE MIN BHP 10110
GEOMETRY  K  0.1  0.0199  1.0  0.0
PERF  GEO  'PROD'
100 7 1:20  1.0  OPEN    FLOW-TO  'SURFACE'  REFLAYER

TIME 1
TIME 3650

WELL 'INJ'
INJECTOR UNWEIGHT 'INJ'
INCOMP WATER 0.9985 0.0015 0
OPERATE MAX STW 1500 CONT
GEOMETRY  K  0.1  0.0199  1.0  0.0
PERF  GEO  'INJ'
1 7 1:20  1.0  OPEN    FLOW-FROM  'SURFACE'  REFLAYER

TIME 3660
TIME 7300

STOP
```

Appendix D- Highsal-Lowsal-Lowsal&Polymer data file, coarse

```
** ==============  INPUT/OUTPUT CONTROL  ======================= **

RESULTS SIMULATOR STARS 201210
INTERRUPT *STOP
TITLE1 'Highsal-Lowsal-Lowsal&Polymer'
TITLE2 'Dead oil, water, and polymers'

INUNIT *SI

OUTPRN GRID *PRES *SW *SO *SG *TEMP *X *W *OBHLOSS *ADSORP
          *MASDENO *MASDENG *MASDENW *KRINTER *IFT
          *MASFR
OUTPRN WELL ALL

OUTSRF WELL DOWNHOLE
OUTSRF WELL DOWNHOLE
OUTSRF SPECIAL DELP  'INJ' 'PROD'
OUTSRF SPECIAL MOLEFRAC  'PROD' 'NaCl'
OUTSRF SPECIAL AVGVAR PRES
OUTSRF WELL LAYER ALL

WRST 100
WPRN *GRID 100
WPRN *ITER 100
OUTSRF WELL COMPONENT ALL
OUTSRF GRID ALL

OUTSRF SPECIAL DELPBLK 1,4,1 50,4,1
OUTSRF SPECIAL DELPBLK 1,4,5 50,4,5
OUTSRF SPECIAL DELPBLK 1,4,6 50,4,6
OUTSRF SPECIAL DELPBLK 1,4,10 50,4,10
OUTSRF SPECIAL DELPBLK 1,4,11 50,4,11
OUTSRF SPECIAL DELPBLK 1,4,15 50,4,15
OUTSRF SPECIAL DELPBLK 1,4,16 50,4,16
OUTSRF SPECIAL DELPBLK 1,4,20 50,4,20

**$  Distance units: m
RESULTS XOFFSET         0.0000
RESULTS YOFFSET         0.0000
RESULTS ROTATION         0.0000  **$  (DEGREES)
RESULTS AXES-DIRECTIONS 1.0 -1.0 1.0

** ============ GRID AND RESERVOIR DEFINITION ================ **

RANGECHECK OFF

GRID VARI 50 7 20
KDIR DOWN

DI IVAR
 50*40
DJ JVAR
 7*40
DK ALL
 7000*2
```

```
DTOP
 350*1500

NULL CON 1
POR CON
0.25

PERMI
1750*200
1750*2000
1750*200
1750*2000

PERMJ EQUALSI
PERMK
1750*20
1750*200
1750*20
1750*200

PINCHOUTARRAY CON          1

RANGECHECK ON

** ==================  COMPONENT PROPERTIES  ============== **

MODEL 4 4 4 3
COMPNAME       'WATER'  'NaCl'              'Polymer'           'DEAD_OIL'
CMM            0.018   0.058 6000 0.4
PCRIT          0   0  0  0
TCRIT          0   0  0  0
CP             0   0  0  1.2E-6
MASSDEN        1000      2165      1000      750
AVISC          0.5   0.5  5  8
BVISC          0     0    0    0

VSMIXCOMP 'NaCl'
VSMIXENDP 0.0015 0.0099

VSMIXCOMP 'Polymer'
VSMIXENDP 0 1.50491E-9

SOLID_DEN  'NaCl'   2165  0  0

PRSR 10110
TEMR 75
PSURF 101
TSURF 31

** ==================  ROCK-FLUID DATA  ================== **

ROCKFLUID
RPT 1 STONE1 WATWET
INTCOMP 'NaCl' WATER
KRINTRP 1
DTRAPW 0.0099
```

SWT
SMOOTHEND QUAD

**	Sw	krw	kro
	0.234	0	1
	0.25	5.99125E-06	0.996106325
	0.27	7.17668E-05	0.983370779
	0.29	0.000284647	0.962240268
	0.31	0.000751088	0.932331782
	0.349979192	0.002986857	0.844899047
	0.37	0.005101713	0.787347713
	0.41	0.012403842	0.648763729
	0.43	0.018114779	0.57098451
	0.45	0.025575898	0.490610345
	0.47	0.035063181	0.410326485
	0.49	0.046809721	0.332832661
	0.510160267	0.061085553	0.260030946
	0.5428828	0.089414723	0.158222176
	0.556943893	0.103345501	0.12185257
	0.565259814	0.111991956	0.102580085
	0.571303904	0.118436683	0.089630648
	0.580425203	0.128373266	0.071779123
	0.587468028	0.136180827	0.059382728
	0.593179822	0.142573833	0.050210539
	0.597861826	0.147840806	0.043275877
	0.601594746	0.152049684	0.038120791
	0.612666845	0.164528103	0.024757607
	0.619487584	0.172165403	0.017940839
	0.624500453	0.177730961	0.01361028
	0.628429651	0.182056045	0.01061618
	0.641291499	0.195909585	0.003287684
	0.647129118	0.202006703	0.001252063
	0.65	0.204954075	0.000572556
	0.655	0.21	0

** Set #2: Low-sal. water injection

KRINTRP 2
DTRAPW 0.0015
SWT
SMOOTHEND QUAD

**	sw	krw	kro
	0.234	0	1
	0.25	0.000936841	0.918442297
	0.27	0.003265858	0.846816847
	0.29	0.006521471	0.7808626
	0.31	0.010580916	0.716878935
	0.349979192	0.020840615	0.591561006
	0.37	0.02695018	0.530118338
	0.41	0.040851329	0.412039763
	0.43	0.048542824	0.356489747
	0.45	0.056651524	0.304060013
	0.47	0.065115374	0.255292317
	0.49	0.073869215	0.21063927
	0.510160267	0.082918082	0.170134401
	0.5428828	0.097903718	0.114504745

0.556943893	0.104392132	0.094480411
0.565259814	0.108228334	0.083717782
0.571303904	0.111012407	0.076390308
0.580425203	0.11520267	0.066106011
0.587468028	0.118425197	0.058788422
0.593179822	0.121028159	0.053243022
0.597861826	0.123153582	0.04895182
0.601594746	0.124842209	0.045691595
0.612666845	0.1298152	0.036838472
0.619487584	0.132848481	0.031972105
0.624500453	0.135061164	0.028669878
0.628429651	0.136784891	0.026239206
0.641291499	0.14235533	0.019209789
0.647129118	0.14484363	0.016465237
0.65	0.146057409	0.015212537
0.655	0.148154899	0.013178367
0.671148956	0.154773722	0.007808585
0.696129084	0.164461177	0.002635241
0.702348709	0.166749773	0.001843751
0.709204197	0.16920569	0.001164154
0.711132705	0.169882989	0.00100659
0.71348691	0.170701198	0.000832972
0.714273393	0.17097237	0.000779413
0.715830505	0.171505938	0.000679737
0.716743827	0.171816809	0.000625119
0.716968417	0.171893012	0.000612115
0.717165112	0.171959672	0.000600864
0.717338681	0.172018432	0.000591042
0.717754543	0.172158983	0.00056791
0.717968047	0.172231011	0.000556253
0.718060613	0.172262212	0.000551245
0.718145311	0.172290746	0.000546687
0.718223155	0.172316958	0.000542518
0.718294799	0.172341073	0.000538698
0.718422413	0.172384001	0.000531936
0.718479455	0.172403178	0.00052893
0.718532562	0.172421028	0.000526141
0.718672156	0.172467919	0.000518852
0.718787849	0.172506751	0.000512859
0.718854547	0.172529126	0.000509423
0.718885243	0.172539421	0.000507846
0.73	0.176129464	0.000115883
0.74	0.179037491	4.98189E-06
0.744	0.18	0

DISPI_WAT 'NaCl' *CON 0.01
DISPJ_WAT 'NaCl' *CON 0.01
DISPK_WAT 'NaCl' *CON 0.01

DISPI_WAT 'Polymer' *CON 0.001
DISPJ_WAT 'Polymer' *CON 0.001
DISPK_WAT 'Polymer' *CON 0.001

ADSCOMP 'Polymer' WATER
ADSLANG 2 0 8000000000

```
ADMAXT 2.3E-10
ADRT 2.3E-10

** ================= INITIAL CONDITIONS ====== ============== **


INITIAL
INITREGION 1
VERTICAL DEPTH_AVE
REFDEPTH  1500
REFPRES 40110
SW ALL
7000*0.234
MFRAC_OIL 'DEAD_OIL' CON          1
MFRAC_WAT 'WATER' CON     0.9901
MFRAC_WAT 'NaCl' CON      0.0099

** ================= NUMERICAL CONTROL ====================== **

NUMERICAL
TFORM ZT
ISOTHERMAL
NORTH 300
ITERMAX 300
CONVERGE TOTRES TIGHTER

** =================  RECURRENT DATA  ====================== **

RUN
TIME 0
DTWELL 0.1
DTMAX 10

WELL 'INJ'
INJECTOR UNWEIGHT 'INJ'
INCOMP WATER 0.9901 0.0099 0 0
OPERATE MAX STW 1500 CONT
GEOMETRY  K  0.1  0.0199  1.0  0.0
PERF  GEO  'INJ'
1 4 1:20  1.0  OPEN    FLOW-FROM  'SURFACE'  REFLAYER

WELL 'PROD'
PRODUCER 'PROD'
OPERATE MAX STL 1534 CONT
OPERATE MIN BHP 10110
GEOMETRY  K  0.1  0.0199  1.0  0.0
PERF  GEO  'PROD'
50 4 1:20  1.0  OPEN    FLOW-TO  'SURFACE'  REFLAYER

TIME 1
TIME 2200,

WELL 'INJ'
INJECTOR UNWEIGHT 'INJ'
INCOMP WATER 0.9985 0.0015 0 0

OPERATE MAX STW 1500 CONT
```

```
GEOMETRY  K  0.1  0.0199  1.0  0.0
PERF  GEO  'INJ'
1 4 1:20  1.0  OPEN    FLOW-FROM  'SURFACE'  REFLAYER

TIME 2300
TIME 4750

WELL 'INJ'
INJECTOR UNWEIGHT 'INJ'
INCOMP WATER 0.998499998 0.0015 0.00000000150491 0

OPERATE MAX STW 1500 CONT
GEOMETRY  K  0.1  0.235  1.0  -4.3
PERF  GEO  'INJ'
 1 4 1:20  1.0  OPEN    FLOW-FROM  'SURFACE'  REFLAYER

TIME 4760
TIME 7300

STOP
```

References

AGBALAKA, C., DANDEKAR, A., PATIL, S., KHATANIAR, S. & HEMSATH, J. 2009. Coreflooding Studies to Evaluate the Impact of Salinity and Wettability on Oil Recovery Efficiency. *Transport in Porous Media,* 76**,** 77-94.

ALZAYER, H. & SOHRABI, M. 2013. Numerical Simulation of Improved Heavy Oil Recovery by Low-Salinity Water Injection and Polymer Flooding. Society of Petroleum Engineers.

ANDERSON, W. G. 1987a. Wettability Literature Survey- Part 4: Effects of Wettability on Capillary Pressure.

ANDERSON, W. G. 1987b. Wettability Literature Survey-Part 6: The Effects of Wettability on Waterflooding.

ANDERSON, W. G. 1987c. Wettability Literature Survey Part 5: The Effects of Wettability on Relative Permeability.

ARYA, A., HEWETT, T. A., LARSON, R. G. & LAKE, L. W. 1988. Dispersion and Reservoir Heterogeneity.

ASHRAF, A., HADIA, N., TORSAETER, O. & TWEHEYO, M. T. 2010. Laboratory Investigation of Low Salinity Waterflooding as Secondary Recovery Process: Effect of Wettability. Society of Petroleum Engineers.

BASU, S. & SHARMA, M. M. 1997. Characterization of Mixed-Wettability States in Oil Reservoirs by Atomic Force Microscopy.

BEAR, J. 1972. *Dynamics of Fluids in Porous Media*.

BERNARD, G. G. 1967. Effect of Floodwater Salinity on Recovery Of Oil from Cores Containing Clays. Society of Petroleum Engineers.

BROWNELL, L. E. 1948. *FLOW OF FLUIDS THROUGH POROUS MEDIA*, University of MICHIGAN.

BUCKLEY, J. S., LIU, Y. & MONSTERLEET, S. 1998. Mechanisms of Wetting Alteration by Crude Oils.

COREY, A. T. 1954. The Interrelation Between Gas and Oil Relative Permeabilities.

CRAIG, F. F. 1971. *Reservoir engineering aspects of waterflooding*.

EHRLICH, R. & WYGAL, R. J., JR. 1977. Interrelation of Crude Oil and Rock Properties With the Recovery of Oil by Caustic Waterflooding.

HAAJIZADEH, M. & BEGG, S. H. 1993. Sensitivity of Oil Recovery to Grid Size and Reservoir Description in Fluvially Dominated Deltaic Facies. Society of Petroleum Engineers.

JADHUNANDAN, P. P. & MORROW, N. R. 1995. Effect of wettability on waterflood recovery for crude-oil/brine/rock systems. *Journal Name: SPE Reservoir Engineering (Society of Petroleum Engineers); (United States); Journal Volume: 10:1***,** Medium: X; Size: Pages: 40-46.

JENSEN, J. A. & RADKE, C. J. 1988. Chromatographic Transport of Alkaline Buffers Through Reservoir Rock.

JERAULD, G. R., WEBB, K. J., LIN, C.-Y. & SECCOMBE, J. 2006. Modeling Low-Salinity Waterflooding. Society of Petroleum Engineers.

KALLEVIK, G. 2010. Implementations of Methods for Modeling Low Salinity Waterflood and Low Salinity Surfactant Flooding.

LAGER, A., WEBB, K. J., COLLINS, I. R. & RICHMOND, D. M. 2008. LoSal Enhanced Oil Recovery: Evidence of Enhanced Oil Recovery at the Reservoir Scale. Society of Petroleum Engineers.

LAKE, L. W. 1989. *Enhanced oil recovery / Larry W. Lake,* Englewood Cliffs, N.J, Prentice Hall.

LEE, S. Y., WEBB, K. J., COLLINS, I., LAGER, A., CLARKE, S., APOS, SULLIVAN, M., ROUTH, A. & WANG, X. 2010. Low Salinity Oil Recovery: Increasing Understanding of the Underlying Mechanisms. Society of Petroleum Engineers.

LIU, K. 2001. Reduce the Number of Components for Compositional Reservoir Simulation. Society of Petroleum Engineers.

LOMELAND, F., EBELTOFT, E. & THOMAS, W. H. 2005. A NEW VERSATILE RELATIVE PERMEABILITY CORRELATION. *Symposium on Computer Animation.*

LTD., C. M. G. 2012. *User`s guide STARS,* Calgary, Alberta Canada, Computer Modelling Group Ltd.

MOHAMMADI, H. & JERAULD, G. 2012. Mechanistic Modeling of the Benefit of Combining Polymer with Low Salinity Water for Enhanced Oil Recovery. Society of Petroleum Engineers.
MORROW, N. & BUCKLEY, J. 2011. Improved Oil Recovery by Low-Salinity Waterflooding.
RIVET, S., LAKE, L. W. & POPE, G. A. 2010. A Coreflood Investigation of Low-Salinity Enhanced Oil Recovery. Society of Petroleum Engineers.
SALATHIEL, R. A. 1973. Oil Recovery by Surface Film Drainage In Mixed-Wettability Rocks.
SALTER, S. J. & MOHANTY, K. K. 1982. Multiphase Flow in Porous Media: I. Macroscopic Observations and Modeling. Society of Petroleum Engineers.
SKRETTINGLAND, K., HOLT, T., TWEHEYO, M. T. & SKJEVRAK, I. 2010. Snorre Low Salinity Water Injection - Core Flooding Experiments And Single Well Field Pilot. Society of Petroleum Engineers.
SORBIE, K. S. & COLLINS, I. 2010. A Proposed Pore-Scale Mechanism for How Low Salinity Waterflooding Works. Society of Petroleum Engineers.
TANG, G.-Q. & MORROW, N. R. 1999. Influence of brine composition and fines migration on crude oil/brine/rock interactions and oil recovery. *Journal of Petroleum Science and Engineering,* 24**,** 99-111.
TANG, G. Q. & MORROW, N. R. 1997. Salinity, Temperature, Oil Composition, and Oil Recovery by Waterflooding.
VIJAPURAPU, C. S. & RAO, D. N. 2004. Compositional effects of fluids on spreading, adhesion and wettability in porous media. *Colloids and Surfaces A: Physicochemical and Engineering Aspects,* 241**,** 335-342.
WANG, D., CHENG, J., WU, J. & WANG, Y. 2002. Producing by Polymer Flooding more than 300 Million Barrels of Oil, What Experiences Have Been Learnt? : Society of Petroleum Engineers.
WILLHITE, P. G. 1986. *Waterflooding*.
YILDIZ, H. O. & MORROW, N. R. 1996. Effect of brine composition on recovery of Moutray crude oil by waterflooding. *Journal of Petroleum Science and Engineering,* 14**,** 159-168.